SUSY Seesaw Model and Phenomenological Implications for Leptonic Processes at Low Energies and Leptogenesis

Dissertation zur Erlangung des
naturwissenschaftlichen Doktorgrades
der Bayerischen Julius-Maximilians-Universität
Würzburg

vorgelegt von

Andreas Redelbach

aus Marktheidenfeld

Würzburg 2004

Eingereicht am: 02.02.2004
bei der Fakultät für Physik und Astronomie

1. Gutachter: Prof. Dr. R. Rückl
2. Gutachter: Prof. Dr. H. Fraas
der Dissertation

1. Prüfer: Prof. Dr. R. Rückl
2. Prüfer: Prof. Dr. J. Niemeyer
der mündlichen Prüfung

Tag der mündlichen Prüfung: 20.02.2004

Doktorurkunde ausgehändigt am: . . . .

Contents

Chapter 1

Introduction

During the last years there have been many fascinating new insights into the nature of leptonic interactions. The evidence for neutrino oscillations in solar [1] and atmospheric [2] neutrino experiments and the resulting neutrino mixing and mass squared difference parameters [3] are now widely accepted. In the near future, the ongoing efforts of testing neutrino properties will become precision measurements. The research in the neutrino sector is nicely complemented by precision experiments studying charged leptons [4]. Among these are the searches for lepton-flavor violating rare decays, muon-electron conversion on nuclei and electric and magnetic dipole moments. In order to give an overview of the present results and the expected future sensitivities of these experiments, we summarize them below:

- $Br\left(\mu \to e\gamma\right) < 1.2 \cdot 10^{-11} \; (10^{-13} - 10^{-14})$ [5, 4] [6]

- $Br\left(\tau \to e\gamma\right) < 3.7 \cdot 10^{-7} \; (10^{-8})$ [7]

- $Br\left(\tau \to \mu\gamma\right) < 3.1 \cdot 10^{-7} \; (10^{-8} - 10^{-9})$ [8] [9, 7]

- $Br\left(\mu^+ \to e^+e^+e^-\right) < 1.0 \cdot 10^{-12} \; (10^{-16})$ [5] [10]

- $R\left(\mu^- Ti \to e^- Ti\right) < 6.1 \cdot 10^{-13} \; (10^{-16})$ [5] [4, 11]

- $d_e < 1.5 \cdot 10^{-27} \; (10^{-33})$ ecm [12] [13]

- $d_\mu < 1.5 \cdot 10^{-18} \; (10^{-26})$ ecm [14] [10]

A natural framework for neutrino masses is provided by the seesaw mechanism [15] in which the smallness of neutrino masses is explained by a very large mass scale of right-handed neutrinos. These are Majorana fermions and singlets under the Standard Model (SM) gauge symmetry. Their existence leads to a possible solution of the puzzle of baryogenesis, i. e. the matter-antimatter asymmetry of the universe in the framework of leptogenesis [16], where an asymmetry in the lepton number L, generated by interactions of the heavy Majorana neutrinos is eventually converted into the baryon asymmetry observed in the present universe. The generation of a baryon asymmetry of the right order of magnitude clearly restricts the parameter space of the seesaw model.

The aforementioned lepton-flavor violating processes are strongly suppressed due to the small neutrino masses if only right-handed neutrino singlets are added to the Standard Model [17]. Therefore an observation of lepton-flavor violation (LFV) in rare decays is a clear proof of physics beyond the SM. Well-motivated candidates for physics beyond the SM are supersymmetric theories which can be constructed to be consistent with all experimental data. Apart from an elegant solution to the hierarchy problem, i. e. the large discrepancy between the electroweak scale and the Plack scale, supersymmetric theories generically lead to gauge coupling unification, thus allowing the construction of Grand Unified Theories (GUTs) at ultra high energy scales. From a phenomenological point of view, low-energy supersymmetry (SUSY) is expected to manifest itself at upcoming collider projects, i. e. the Large Hadron Collider (LHC) and the future Linear Collider (LC). Other possible indications of SUSY are the current deviation [18] of the measurement of the muon anomalous magnetic moment [19] from the Standard Model prediction [18]. The interpretation of the lightest supersymmetric particle (LSP) as the cosmological dark matter candidate [20] is also an interesting phenomenological aspect of SUSY.

A challenging problem of supersymmetric theories is the mechanism of soft supersymmetry breaking (SSB). At present, there are several theoretical suggestions in order to explain phenomenologically interesting SSB masses in the TeV range. Among these scenarios of SSB, the so-called minimal supergravity (mSUGRA) scenario [21] has gained much attention in studies of SUSY LFV, see e. g. [22]. In this work however, we also want to discuss the SUSY seesaw model in the framework of anomaly mediated supersymmetry breaking (AMSB) [23] and in the case of gaugino mediated supersymmetry breaking ($\tilde{G}$MSB) [24]. Moreover we study sizeable LFV effects in a scenario of gauge mediated SUSY breaking (GMSB) [25] motivated by the recent analysis of [26], where a very high messenger scale has been considered. It is demonstrated that in a large portion of the parameter space of the SUSY seesaw model, one can expect decay rates for $\mu \rightarrow e\gamma$ accessible by future searches irrespective of the mechanism of SUSY breaking. We point out that relations among different LFV rare processes are expected to probe the parameters of the SUSY seesaw model, and furthermore to distinguish it from other SUSY approaches, such as trilinear R-parity violation.

This work is organized as follows: In the second chapter, different supersymmetric models are introduced and their basic features relevant for further phenomenological and numerical study are outlined. We summarize the analytical results for leptonic processes at low energies and leptogenesis in chapter 3. The fundamental parameters of the SUSY scenarios under study as well as the neutrino data used in the numerical analysis are specified in the fourth chapter. In this chapter we also present numerical predictions, so that we can discuss consequences of the different scenarios and effects of various parameters in detail. The most important results are presented in the conclusions. This work is completed by several appendices containing e. g. a complete one-loop calculation of SUSY contributions to leptonic dipole operators relevant in the SUSY seesaw model.

Chapter 2

Theoretical framework

2.1 Aspects of supersymmetry

A supersymmetric transformation turns a fermionic state into a bosonic state and vice versa. The generator of SUSY transformations is given by the anticommuting spinor object Q [27, 28]. Moreover, Q commutes with P^μ, i. e. the generator of space-time translations. The SUSY algebra is completed by the anticommutator of Q and $Q^\dagger$, which is related to P^μ. We do not want to introduce the full index formalism for Weyl spinor objects here, because we do not need it in the following parts of this work. For formal presentations of the SUSY algebra see e. g. [27, 28]. The irreducible representations of the SUSY algebra consisting of single particle states form supermultiplets. In an unbroken supersymmetric theory, the bosonic and fermionic states of the same supermultiplet have equal masses, since the (mass)^2 operator P^2 commutes with Q, $Q^\dagger$ and all space-time rotation and translation operators. Moreover, Q and $Q^\dagger$ commute with the generators of gauge transformations. It follows that the states of the same supermultiplet are in the same representation of the gauge group, i. e. they have the same $SU(3)_C \times SU(2)_L \times U(1)_Y$ quantum numbers. The supermultiplets consist of bosonic and fermionic superpartners with equal number of bosonic and fermionic degrees of freedom.

Each chiral supermultiplet is a combination of a left-handed, two-component Weyl-fermion and a complex scalar field accompanied by an auxiliary field F_{aux}. The complex scalar field F_{aux} is necessary in order for the SUSY algebra to close off-shell. Since F_{aux} is introduced through $F_{aux}^* F_{aux}$ in the Lagrangian, it has mass dimension 2 and no kinetic term, so that it can be eliminated by using its equation of motion. Vector supermultiplets consist of gauge bosons, the spin-$\frac{1}{2}$ gauginos and auxiliary fields D^a, where the index a refers to the adjoint representation of the gauge group. Prior to spontaneous breaking of electroweak symmetry, gauge bosons and gauginos are massless. The real bosonic fields D^a is introduced in the Lagrangian through $\mathcal{L}_{aux} = \frac{1}{2} D^a_{aux} D^a_{aux}$, allowing the SUSY algebra for vector supermultiplets to close also off-shell, a necessary condition for viable SUSY calculations at the quantum level.

One of the main advantages of supersymmetric theories is that they provide a natural solution to the hierarchy problem [28]: In the SM the quantum corrections to scalar

masses squared diverge quadratically. This leads to Higgs $(\text{mass})^2$ contributions of the order of the cut-off scale squared, so that an extreme amount of fine-tuning would be necessary to obtain a Higgs mass at the electroweak scale.

Because of the experimental evidence that no mass-degenerate SUSY partners of the SM particles exist, supersymmetry is a broken symmetry in the vacuum state. If broken supersymmetry is required to provide a solution of the hierarchy problem at the quantum level, the Lagrangian must contain only couplings with positive mass dimension, so-called soft SUSY breaking terms [29]. In that work it has been shown that a generic renormalizable SSB Lagrangian is given by

$$\mathcal{L}^{gen}_{soft} = -\frac{1}{2}\left(\tilde{M}_{\lambda_a}\lambda_a\lambda_a + h.c.\right) - m^2_{ij}\phi^*_i\phi_j - \left(\frac{1}{2}b_{ij}\phi_i\phi_j + \frac{1}{6}a_{ijk}\phi_i\phi_j\phi_k + h.c.\right), \quad (2.1)$$

specifying the structure of mass terms for gauginos λ_a, scalar fields ϕ_i, bilinear terms b_{ij} and trilinear terms a_{ijk}. Hermitian conjugate of a term is abbreviated by "$h.c.$".

In a renormalizable supersymmetric theory, the interactions of all particles are determined by their gauge transformation properties and the superpotential. The superpotential is an analytic function of the chiral superfields Φ_i of the generic form [27]

$$\mathcal{W}_{gen} = \frac{1}{2}M_{ij}\Phi_i\Phi_j + \frac{1}{6}y_{ijk}\Phi_i\Phi_j\Phi_k. \quad (2.2)$$

If SUSY is broken spontaneously in the vacuum state, the vacuum state is not invariant under a supersymmetric transformation. According to the Goldstone theorem, see e. g. [30], the spontaneous breaking of a global symmetry leads to a massless Goldstone mode having the same quantum numbers as the broken symmetry generator. Broken global SUSY implies the breaking of the fermionic SUSY generator Q, leading to a massless neutral Weyl-fermion, the goldstino.

The mechanism of SUSY breaking is often supposed to occur in a "hidden sector" having only very small direct couplings to the "visible sector" of low-energy supersymmetry. If the theory is locally supersymmetric, it is referred to as supergravity [21], unifying the spacetime symmetries of General Relativity with local supersymmetry transformations. The graviton is then accompanied by its spin-$\frac{3}{2}$ partner, the gravitino. If SUSY is spontaneously broken, the gravitino acquires a mass $m_{3/2}$ in the "super-Higgs mechanism", see e. g. [28] by absorbing the goldstino which becomes its spin-$\frac{1}{2}$ component. It is important to mention that SUSY is spontaneously broken if and only if auxiliary fields have non-vanishing vacuum expectation values (VEVs) [28]. For F-term breaking of SUSY, the gravitino mass is roughly given by

$$m_{3/2} \sim \frac{\langle F_{aux}\rangle}{M_{Pl}} \quad (2.3)$$

which becomes zero in the case of unbroken SUSY, i. e. $\langle F_{aux}\rangle = 0$ or by "switching off" gravity, i. e. $M_{Pl} \to \infty$. Gravitinos can have important effects in cosmology which will be discussed later.

2.2   Minimal supersymmetric Standard Model

The minimal supersymmetric Standard Model (MSSM) is a minimal supersymmetric theory in the sense that one SUSY degree of freedom is introduced for every bosonic or fermionic degree of freedom of the Standard Model. The MSSM shows the following features [27]:

- The MSSM is gauge invariant under the groups $SU(3)_C \times SU(2)_L \times U(1)_Y$.

- The MSSM possesses the minimal structure for the Higgs sector of an anomaly free extension of the Standard Model with two hypercharge $Y = \pm 1/2$ doublets.

- The most general soft SUSY breaking terms are included.

- R-parity is conserved. This multiplicative quantum number is defined as $R = (-1)^{3(B-L)+2S}$ (B: baryon number, L: lepton number, S: spin), yielding an even value for SM particles and an odd number for their superpartners.

The conservation of R-parity is related to $B - L$ invariance and implies important phenomenological consequences:

- If the initial state for any process consists of SM particles (with even R-parity), then SUSY particles can only be produced in even numbers.

- The lightest supersymmetric particle (LSP) has to be absolutely stable if R-parity is exactly conserved.

- Every supersymmetric particle heavier than the LSP must finally decay into a state with an odd number of LSPs.

From cosmological, experimental and theoretical considerations the LSP should neither carry charge nor color [20]. Therefore a LSP having only electroweak interactions appears as a promising candidate for dark matter.

In the MSSM the superpartners for quarks and leptons are shown in Tab. 2.1. The (charge) conjugated fields of right-handed quarks, leptons and their superpartners appear in this table, because it is standard convention that all chiral superfields are defined in terms of left-handed Weyl spinors [27].

The MSSM superpotential is [31]

$$\mathcal{W}_{MSSM} = u_R^{c\,T} Y_u \, q \cdot h_2 + d_R^{c\,T} Y_d \, q \cdot h_1 + e_R^{c\,T} Y_e \, l \cdot h_1 + \mu h_1 \cdot h_2, \qquad (2.4)$$

where the fields are understood as chiral superfields. Here the dot-symbol denotes a summation over $SU(2)_L$ indices, e. g. $\mu h_1 \cdot h_2 = \mu \, (h_1)^{\alpha} \, (h_2)^{\beta} \, \epsilon_{\alpha\beta}$, where $\epsilon_{\alpha\beta}$ is the antisymmetric tensor with $\epsilon_{12} = 1$. A summation over family indices and also $SU(3)_C$ color indices for quarks is understood.

The MSSM contains two Higgs supermultiplets with hypercharges $\pm\frac{1}{2}$. The Higgs chiral supermultiplet with $Y = +1/2$ has the Yukawa couplings necessary to give masses to

Names	spin 0	spin 1/2	$SU(3)_C, SU(2)_L, U(1)_Y$
squarks, quarks	$\tilde{q} = \left(\tilde{u}_L \ \tilde{d}_L \right)$	$q = (u_L \ d_L)$	$\left(\mathbf{3}, \mathbf{2}, \frac{1}{6} \right)$
($\times$ 3 families)	$\tilde{u}_R^*$	$(u_R)^c$	$\left(\overline{\mathbf{3}}, \mathbf{1}, -\frac{2}{3} \right)$
	$\tilde{d}_R^*$	$(d_R)^c$	$\left(\overline{\mathbf{3}}, \mathbf{1}, \frac{1}{3} \right)$
sleptons, leptons	$\tilde{l} = (\tilde{\nu}_L \ \tilde{e}_L)$	$l = (\nu_L \ e_L)$	$\left(\mathbf{1}, \mathbf{2}, -\frac{1}{2} \right)$
($\times$ 3 families)	$\tilde{e}_R^*$	e_R^c	$\left(\mathbf{1}, \mathbf{1}, 1 \right)$
Higgs, higgsinos	$h_2 = \left(h_2^+ \ h_2^0 \right)$	$\tilde{h}_2 = \left(\tilde{h}_2^+ \ \tilde{h}_2^0 \right)$	$\left(\mathbf{1}, \mathbf{2}, \frac{1}{2} \right)$
	$h_1 = \left(h_1^0 \ h_1^- \right)$	$\tilde{h}_1 = \left(\tilde{h}_1^0 \ \tilde{h}_1^- \right)$	$\left(\mathbf{1}, \mathbf{2}, -\frac{1}{2} \right)$

Table 2.1: Physical components of chiral supermultiplets in the MSSM; fields of the SUSY partners are written with tildes on the SM counterpart.

Names	spin 1/2	spin 1	$SU(3)_C, SU(2)_L, U(1)_Y$
Gluino, gluon	$\tilde{G}$	G	$(\mathbf{8}, \mathbf{1}, 0)$
winos, W-bosons	$\tilde{W}^{\pm} \ \tilde{W}^0$	$W^{\pm} \ W^0$	$(\mathbf{1}, \mathbf{3}, 0)$
bino, B-boson	$\tilde{B}^0$	B^0	$(\mathbf{1}, \mathbf{1}, 0)$

Table 2.2: Physical components of vector supermultiplets in the MSSM.

up-type quarks. On the other hand, the $Y = -1/2$ supermultiplet leads to masses of down-type quarks and charged leptons after electroweak symmetry breaking. The VEV v_2 of the $Y = +1/2$ Higgs field and the VEV v_1 of the $Y = -1/2$ Higgs field are connected to the mass of the Z boson, the weak coupling constant g and the hypercharge coupling constant g' [27],

$$v_1^2 + v_2^2 = v^2 = \frac{2m_Z^2}{g^2 + g'^2}. \tag{2.5}$$

The ratio of the Higgs vacuum expectation values defines $\tan \beta$,

$$\tan \beta = \frac{v_2}{v_1}. \tag{2.6}$$

The gauge supermultiplets of the MSSM are shown in Tab. 2.2, see also [27]. The mixing of the gauginos and higgsino states to the neutralinos and charginos as well as the mixing of sfermion gauge eigenstates to the physical sfermions will be summarized in appendix C.

In the case of the MSSM one can write down the possible soft SUSY breaking terms in the following way [31],

$$
\begin{aligned}
-\mathcal{L}_{soft}^{MSSM} \;=\; & \frac{1}{2}\left(\tilde{M}_1\tilde{B}^0\tilde{B}^0 + \tilde{M}_2\tilde{W}^a\tilde{W}^a + \tilde{M}_3\tilde{G}^a\tilde{G}^a + h.c.\right) \\
& + \left(m_{\tilde{Q}}^2\right)_{ij}\tilde{q}_{L_i}^\dagger\tilde{q}_{L_j} + \left(m_{\tilde{u}}^2\right)_{ij}\tilde{u}_{R_i}^*\tilde{u}_{R_j} + \left(m_{\tilde{d}}^2\right)_{ij}\tilde{d}_{R_i}^*\tilde{d}_{R_j} + \left(m_{\tilde{L}}^2\right)_{ij}\tilde{l}_{L_i}^\dagger\tilde{l}_{L_j} \\
& + \left(m_{\tilde{e}}^2\right)_{ij}\tilde{e}_{R_i}^*\tilde{e}_{R_j} + m_{h_1}^2 h_1^\dagger h_1 + m_{h_2}^2 h_2^\dagger h_2 + (B\mu h_1 h_2 + h.c.) \\
& + \left((A_u)_{ij}\,h_2\tilde{u}_{R_i}^*\tilde{q}_{L_j} + (A_d)_{ij}\,h_1\tilde{d}_{R_i}^*\tilde{q}_{L_j} + (A_e)_{ij}\,h_1\tilde{e}_{R_i}^*\tilde{l}_{L_j} + h.c.\right). \quad (2.7)
\end{aligned}
$$

The labels i and j are generation indices. Eq. (2.7) introduces SSB masses for gauginos, squared mass terms for sfermions, SUSY breaking contributions to the Higgs potential and trilinear couplings, respectively. The matrices A are complex matrices in generation space with entries having dimension of mass.

Many unknown masses, phases and mixing angles arise with these soft SUSY breaking terms. There are actually more than 100 new parameters in the MSSM Lagrangian that cannot be rotated away by a redefinition of phases and the flavor basis for the supermultiplets. As a result, some of these new phases and parameters can lead to potentially large flavor-changing neutral currents (FCNCs) and CP-violating effects.

It has been noted that even if one takes $m_{h_1}^2$, $m_{h_2}^2$ and μ^2 positive at some high energy scale, large top Yukawa couplings can drive $m_{h_2}^2$ negative at lower scales through renormalization group (RG) running, see e. g. [28]. This mechanism is known as radiative electroweak symmetry breaking (REWSB). The necessary conditions for REWSB to work are that the Higgs potential is bounded from below and that the minimum of the Higgs potential occurs at non-zero field configurations. These conditions can be expressed in terms of μ and B at tree-level, see e. g. [32],

$$
\mu^2 \;=\; \frac{1}{2}\left(\tan 2\beta\left(m_{h_2}^2\tan\beta - m_{h_1}^2\cot\beta\right) - m_Z^2\right) \tag{2.8}
$$

$$
B \;=\; \frac{-\sin 2\beta}{2\mu}\left(m_{h_1}^2 + m_{h_2}^2 + 2\mu^2\right). \tag{2.9}
$$

The above equations have important consequences: If the Higgs mass parameters and $\tan\beta$ are known at low energy, μ^2 and B can be determined so that REWSB occurs. Moreover, naturalness requires that $|\mu|$ as determined from eq. (2.8) should not be too far away from the electroweak scale, typically $|\mu| \lesssim 1$ TeV. To be more precise about the energy scale in eq. (2.8): It has been found that at the so-called SUSY-scale, defined through the geometric mean of the stop masses,

$$
M_{SUSY} = \sqrt{m_{\tilde{t}_1}m_{\tilde{t}_2}}, \tag{2.10}
$$

the scale dependence of the electroweak breaking conditions is smallest, see e. g. [33] and references therein. This minimizes most SUSY-threshold effects, because below the stop mass scale the RG running of SSB parameters is negligible. Therefore eqs. (2.8) and

(2.9) should be understood at M_{SUSY}. The μ-parameter enters in the mass matrices of charginos and neutralinos, making them more scale independent at the SUSY-scale. It is therefore convenient to define the SSB masses at M_{SUSY} [34].

2.3   SUSY seesaw model

The seesaw mechanism is an elegant and natural way to generate very light neutrino masses by the introduction of super heavy right-handed Majorana neutrinos, being singlets under the SM gauge group. A non-supersymmetric version of the seesaw mechanism would lead to a serious hierarchy problem [35]: The presence of very massive fermions, i. e. the right-handed neutrinos coupled to the Higgs field generates radiative corrections to the Higgs mass, which are proportional to the mass scale of right-handed neutrinos squared. However, in the supersymmetric framework, this problem is automatically cured by contributions of right-handed sneutrinos having similar mass as their fermionic partners.
The supersymmetric version of the seesaw mechanism is characterized by the superpotential [31]

$$\mathcal{W} = \mathcal{W}_{MSSM} + \frac{1}{2}\nu_R^c{}^T M \nu_R^c + \nu_R^c{}^T Y_\nu\, l \cdot h_2, \tag{2.11}$$

where $\mathcal{W}_{MSSM}$ is the superpotential of the MSSM. The Lagrangian for the SSB terms gets modified according to [31]

$$
\begin{aligned}
-\mathcal{L}_{soft} \;=\; & -\mathcal{L}_{soft}^{MSSM} + \left(m_{\tilde{\nu}}^2\right)_{ij}\tilde{\nu}_{R_i}^*\tilde{\nu}_{R_j} + \left(\frac{1}{2}\left(B_\nu\right)_{ij} M_{ij}\tilde{\nu}_{R_i}^*\tilde{\nu}_{R_j}^* + h.c.\right) \\
& + \left((A_\nu)_{ij}\, h_2 \tilde{\nu}_{R_i}^*\tilde{l}_{L_j} + h.c\right).
\end{aligned}
\tag{2.12}
$$

Below the mass scale of the lightest right-handed Majorana neutrino, the effective superpotential [35] is obtained by integrating out all heavy neutrino fields,

$$\mathcal{W}_{eff} = \mathcal{W}_{MSSM} + \frac{1}{2}(Y_\nu\, l \cdot h_2)^T M^{-1}(Y_\nu\, l \cdot h_2). \tag{2.13}$$

After electroweak symmetry breaking, the effective superpotential [35] leads to a mass term for the light neutrinos,

$$m_\nu = m_D^T M^{-1} m_D = Y_\nu^T M^{-1} Y_\nu \langle h_2^0 \rangle^2 \equiv \kappa \langle h_2^0 \rangle^2, \tag{2.14}$$

where $\langle h_2^0 \rangle^2 = v_2^2 \equiv v^2 \sin^2\beta$ and the neutrino Dirac mass terms are denoted by m_D. It is convenient to work in the flavor basis in which the charged lepton Yukawa matrix is diagonal, so that the symmetric matrix κ is diagonalized by the MNS matrix U,

$$U^T \kappa U = \text{Diag}(\kappa_1, \kappa_2, \kappa_3) \equiv D_\kappa, \tag{2.15}$$

being related to the light neutrino masses by

$$m_i = v_2^2 \kappa_i, \qquad i = 1, 2, 3. \tag{2.16}$$

This unitary matrix U relates flavor to mass eigenstates,

$$\begin{pmatrix} \nu_e \\ \nu_\mu \\ \nu_\tau \end{pmatrix} = U \begin{pmatrix} \nu_1 \\ \nu_2 \\ \nu_3 \end{pmatrix}. \tag{2.17}$$

If one chooses $\kappa_i \geq 0$, then U can be written in the form

$$U = V \cdot \text{Diag}(e^{-i\phi/2}, e^{-i\phi'/2}, 1), \tag{2.18}$$

where ϕ, ϕ' are Majorana phases and V can be parametrized in the standard CKM form

$$V = \begin{pmatrix} c_{13}c_{12} & c_{13}s_{12} & s_{13}e^{-i\delta} \\ -c_{23}s_{12} - s_{23}s_{13}c_{12}e^{i\delta} & c_{23}c_{12} - s_{23}s_{13}s_{12}e^{i\delta} & s_{23}c_{13} \\ s_{23}s_{12} - c_{23}s_{13}c_{12}e^{i\delta} & -s_{23}c_{12} - c_{23}s_{13}s_{12}e^{i\delta} & c_{23}c_{13} \end{pmatrix}, \tag{2.19}$$

where $c_{ij} = \cos\theta_{ij}$ and $s_{ij} = \sin\theta_{ij}$. The symmetric mass matrix M of the heavy Majorana neutrinos can be diagonalized by the unitary matrix U_M, such that

$$U_M^T M U_M = \text{Diag}(M_1, M_2, M_3) \equiv D_M \tag{2.20}$$
$$M^{-1} = U_M D_M^{-1} U_M^T. \tag{2.21}$$

Diagonalization of the seesaw relation

$$m_\nu = v_2^2 Y_\nu^T U_M D_M^{-1} U_M^T Y_\nu \tag{2.22}$$

leads to the complex orthogonal matrix R defined as [35]

$$R = \sqrt{D_M^{-1}} U_M^T Y_\nu U \sqrt{D_\kappa^{-1}}. \tag{2.23}$$

The neutrino Yukawa couplings are then expressed as [35]

$$Y_\nu = U_M^* \sqrt{D_M} R \sqrt{D_\kappa} U^\dagger. \tag{2.24}$$

The renormalization group evolution of neutrino Yukawa couplings from m_Z to the GUT-scale M_{GUT} for non-degenerate seesaw scales is summarized below, see also [36] for a top-down approach:

Below M_1, the heavy Majorana neutrinos are decoupled, so that $Y_\nu = \mathbf{0}$ and only the effective light neutrino mass matrix κ evolves, starting from the input value $\kappa(m_Z) = U^* D_\kappa U^\dagger$. At the M_1-threshold, the corresponding right-handed Majorana neutrino is integrated in, according to the seesaw formula

$$(Y_\nu)_{ij}\Big|_{M_1} \to \delta_{i1} \left(\sqrt{D_M} R \sqrt{D_\kappa} U^\dagger\right)_{ij}\Big|_{M_1}. \tag{2.25}$$

The tree-level matching condition for κ at M_1 is given by

$$(\kappa)_{ij}\Big|_{M_1} \to (\kappa)_{ij}\Big|_{M_1} - \left(Y_\nu^T\right)_{i1} \frac{1}{M_1} (Y_\nu)_{1j}\Big|_{M_1}. \tag{2.26}$$

The masses of heavy neutrinos evolve above the respective mass thresholds. For the evolution between M_1 and M_2, the input values are $\kappa|_{M_1}$, $Y_\nu|_{M_1}$ and $M_1(M_1)$, evolving to $\kappa|_{M_2}$, $Y_\nu|_{M_2}$ and $M_1(M_2)$ at the M_2-threshold. The matching at M_2 is analogous to the matching at M_1, when replacing M_1 by M_2 and indices 1 by 2, respectively,

$$(Y_\nu)_{ij}\Big|_{M_2} \quad \rightarrow \quad (Y_\nu)_{ij}\Big|_{M_2} + \delta_{i2}\left(\sqrt{D_M}R\sqrt{D_\kappa}U^\dagger\right)_{ij}\Big|_{M_2} \tag{2.27}$$

$$(\kappa)_{ij}\Big|_{M_2} \quad \rightarrow \quad (\kappa)_{ij}\Big|_{M_2} - \left(Y_\nu{}^T\right)_{i2}\frac{1}{M_2}(Y_\nu)_{2j}\Big|_{M_2}. \tag{2.28}$$

Above the M_2 threshold, the 2×2 submatrix of M obtains small off-diagonal elements, so that at the M_3 scale M has to be diagonalized by U_M. The diagonalization of M leads to the redefinition $Y_\nu \rightarrow U_M^* Y_\nu$. As has been noted in [36], the renormalization group equations (RGEs) are invariant under the transformations that diagonalize M. In the corresponding RGEs, see appendix H, U_M drops out in the combination $Y_\nu^\dagger Y_\nu$. It can also be checked that the RG equation (H.14) for M, where the combination $Y_\nu Y_\nu^\dagger$ enters, is not modified under the transformations $M \rightarrow U_M^* D_M U_M^\dagger$ and $Y_\nu \rightarrow U_M^* Y_\nu$. Therefore the matching conditions at M_3 are given by

$$(Y_\nu)_{ij}\Big|_{M_3} \quad \rightarrow \quad (U_M^* Y_\nu)_{ij}\Big|_{M_3} + \delta_{i3}\left(U_M^*\sqrt{D_M}R\sqrt{D_\kappa}U^\dagger\right)_{ij}\Big|_{M_3} \tag{2.29}$$

$$(\kappa)_{ij}\Big|_{M_3} \quad \rightarrow \quad \mathbf{0}. \tag{2.30}$$

Between M_3 and M_{GUT}, all right-handed neutrinos are active degrees of freedom, so that in principle all matrix elements of Y_ν and M evolve in this regime. It turns out however, that the off-diagonal elements of M are many orders of magnitude smaller than the diagonal entries, in all cases considered in this study. Also the corrections to the diagonal mass terms in M are at the percent level or below.

By inspection of the RGEs (H.16, H.19, H.25), one sees that the additional contributions from right-handed neutrino singlets to the SSB terms $m_{\tilde{L}}^2$, $m_{\tilde{e}}^2$ and A_e are given by

$$16\pi^2\frac{dm_{\tilde{L}}^2}{d\ln\mu} \quad = \quad m_{\tilde{L}}^2 Y_\nu^\dagger Y_\nu + Y_\nu^\dagger Y_\nu m_{\tilde{L}}^2 + 2\left(Y_\nu^\dagger m_{\tilde{\nu}}^2 Y_\nu + m_{h_2}^2 Y_\nu^\dagger Y_\nu + A_\nu^\dagger A_\nu\right) \tag{2.31}$$

$$16\pi^2\frac{dm_{\tilde{e}}^2}{d\ln\mu} \quad = \quad \mathbf{0} \tag{2.32}$$

$$16\pi^2\frac{dA_e}{d\ln\mu} \quad = \quad 2Y_e Y_\nu^\dagger A_\nu + A_e Y_\nu^\dagger Y_\nu. \tag{2.33}$$

These contributions induce lepton-flavor violating mass terms in the left-handed slepton masses through diagrams depicted in Fig. 2.3 and also in the corresponding trilinear couplings.
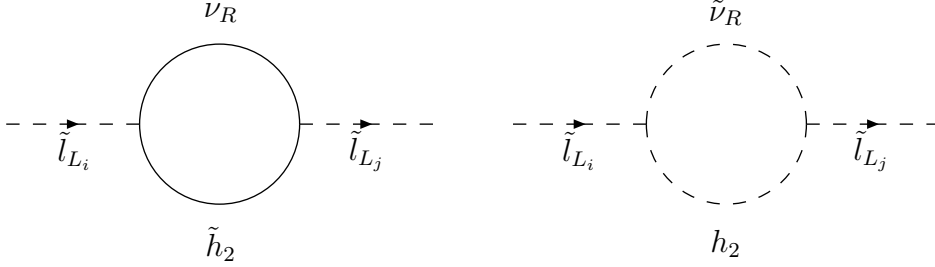
Figure 2.1: Generation of LFV mass terms for left-handed sleptons; the right diagram is the supersymmetric version of the left one and i, j are lepton flavor indices.

Parametrization of R

Requiring that the neutrino Yukawa couplings remain perturbative is equivalent to $\left|(Y_\nu)_{ij}\right| \lesssim \mathcal{O}(1)$. For $U_M = \mathbf{1}$, this corresponds to the constraint

$$\sum_{l=1}^{3} \left|R_{il} U_{jl}^*\right| \sqrt{(D_\kappa)_l} \lesssim \mathcal{O}\left(\frac{1}{\sqrt{(D_M)_i}}\right), \tag{2.34}$$

implying that either the heavy Majorana masses and/or the elements of R have to be sufficiently small. The complex orthogonal matrix R can be parametrized [35] as

$$R = \begin{pmatrix} \hat{c}_2\hat{c}_3 & -\hat{c}_1\hat{s}_3 - \hat{s}_1\hat{s}_2\hat{c}_3 & \hat{s}_1\hat{s}_3 - \hat{c}_1\hat{s}_2\hat{c}_3 \\ \hat{c}_2\hat{s}_3 & \hat{c}_1\hat{c}_3 - \hat{s}_1\hat{s}_2\hat{s}_3 & -\hat{s}_1\hat{c}_3 - \hat{c}_1\hat{s}_2\hat{s}_3 \\ \hat{s}_2 & \hat{s}_1\hat{c}_2 & \hat{c}_1\hat{c}_2 \end{pmatrix}, \tag{2.35}$$

where $\hat{c}_i \equiv \cos(x_i + iy_i)$ and $\hat{s}_i \equiv \sin(x_i + iy_i)$. In the case of imaginary angles one obtains $\cos(iy) = \cosh(y)$ and $\sin(iy) = i\sinh(y)$, demonstrating that $\left|(Y_\nu)_{ij}\right|$ is expected to be very sensitive to the imaginary parts of the angles if they are of order 1 or larger. If only one angle in R is non-vanishing, one obtains the following matrices

$$R_1 = \begin{pmatrix} 1 & 0 & 0 \\ 0 & \hat{c}_1 & -\hat{s}_1 \\ 0 & \hat{s}_1 & \hat{c}_1 \end{pmatrix} \tag{2.36}$$

$$R_2 = \begin{pmatrix} \hat{c}_2 & 0 & -\hat{s}_2 \\ 0 & 1 & 0 \\ \hat{s}_2 & 0 & \hat{c}_2 \end{pmatrix} \tag{2.37}$$

$$R_3 = \begin{pmatrix} \hat{c}_3 & -\hat{s}_3 & 0 \\ \hat{s}_3 & \hat{c}_3 & 0 \\ 0 & 0 & 1 \end{pmatrix}. \tag{2.38}$$

As we will show later, assuming relatively small values for the imaginary angles, $y_i \simeq 10^{-1}$, and setting the real angles in R to zero, can lead to successful leptogenesis. Under these assumptions, the R-matrix is approximately given by

$$R \simeq \begin{pmatrix} 1 + \frac{1}{2}\left(y_2^2 + y_3^2\right) & -iy_3 + y_1 y_2 & -iy_2 - y_1 y_3 \\ iy_3 & 1 + \frac{1}{2}\left(y_1^2 + y_3^2\right) & -iy_1 + y_2 y_3 \\ iy_2 & iy_1 & 1 + \frac{1}{2}\left(y_1^2 + y_2^2\right) \end{pmatrix}. \tag{2.39}$$

The form (2.35) of the complex orthogonal R-matrix can be obtained from the CKM parametrization (2.19) by taking the transponent matrix, neglecting the Dirac phase and using complex angles. This parametrization of R is particularly useful in the case of dominant M_3 and hierarchical κ, i. e. $D_M \simeq (0, 0, M_3), D_\kappa \simeq (0, \kappa_2, \kappa_3)$ [35]. In this limit the only non-vanishing Y_ν-elements are given by

$$(Y_\nu)_{3j} = \sqrt{M_3}\hat{c}_2 \left(\hat{s}_1 \sqrt{(D_\kappa)_2} U_{j2}^* + \hat{c}_1 \sqrt{(D_\kappa)_3} U_{j3}^* \right). \tag{2.40}$$

The authors of [35] have found that if one further assumes that the largest eigenvalue of $Y_\nu^\dagger Y_\nu$ is fixed at M_{GUT}, then the neutrino Yukawa coupling matrix only depends on the phase of $\hat{c}_2$ and the complex angle $x_1 + iy_1$ in this limit. Then the perturbativity of neutrino Yukawa couplings leads to

$$|R_{32}| \lesssim (M_3 \kappa_2)^{-\frac{1}{2}}, \qquad |R_{33}| \lesssim (M_3 \kappa_3)^{-\frac{1}{2}}, \tag{2.41}$$

using $|U_{33}| \simeq \mathcal{O}(1)$ and $|U_{22}| \simeq \mathcal{O}(1)$.
If both light and heavy neutrino states are quasi-degenerate, i. e. $M_{ij} \simeq M_R \delta_{ij}$ and $\kappa_{ij} \simeq \kappa_d \delta_{ij}$, perturbativity requires

$$\sum_{l=1}^{3} \left| R_{il} U_{jl}^* \right| \lesssim \frac{1}{\sqrt{\kappa_d M_R}}. \tag{2.42}$$

2.4   Minimal supergravity

In gravity mediated SUSY breaking, the hidden sector is connected to the MSSM sector through interactions of gravitational strength. One can assume that SUSY is broken in the hidden sector by a vacuum expectation value $\langle F_X \rangle$ of a complex scalar auxiliary field. Then the very rough approximation

$$m_{soft} \sim \frac{\langle F_X \rangle}{M_{Pl}} \tag{2.43}$$

gives the order of the soft SUSY breaking mass terms [27]. In an effective field theory the interactions between the two sectors are described by a supergravity Lagrangian with non-renormalizable terms that are suppressed by powers of the Planck scale, because the gravitational coupling is proportional to $1/M_{Pl}$. One might ask if this non-renormalizability

is reasonable. However it is due to the fact that even a renormalizable model will lose this property at least at the Planck scale where the non-renormalizable effects of gravity are included. In practice one introduces a cutoff at the Planck scale.

The non-renormalizable part of a supergravity Lagrangian [27] includes the terms

$$-\mathcal{L}_{nr} = \frac{1}{M_{Pl}}F_X\left(\frac{c_a}{2}\lambda_a\lambda_a + h.c.\right) + \frac{1}{M_{Pl}^2}F_X F_X^* k_{ij}\phi_i^*\phi_j$$
$$+\frac{1}{M_{Pl}}F_X\left(\frac{1}{6}y'_{ijk}\phi_i\phi_j\phi_k + \frac{1}{2}\mu'_{ij}\phi_i\phi_j + h.c.\right). \tag{2.44}$$

Here ϕ_i stands for scalar fields in the MSSM and λ_a denotes the gaugino fields of the MSSM. If one assumes that $\sqrt{\langle F_X\rangle} \sim 10^{10}$ GeV, then $\mathcal{L}_{nr}$ yields a soft SUSY breaking Lagrangian of the form (2.1) with dimensionless couplings c_a, k_{ij}, y'_{ijk} and mass dimension coupling μ'_{ij}.

In the special case of a "minimal" form for the normalization of kinetic terms and gauge interactions in the full, non-renormalizable Lagrangian of supergravity there is a common dimensionless $c_a = c_\lambda$ for the three gauginos and the same $k_{ij} = c_k\delta_{ij}$ for all scalars. Moreover the coupling characterized by y'_{ijk} is proportional to the trilinear term a_{ijk} in the Lagrangian eq. (2.1), $y'_{ijk} = c_y a_{ijk}$ and the mass dimension coupling is proportional to the bilinear coupling μ_{ij}, $\mu'_{ij} = c_\mu \mu_{ij}$ with universal and dimensionless constants c_y and c_μ. Then the soft terms of the MSSM can be written in terms of four parameters [27],

$$\tilde{M}_{1/2} = c_\lambda \frac{\langle F_X\rangle}{M_{Pl}}, \quad m_0^2 = c_k \frac{|\langle F_X\rangle|^2}{M_{Pl}^2}, \quad A_0 = c_y \frac{\langle F_X\rangle}{M_{Pl}}, \quad B_0 = c_\mu \frac{\langle F_X\rangle}{M_{Pl}}. \tag{2.45}$$

At the (reduced) Planck scale $M_{Pl} = (8\pi G_{\text{Newton}})^{-1/2} \approx 2.4 \cdot 10^{18}$ GeV the gaugino masses are unified, [27],
$$\tilde{M}_{1/2} = \tilde{M}_1 = \tilde{M}_2 = \tilde{M}_3 \tag{2.46}$$

and the scalar masses in the minimal form are fixed by a common scale m_0

$$m_0^2\mathbf{1} = m_{\tilde{Q}}^2 = m_{\tilde{u}}^2 = m_{\tilde{d}}^2 = m_{\tilde{L}}^2 = m_{\tilde{e}}^2 = m_{\tilde{\nu}}^2 \tag{2.47}$$
$$m_0^2 = m_{h_1}^2 = m_{h_2}^2. \tag{2.48}$$

Trilinear and bilinear parameters are given by

$$A_u = A_0 Y_u, \quad A_d = A_0 Y_d, \quad A_e = A_0 Y_e, \quad A_\nu = A_0 Y_\nu \tag{2.49}$$

and B_0, respectively.

In this framework both the scalar squared masses and the A-parameters are flavor diagonal and universal. This kind of universality relations evades unwanted FCNCs and CP-violating effects at high energy scales. The mentioned form of SSB parameters represents a set of boundary conditions for the renormalization group equations at the Planck scale. In practice, phenomenological studies often assume that the mSUGRA boundary conditions are valid at the GUT-scale M_{GUT} where gauge couplings and also gaugino masses are

unified. The existence of M_{GUT} near 10^{16} GeV is a general prediction of the two-loop RGEs in the MSSM [27]. The predictions of SUSY GUT theories between M_{GUT} and M_{Pl} on the other hand are highly model-dependent. The RG evolution of the soft parameters down to the SUSY-scale leads to the mass spectrum of the MSSM in terms of five basic parameters, namely $\tilde{M}_{1/2}, m_0^2, A_0, B_0, \mu$ (plus the gauge and Yukawa couplings of the MSSM). The model described above is called the minimal supergravity scenario for the soft SUSY breaking terms.

For the mSUGRA scenarios considered in this work, we refer to the new parameters $\tan\beta$ and $\text{sign}(\mu)$ instead of B_0 and $|\mu|$. From the conditions for REWSB, eqs. (2.8) and (2.9), one can introduce these new parameters by removing $|\mu|$ and B_0 in favor of m_Z and $\tan\beta$, however the sign of μ is not fixed in that procedure.

The presence of the neutrino Yukawa couplings at high energies above the mass scales of right-handed neutrinos modifies the RGEs of the slepton soft terms. In the leading logarithmic (LL) approximation, this leads to the additional contributions

$$\delta m_{\tilde{L}}^2 \;\simeq\; -\frac{1}{8\pi^2}\left(3m_0^2 + A_0^2\right)Y_\nu^\dagger L Y_\nu \tag{2.50}$$

$$\delta m_{\tilde{e}}^2 \;\simeq\; \mathbf{0} \tag{2.51}$$

$$\delta A_e \;\simeq\; -\frac{3A_0}{16\pi^2}Y_e Y_\nu^\dagger L Y_\nu, \tag{2.52}$$

assuming mSUGRA conditions at M_{GUT} and

$$L_{ij} = \ln\left(\frac{M_{GUT}}{M_i}\right)\delta_{ij}, \tag{2.53}$$

see also [37], [38]. Note that in (2.50) to (2.52) the Yukawa couplings are evaluated at M_{GUT} and these terms are only the leading contributions originating from right-handed neutrinos. Higher corrections of the form Y_l^4, i. e. quartic terms in the lepton Yukawa couplings have been neglected, see also [38] for the discussion of further contributions. In the SUSY seesaw model, the SSB terms for the right-handed sneutrinos, i. e. $m_{\tilde{\nu}}^2$, and trilinear terms A_ν can be neglected in the sneutrino (mass)^2 matrix, because of the dominance of the right-handed neutrino masses. The terms in eqs. (2.50) to (2.52) give rise to LFV processes such as $l_j \to l_i\gamma$ and μ-e conversion to be discussed later.

In general, the combination $Y_\nu^\dagger L Y_\nu$ entering the RGEs of left-handed sleptons reads

$$\left(Y_\nu^\dagger L Y_\nu\right)_{ij} = \left(U\sqrt{D_\kappa}R^\dagger\sqrt{D_M}U_M^T\right)_{ik}\ln\left(\frac{M_{GUT}}{M_k}\right)\left(U_M^*\sqrt{D_M}R\sqrt{D_\kappa}U^\dagger\right)_{kj}. \tag{2.54}$$

In the following, we choose a basis in which M is diagonal, so that $U_M = \mathbf{1}$. Assuming degenerate right-handed neutrinos, i. e. $M_i \equiv M_R$ at a large scale, e. g. M_{GUT}, and neglecting small radiative corrections to M and correspondingly to U_M, one can approximate

$$Y_\nu^\dagger L Y_\nu \simeq M_R \ln\left(\frac{M_{GUT}}{M_R}\right)U\sqrt{D_\kappa}R^\dagger R\sqrt{D_\kappa}U^\dagger. \tag{2.55}$$

In this case it is obvious that if the orthogonal matrix R is real, it drops out in the combination $Y_\nu^\dagger L Y_\nu$.

2.5 Gauge mediation

The basic concept of gauge mediated SUSY breaking is that chiral supermultiplet fields, so-called messengers couple both to the SUSY breaking sector and also indirectly to sparticles through $SU(3)_C \times SU(2)_L \times U(1)_Y$ gauge and gaugino interactions [27]. Gravitational strength interactions can then be neglected. The messenger fields are a set of new chiral supermultiplets containing very heavy (s)quarks and (s)leptons which transform under the SM gauge group as a real non-trivial representation. The messengers Φ_i couple at tree-level to a chiral superfield X_m by the superpotential [25]

$$\mathcal{W}_{mess} = (\lambda_m)_{ij} \, \bar{\Phi}_i X_m \Phi_j. \tag{2.56}$$

The chiral supermultiplet X_m is assumed to overlap with the goldstino field thus being in contact with the source of SUSY breaking which is left unspecified here. If the scalar component of X_m and the auxiliary F-term component of X_m obtain VEVs denoted by $\langle S \rangle$ and F_S, respectively, the masses of the scalar and fermionic messenger components are split apart, provided that $F_S \neq 0$ [25]. This effect of SUSY breaking is then communicated to the visible sector fields by radiative quantum corrections involving loops of messenger fields.

It is important to study whether GMSB spoils the unification of gauge couplings. It has been shown that if the messengers have similar masses and are in complete multiplets of $SU(5)$ GUT symmetry, then gauge coupling unification can still occur at M_{GUT} [25]. Therefore, one often assumes that messenger supermultiplets transform under $SU(5)$ in N_m copies of the fundamental representation. The unified value of gauge couplings is shifted according to

$$\delta \alpha_{GUT}^{-1} = -\frac{N_m}{2\pi} \ln \frac{M_{GUT}}{M_m}, \tag{2.57}$$

where N_m is the so-called messenger index. Requiring perturbativity of gauge couplings up to the GUT-scale then restricts the messenger index [25]

$$N_m \lesssim 150 \frac{1}{\ln \frac{M_{GUT}}{M_m}}, \tag{2.58}$$

so that $N_m \lesssim 5$ or $N_m \lesssim 10$ for $M_m = 100$ TeV or $M_m = 10^{10}$ GeV, respectively. In this work we consider only a messenger index $N_m = 1$.

Due to the gauge charges of the messenger fields under $SU(3)_C \times SU(2)_L \times U(1)_Y$, the messengers couple to gauge bosons and gauginos. Therefore gaugino masses arise at the one-loop level, see Fig. 2.2, at the messenger scale M_m [25], which is approximately $M_m \sim \langle S \rangle$ for $(\lambda_m)_{ij}$ of order 1. Positive scalar (mass)^2 terms are generated at the two-loop level, because there are no direct couplings between scalars and messengers. At M_m, the gaugino masses are given by [25],

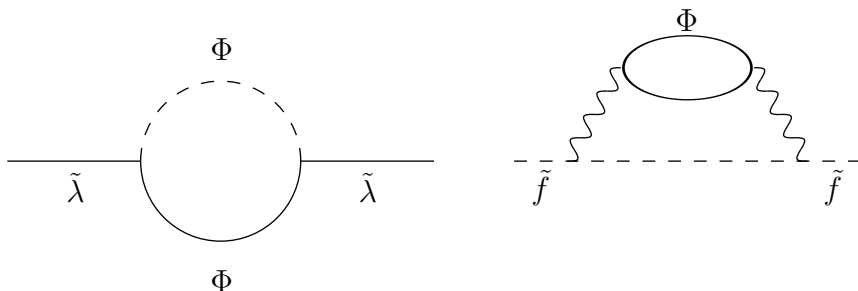$$\tilde{M}_i (M_m) = \frac{\alpha_i (M_m)}{4\pi} \frac{F_S}{M_m}. \tag{2.59}$$

Figure 2.2: Generation of gaugino masses is shown in the left diagram; the right diagram is an example of a two-loop diagram leading to scalar masses at M_m.

The gauge coupling constants are normalized such that they are all equal at the GUT-scale, so that $\frac{5}{3}\alpha_1$ enters in eq. (2.59). This also implies that for very high messenger scales close to the gauge coupling unification scale M_{GUT}, as motivated in [26], the initial value of $\tilde{M}_1$ is approximately $\tilde{M}_1(M_m) \simeq \frac{5}{3}\tilde{M}_2(M_m) \simeq \frac{5}{3}\tilde{M}_3(M_m)$, leading to a relatively heavy bino at the SUSY-scale.

The scalar SSB masses are given by [25],

$$\left(m_s^2\right)_{ij} = \frac{1}{8\pi^2}\left(c_1\alpha_1^2(M_m) + c_2\alpha_2^2(M_m) + c_3\alpha_3^2(M_m)\right)\left(\frac{F_S}{M_m}\right)^2\delta_{ij}, \qquad (2.60)$$

where the c_i denote the quadratic Casimir invariants which are given by $c_N = \frac{N^2-1}{2N}$ for $SU(N)$ groups and by $c_1 = \frac{3}{5}Y^2$ for the hypercharge $U(1)_Y$ in the normalization $Y = Q_{em} - T_3$ making use of the electromagnetic charge Q_{em} and the third component of weak isospin T_3. Due to the different couplings of scalar particles under $SU(3)_C \times SU(2)_L \times U(1)_Y$ at M_m, it is naturally expected that strongly interacting scalars become heavier than only weakly interacting sparticles. Moreover, in order to obtain a SUSY-scale near the TeV-scale, the ratio $\Lambda_m = \frac{F_S}{M_m}$, determining the size of the SSB mass terms, has to be roughly $10^4 - 10^5$ GeV [25]. MSSM gauge bosons cannot get a corresponding mass shift, because they are protected by gauge invariance [27]. Moreover, the trilinear terms A_f arise at two-loop order at M_m, suppressed by an additional factor of $\frac{\alpha_a}{4\pi}$ compared to the gaugino masses, so that they can be neglected at this scale. The bilinear B-parameter may be taken to vanish at M_m; in practice it is determined by successful REWSB [27], see eq. (2.9).

It is often claimed that for gauge mediated SUSY breaking [25] there are no new sources of flavor violation. In this class of models the SSB terms are generated at the messenger scale M_m which is a priori unrelated to the flavor scale Λ_F above which the flavor symmetry is broken.

In the case of the MSSM with flavor breaking at a very high scale $\Lambda_F \gg M_m$, the flavor

breaking is communicated to the soft terms only through Yukawa interactions. All other sources of flavor violation at the messenger scale then correspond to operators of dimension greater than 4, suppressed by powers of $\frac{1}{\Lambda_F}$. The contribution of these operators to soft masses is therefore suppressed by powers of $\frac{M_m}{\Lambda_F}$. In other words the flavor problem is naturally decoupled if flavor breaking occurs at a very high scale compared to M_m.

In the SUSY seesaw model the Λ_F-scale can be identified with the mass scale M_R of right-handed Majorana neutrinos. Below M_R, the neutrino Yukawa couplings vanish, so that for $M_R \gg M_m$ only operators suppressed by $\frac{M_m}{M_R}$ can contribute to the lepton-flavor violating soft masses. One can obtain an upper bound on M_m if one requires that gravity mediated contributions do not reintroduce large flavor violations [25]. Requiring that gravity mediated contributions of the order of $\frac{F_S}{M_{Pl}}$ are below the 0.1 percent level in the GMSB soft squared masses, leads to

$$\frac{F_S}{M_{Pl}} \lesssim \left(10^{-3} \left(\frac{\alpha}{4\pi} \right)^2 \left(\frac{F_S}{M_m} \right)^2 \right)^{1/2}, \tag{2.61}$$

being equivalent to

$$M_m \lesssim 10^{-3/2} \frac{\alpha}{4\pi} M_{Pl}. \tag{2.62}$$

Inserting the numerical value $M_{Pl} = 2.4 \cdot 10^{18}$ GeV and a value for the unified coupling constant parameter $\alpha \sim \frac{1}{24}$ gives rise to an rough upper bound on the messenger scale, $M_m \lesssim \mathcal{O}\left(10^{14}\right) - \mathcal{O}\left(10^{15}\right)$ GeV [25].

Recently, however, the authors of [26] have shown that high values of F_S in the range of $10^{17} \text{GeV}^2 \lesssim \text{F}_S \lesssim 10^{19}$ GeV^2 can be motivated in the SUSY seesaw model and it is therefore possible to obtain sizeable rates for low-energy LFV. Such high values of F_S lead to gravitino masses up to $m_{3/2} \lesssim 1$ GeV according to eq. (2.3), while e. g. for the GMSB scenarios of [39], $m_{3/2}$ is roughly in the eV-range. Therefore, the gravitino is the natural LSP in GMSB models being stable if R-parity conservation is assumed. The analysis of [40] provided a natural solution to the cosmological gravitino problem in GMSB: In the case of a gravitino LSP, thermal relics of the gravitinos tend to overclose the universe once they are thermalized in the early universe. Moreover the abundance of gravitinos is roughly proportional to the reheating temperature of the universe after inflation. Note that if the gravitino is very light, i. e. $m_{3/2} \lesssim 1$ keV, there is no cosmological gravitino problem, since in this case the gravitino does not overclose the energy density of the universe even if it is thermalized [41]. The overproduction of gravitinos can be avoided if there is a strong upper bound on the reheating temperature T_R of inflation, e. g. $T_R \lesssim 10^9$ GeV for $m_{3/2}$=1 GeV, $T_R \lesssim 10^6$ GeV for $m_{3/2}$=10 MeV or $T_R \lesssim 10^3$ GeV for $m_{3/2}$=100 keV [42]. For such low values of T_R it is very difficult for thermal leptogenesis to work, see section 3.4 for more details concerning a heavier i. e. unstable gravitino and its implications. The authors of [40] have found a solution to this problem by taking into account small mixings between the messenger supermultiplets and MSSM fields. As a result, the late-time decays of the lightest messenger provide an amount of energy sufficient to dilute the thermal relics of the gravitinos down to the observed mass density

of dark matter in the universe. It is important to mention that in this case the mass of the gravitino or the reheating temperature are not severely restricted, once gravitinos and messenger particles are thermalized in the early universe. The analysis of [40] has demonstrated that the gravitinos are indeed in thermal equilibrium at high temperatures such as $T_R \gtrsim 10^{10}$ GeV for $m_{3/2} \lesssim 1$ GeV. Therefore, in this class of GMSB models, the severe upper bound on the reheating temperature is completely evaded and thermal leptogenesis can naturally generate the baryon asymmetry of the universe.

It is a direct consequence of (2.60) that the SSB masses of singlet right-handed sneutrinos vanish at the messenger mass scale and that the masses of left-handed sleptons are equal to those of the SSB Higgs masses at M_m. Therefore the lepton-flavor violating terms are given by

$$\delta m_{\tilde{L}}^2 \quad \simeq \quad -\frac{1}{4\pi^2} \left(m_{\tilde{L}}^2 \left(M_m \right) Y_\nu^\dagger L Y_\nu \right) \tag{2.63}$$

$$\delta m_{\tilde{e}}^2 \quad \simeq \quad \mathbf{0} \tag{2.64}$$

$$\delta A_e \quad \simeq \quad \mathbf{0}, \tag{2.65}$$

in the leading logarithmic approximation, where the neutrino Yukawa couplings are evaluated at M_m. In this case, L denotes

$$L_{ij} = \ln \left(\frac{M_m}{M_i} \right) \delta_{ij}. \tag{2.66}$$

Inserting the explicit form of $m_{\tilde{L}}^2 \left(M_m \right)$ yields

$$\delta m_{\tilde{L}}^2 \simeq -\frac{1}{2 \left(4\pi^2 \right)^2} \left(\frac{3}{20} \alpha_1^2 \left(M_m \right) + \frac{3}{4} \alpha_2^2 \left(M_m \right) \right) \left(\frac{F_S}{M_m} \right)^2 Y_\nu^\dagger L Y_\nu, \tag{2.67}$$

provided that M_m is above the right-handed neutrino mass scales.

2.6   Minimal anomaly mediation

Anomaly mediated breaking of SUSY originates from the super-Weyl anomaly [23]. This can be the dominant source of SSB in a higher dimensional framework, where one extra dimension is assumed to be compactified roughly one to two orders of magnitude below the four-dimensional Planck-scale. Assuming that the SUSY breaking and visible sectors reside on different branes, and are "sufficiently separated" in the higher dimensional space [23], the gravity contributions to scalar masses are strongly suppressed.

Unfortunately, however, the anomaly contribution turns out to be negative for sleptons. From a phenomenological point of view, it suffices to add an universal contribution m_0^2 in order to cure this problem [43]. In the framework of minimal anomaly mediation of SUSY breaking, see [43] and [44], the SSB terms are determined by the parameters $m_{3/2}$,

m_0, $\tan\beta$ and $\text{sign}(\mu)$ at the GUT-scale,

$$\tilde{M}_i = \frac{1}{16\pi^2} B_i^{(1)} g_i^2 m_{3/2} \tag{2.68}$$

$$(A_f)_{ij} = -\left(\beta_{Y_f}\right)_{ij} m_{3/2} \tag{2.69}$$

$$\left(m_s^2\right)_{ij} = \frac{1}{2} \frac{d\left(\gamma_s\right)_{ij}}{d\ln\mu} m_{3/2}^2 + m_0^2 \delta_{ij}, \tag{2.70}$$

where the beta functions $\beta_P \equiv \frac{\partial P}{\partial \ln\mu}$ for the RGEs in the MSSM are defined in appendix H and the anomalous dimensions are denoted by γ_s. At M_{GUT} the trilinear couplings are multiplied by the corresponding Yukawa couplings. The coefficients for gaugino masses are $B^{(1)} = \left(\frac{33}{5}, 1, -3\right)$ in GUT normalization [43]. The pattern of the high scale values of gaugino masses yields a characteristic spectrum [43] for them at low energy,

$$\tilde{M}_1 : \tilde{M}_2 : \left|\tilde{M}_3\right| \simeq 2.8 : 1 : 8.3. \tag{2.71}$$

The mixing of gaugino and higgsino states leads to the neutralinos and charginos, as explained in appendix C. The authors of [43] have found that in the case of AMSB, successful REWSB is possible for $\tilde{M}_2 < \tilde{M}_1 < |\mu|$. This implies that the lightest neutralino and charginos consist mainly of wino states and the second lightest neutralino is bino-like. Moreover, higgsino-type states form the heavier neutralinos and chargino [43]. In much of the parameter space the triplet of winos is nearly degenerate. Note that $m_{3/2}$ is proportional to the VEV of an auxiliary field in the supergravity multiplet and is of the order of the gravitino mass [43]. The anomalous dimensions of the MSSM are given by [43] supplemented by those with additional right-handed neutrinos in [45],

$$\gamma_{h_2} = \frac{1}{16\pi^2}\left(3\left(Y_u^*\right)_{ji}\left(Y_u\right)_{ji} + \left(Y_\nu^*\right)_{ji}\left(Y_\nu\right)_{ji} - \frac{3}{2}g_2^2 - \frac{3}{10}g_1^2\right) \tag{2.72}$$

$$\gamma_{h_1} = \frac{1}{16\pi^2}\left(3\left(Y_d^*\right)_{ji}\left(Y_d\right)_{ji} + \left(Y_e^*\right)_{ji}\left(Y_e\right)_{ji} - \frac{3}{2}g_2^2 - \frac{3}{10}g_1^2\right) \tag{2.73}$$

$$\left(\gamma_{\tilde{Q}}\right)_{ij} = \frac{1}{16\pi^2}\left(\left(Y_u^*\right)_{ki}\left(Y_u\right)_{kj} + \left(Y_d^*\right)_{ki}\left(Y_d\right)_{kj} - \frac{8}{3}g_3^2 - \frac{3}{2}g_2^2 - \frac{1}{30}g_1^2\right) \tag{2.74}$$

$$\left(\gamma_{\tilde{u}}\right)_{ij} = \frac{1}{16\pi^2}\left(2\left(Y_u^*\right)_{ik}\left(Y_u\right)_{jk} - \frac{8}{3}g_3^2 - \frac{8}{15}g_1^2\right) \tag{2.75}$$

$$\left(\gamma_{\tilde{d}}\right)_{ij} = \frac{1}{16\pi^2}\left(2\left(Y_d^*\right)_{ik}\left(Y_d\right)_{jk} - \frac{8}{3}g_3^2 - \frac{2}{15}g_1^2\right) \tag{2.76}$$

$$\left(\gamma_{\tilde{L}}\right)_{ij} = \frac{1}{16\pi^2}\left(\left(Y_e^*\right)_{ki}\left(Y_e\right)_{kj} + \left(Y_\nu^*\right)_{ki}\left(Y_\nu\right)_{kj} - \frac{3}{2}g_2^2 - \frac{3}{10}g_1^2\right) \tag{2.77}$$

$$\left(\gamma_{\tilde{e}}\right)_{ij} = \frac{1}{16\pi^2}\left(2\left(Y_e^*\right)_{ik}\left(Y_e\right)_{jk} - \frac{6}{5}g_1^2\right) \tag{2.78}$$

$$\left(\gamma_{\tilde{\nu}}\right)_{ij} = \frac{1}{16\pi^2}\left(2\left(Y_\nu^*\right)_{ik}\left(Y_\nu\right)_{jk}\right). \tag{2.79}$$

This leads to the following SSB terms at the GUT-scale,

$$
\begin{aligned}
m_{h_2}^2 &= \frac{m_{3/2}^2}{32\pi^2} \left(6Re \left(Tr \left(Y_u^\dagger \beta_{Y_u} \right) \right) + 2Re \left(Tr \left(Y_\nu^\dagger \beta_{Y_\nu} \right) \right) - 3g_2 \beta_{g_2} \right. \\
&\qquad \left. - \frac{3}{5} g_1 \beta_{g_1} \right) + m_0^2
\end{aligned}
\tag{2.80}
$$

$$
\begin{aligned}
m_{h_1}^2 &= \frac{m_{3/2}^2}{32\pi^2} \left(6Re \left(Tr \left(Y_d^\dagger \beta_{Y_d} \right) \right) + 2Re \left(Tr \left(Y_e^\dagger \beta_{Y_e} \right) \right) - 3g_2 \beta_{g_2} \right. \\
&\qquad \left. - \frac{3}{5} g_1 \beta_{g_1} \right) + m_0^2
\end{aligned}
\tag{2.81}
$$

$$
\begin{aligned}
m_{\tilde{Q}}^2 &= \frac{m_{3/2}^2}{32\pi^2} \left(\beta_{Y_u}^\dagger Y_u + Y_u^\dagger \beta_{Y_u} + \beta_{Y_d}^\dagger Y_d + Y_d^\dagger \beta_{Y_d} - \frac{16}{3} g_3 \beta_{g_3} - 3g_2 \beta_{g_2} \right. \\
&\qquad \left. - \frac{1}{15} g_1 \beta_{g_1} \right) + m_0^2 \mathbf{1}
\end{aligned}
\tag{2.82}
$$

$$
m_{\tilde{u}}^2 = \frac{m_{3/2}^2}{16\pi^2} \left(\beta_{Y_u}^* Y_u^T + \left(\beta_{Y_u}^* Y_u^T \right)^\dagger - \frac{8}{3} g_3 \beta_{g_3} - \frac{8}{15} g_1 \beta_{g_1} \right) + m_0^2 \mathbf{1}
\tag{2.83}
$$

$$
m_{\tilde{d}}^2 = \frac{m_{3/2}^2}{16\pi^2} \left(\beta_{Y_d}^* Y_d^T + \left(\beta_{Y_d}^* Y_d^T \right)^\dagger - \frac{8}{3} g_3 \beta_{g_3} - \frac{2}{15} g_1 \beta_{g_1} \right) + m_0^2 \mathbf{1}
\tag{2.84}
$$

$$
m_{\tilde{L}}^2 = \frac{m_{3/2}^2}{32\pi^2} \left(\beta_{Y_e}^\dagger Y_e + Y_e^\dagger \beta_{Y_e} + \beta_{Y_\nu}^\dagger Y_\nu + Y_\nu^\dagger \beta_{Y_\nu} - 3g_2 \beta_{g_2} - \frac{3}{5} g_1 \beta_{g_1} \right) + m_0^2 \mathbf{1}
\tag{2.85}
$$

$$
m_{\tilde{e}}^2 = \frac{m_{3/2}^2}{16\pi^2} \left(\beta_{Y_e}^* Y_e^T + \left(\beta_{Y_e}^* Y_e^T \right)^\dagger - \frac{6}{5} g_1 \beta_{g_1} \right) + m_0^2 \mathbf{1}
\tag{2.86}
$$

$$
m_{\tilde{\nu}}^2 = \frac{m_{3/2}^2}{16\pi^2} \left(\beta_{Y_\nu}^* Y_\nu^T + \left(\beta_{Y_\nu}^* Y_\nu^T \right)^\dagger \right) + m_0^2 \mathbf{1}.
\tag{2.87}
$$

These values can be used to obtain the leading logarithmic corrections to the RGEs due to the presence of right-handed neutrinos,

$$
\delta m_{\tilde{L}}^2 \simeq -\frac{1}{8\pi^2} \left(3m_0^2 Y_\nu^\dagger L Y_\nu + m_{3/2}^2 \beta_{Y_\nu}^\dagger L \beta_{Y_\nu} \right)
\tag{2.88}
$$

$$
\delta m_{\tilde{e}}^2 \simeq \mathbf{0}
\tag{2.89}
$$

$$
\delta A_e \simeq \frac{m_{3/2}}{16\pi^2} \left(2Y_e Y_\nu^\dagger L \beta_{Y_\nu} + \beta_{Y_e} Y_\nu^\dagger L Y_\nu \right),
\tag{2.90}
$$

where

$$
L_{ij} = \ln \left(\frac{M_{GUT}}{M_i} \right) \delta_{ij}.
\tag{2.91}
$$

Note that these terms are only the leading contributions originating from right-handed neutrinos. Higher corrections involving additional Yukawa or gauge couplings have been neglected in eqs. (2.88) to (2.90). The lepton-flavor violating terms $\delta m_{\tilde{L}}^2$ in eq. (2.88)

consist of a part proportional to m_0^2 analogous to the mSUGRA case, supplemented by a new contribution proportional to $m_{3/2}^2$. This additional term is proportional to the combination $\beta_{Y_\nu}^\dagger \beta_{Y_\nu}$ of neutrino RGE beta functions assuming degenerate Majorana masses, $M_i \equiv M_R$. Making use of the explicit form of β_{Y_ν} given in eq. (H.9), and keeping only the dominant terms involving Yukawa couplings of up-type quarks or neutrinos, one obtains

$$\beta_{Y_\nu} \simeq \frac{1}{16\pi^2} Y_\nu \left(3Tr \left(Y_u^\dagger Y_u \right) \mathbf{1} + Tr \left(Y_\nu^\dagger Y_\nu \right) \mathbf{1} + 3Y_\nu^\dagger Y_\nu \right). \tag{2.92}$$

Assuming small neutrino Yukawa couplings as compared to the top Yukawa coupling Y_t leads to the approximation

$$m_{3/2}^2 \beta_{Y_\nu}^\dagger \beta_{Y_\nu} \simeq \frac{9m_{3/2}^2}{\left(16\pi^2\right)^2} \left| Y_t \right|^4 Y_\nu^\dagger Y_\nu. \tag{2.93}$$

If the neutrino Yukawa couplings are of similar size as the top Yukawa coupling, additional terms in $\beta_{Y_\nu}^\dagger \beta_{Y_\nu}$ involving more than two factors of Y_ν become important and may enhance or weaken the effect of the $m_{3/2}^2$ contribution in eq. (2.88). Inserting numerical values of the AMSB scenario considered in section 4, i. e. $m_0 = 450$ GeV and $m_{3/2} = 60$ TeV shows that the contribution from $m_{3/2}^2$ to $\delta m_{\tilde{L}}^2$ is expected to be slightly smaller than the m_0^2 contribution under the assumption of large top Yukawa coupling as compared to neutrino Yukawa couplings.

2.7 Minimal gaugino mediation

In this model of SUSY breaking, the chiral supermultiplets of the observable sector reside on a matter brane, whereas the SUSY breaking sector is confined to a different brane [24]. Gravity and gauge superfields propagate in the bulk, and hence, directly couple to fields on both of the branes. As a result of their direct coupling to the SUSY breaking brane, gauginos acquire a mass. However the SUSY breaking parameters for scalar masses, trilinear couplings or the B-parameter only arise from their interactions with gauginos or gravity. In minimal gaugino mediation [46] (see also [24]), the success of the unification of gauge couplings is preserved by assuming that there is a $SU(5)$ or $SO(10)$ SUSY GUT between M_{GUT} and the compactification scale M_C. At the compactification scale M_C the higher dimensional theory is matched to the effective four-dimensional theory. In order to preserve the successful prediction of $\sin^2 \theta_W$ from gauge coupling unification in the MSSM, M_C is limited to $M_C > M_{GUT}$. On the other hand, the scale M_C is restricted to be $M_C \lesssim \frac{M_{Pl}}{10}$, in order to suppress flavor violating soft masses. Otherwise the flavor violating couplings of heavy bulk fields would lead to unwanted large FCNCs. Note that in minimal gaugino mediation the RGEs of the soft terms mainly depend on gauge couplings and gaugino masses, the dependence on other soft masses through gauge/Yukawa couplings above M_{GUT} is loop-suppressed. In its minimal form gaugino mediation has basically two free parameters, the unified gaugino masses at M_C and the compactification scale, plus the sign of the μ-parameter. The Higgs masses are assumed

to be zero at M_C and $\tan\beta$ can be determined by requiring that $B = 0$ at M_C, see [46]. The size of the μ-parameter is fixed by requiring correct electroweak symmetry breaking at the weak scale. In the gaugino mediation framework [46], the SSB-terms vanish at the compactification scale M_C, $M_{GUT} \leq M_C \leq \frac{M_{Pl}}{10}$:

$$m_0^2|_{M_C} = A_0|_{M_C} = \mathbf{0}, \tag{2.94}$$

whereas the common gaugino mass takes a value

$$\tilde{M}_{1/2}|_{M_C} = \tilde{M}_{1/2}^0. \tag{2.95}$$

Between the scales of M_C and M_{GUT}, the unified gauge coupling g_{GUT}^2 and the common gaugino mass $\tilde{M}_{1/2}$ evolve in the same way [46],

$$\frac{d}{dt}\frac{1}{g_{GUT}^2} = -2b_{GUT} \tag{2.96}$$

$$\frac{d}{dt}\frac{\tilde{M}_{1/2}}{g_{GUT}^2} = 0, \tag{2.97}$$

where

$$t = \frac{1}{16\pi^2}\ln\left(\frac{\mu}{M_{GUT}}\right). \tag{2.98}$$

We will consider a SUSY $SU(5)$ GUT with additional right-handed neutrino singlets, in which case $b_{GUT} = -3$. This model [37] has three families of matter multiplets T_i, F_i and $\nu_{R_i}^c$, which are $\mathbf{10}$, $\mathbf{5^*}$ and $\mathbf{1}$ dimension representations of $SU(5)$, respectively. T_i contains the quark doublet, the charged lepton singlet and the up-type quark singlet, while the down-type quark singlet and the lepton doublet are embedded in F_i. Moreover the model has $\mathbf{5}$ and $\mathbf{5^*}$ dimension representations of Higgs multiplets, H and $\overline{H}$. H consists of the MSSM Higgs multiplet h_2 and a colored Higgs multiplet. The other MSSM Higgs multiplet h_1 and another colored Higgs multiplet constitute $\overline{H}$. This model is characterized by the superpotential [37]

$$\begin{aligned}\mathcal{W}^{SU(5)RN} &= \frac{1}{4}(Y_u)_{ij}T_i^{AB}T_j^{CD}H^E\epsilon_{ABCDE} + \sqrt{2}(Y_d)_{ij}T_i^{AB}F_{j_A}\overline{H}_B \\ &\quad + (Y_\nu)_{ij}\nu_{R_i}^c F_{j_A}H^A + \frac{1}{2}M_{ij}\nu_{R_i}^c\nu_{R_j}^c,\end{aligned} \tag{2.99}$$

where $SU(5)$ indices are in capital letters. GUT Higgs sector self-couplings as well as GUT Higgs superpotential mass terms are neglected, see [47] for a general analysis of SUSY $SU(5)$ RGEs and [48] for a more general approach to SUSY $SU(5)$ GUT with additional right-handed neutrino singlets. The additional terms of the Higgs sector are not relevant in the minimal gaugino mediation framework for the study of SSB masses.

The Lagrangian for the soft terms is then given by [37]

$$
\begin{aligned}
-\mathcal{L}_{soft}^{SU(5)RN} &= \left(m_{10}^2\right)_{ij} \tilde{T}_i^\dagger \tilde{T}_j + \left(m_{\bar{5}}^2\right)_{ij} \tilde{F}_i^\dagger \tilde{F}_j + \left(m_\nu^2\right)_{ij} \tilde{\nu}_{R_i}^* \tilde{\nu}_{R_j} + m_h^2 h^\dagger h + m_{\bar{h}}^2 \bar{h}^\dagger \bar{h} \\
&\quad + \left(\frac{1}{4} (A_u Y_u)_{ij} \tilde{T}_i \tilde{T}_j h + \sqrt{2} (A_d Y_d)_{ij} \tilde{T}_i \tilde{F}_j \bar{h} + (A_\nu Y_\nu)_{ij} \tilde{\nu}_{R_i}^* \tilde{F}_j h + h.c. \right) \\
&\quad + \frac{1}{2} \left(\tilde{M}_{1/2} \lambda_L \lambda_L + h.c. \right),
\end{aligned}
\tag{2.100}
$$

where $SU(5)$ indices have been dropped. In accordance with the work [46] on $\tilde{G}$MSB, we define the trilinear couplings such that they multiply the Yukawa couplings in the Lagrangian. Moreover, we do not assume lepton-down quark Yukawa unification, see e. g. [49] for more comments on this point. In the case of minimal $\tilde{G}$MSB, the RGEs of non-gaugino soft terms read

$$
\frac{dm_{10}^2}{dt} = \frac{3}{2}\frac{dm_{\bar{5}}^2}{dt} = \frac{3}{2}\frac{dm_{\bar{5}}^2}{dt} = -\frac{144}{5} g_{GUT}^2 \tilde{M}_{1/2}^2 \mathbf{1}
\tag{2.101}
$$

$$
\frac{dm_\nu^2}{dt} = \mathbf{0}
\tag{2.102}
$$

$$
\frac{3}{2}\frac{dm_{h_1}^2}{dt} = \frac{3}{2}\frac{dm_{h_2}^2}{dt} = -\frac{144}{5} g_{GUT}^2 \tilde{M}_{1/2}^2
\tag{2.103}
$$

$$
\frac{dA_u}{dt} = \frac{8}{7}\frac{dA_d}{dt} = 2\frac{dA_\nu}{dt} = \frac{192}{5} g_{GUT}^2 \tilde{M}_{1/2} \mathbf{1}.
\tag{2.104}
$$

Note that this convention [46] for the sign of the terms proportional to the gaugino masses in the RGEs of trilinear A parameters is consistent with [50], however different from [37]. The analytic solutions to the RGEs in eqs. (2.101) to (2.104) are obtained by first calculating the scale dependence of gauge couplings above the GUT-scale from eq. (2.96),

$$
g^2(t) = \frac{4\pi \alpha_{GUT}}{1 - 8\pi b_{GUT} \alpha_{GUT} t}.
\tag{2.105}
$$

It follows from eq. (2.97) that

$$
\tilde{M}_{1/2}(t) = \frac{\tilde{M}_{1/2}\left(M_{GUT}\right)}{g^2\left(M_{GUT}\right)} g^2(t).
\tag{2.106}
$$

Then the scale dependence of gauge couplings and gaugino masses between M_C and M_{GUT} is known and the solutions to the RGEs in eqs. (2.101) to (2.104) are obtained by analytic integration from M_C to M_{GUT}, as has also been mentioned in [46].

Evolving the RGEs of $SU(5)$ with additional right-handed neutrinos from M_C to M_{GUT} yields the following values of the SSB-terms at M_{GUT}

$$
m_{10}^2 = \frac{3}{2}m_{\bar{5}}^2 = \frac{3}{2}m_{\bar{5}}^2 = \frac{144}{5} \tilde{M}_{1/2}^2 S_2 \mathbf{1}
\tag{2.107}
$$

$$
A_u = \frac{8}{7}A_d = 2A_\nu = -\frac{192}{5} \tilde{M}_{1/2} S_1 \mathbf{1}
\tag{2.108}
$$

$$
m_\nu^2 = \mathbf{0},
\tag{2.109}
$$

where from the RGE solution of gauge couplings and gaugino masses, the analytic solutions

$$S_1 = \frac{\alpha_{GUT}}{4\pi} \ln \frac{M_C}{M_{GUT}} \frac{1}{1 - (2\pi)^{-1}b_{GUT}\alpha_{GUT} \ln \frac{M_C}{M_{GUT}}} \tag{2.110}$$

$$S_2 = \frac{\alpha_{GUT}}{4\pi} \ln \frac{M_C}{M_{GUT}} \frac{1 - (4\pi)^{-1}b_{GUT}\alpha_{GUT} \ln \frac{M_C}{M_{GUT}}}{\left(1 - (2\pi)^{-1}b_{GUT}\alpha_{GUT} \ln \frac{M_C}{M_{GUT}}\right)^2} \tag{2.111}$$

have been determined, as explained before.
In generation space, the following relations at the GUT-scale hold

$$m_{10}^2 = m_{\tilde{Q}}^2 = \left(m_{\tilde{e}}^2\right)^T = \left(m_{\tilde{u}}^2\right)^T \tag{2.112}$$

$$m_{\bar{5}}^2 = m_{\tilde{L}}^2 = \left(m_{\tilde{d}}^2\right) = m_{h_1}^2 \mathbf{1} = m_{h_2}^2 \mathbf{1} \tag{2.113}$$

$$A_e = A_d^T, \tag{2.114}$$

see also [51]. The relevant leading logarithmic contributions from right-handed neutrinos are then given by

$$\delta m_{\tilde{L}}^2 = -\frac{1}{8\pi^2} \left(2m_{\bar{5}}^2 Y_\nu^\dagger L Y_\nu + |A_\nu(M_{GUT})|^2 Y_\nu^\dagger L Y_\nu\right) \tag{2.115}$$

$$\delta m_{\tilde{e}}^2 = \mathbf{0} \tag{2.116}$$

$$\delta A_e = -\frac{1}{16\pi^2} \left(2Y_e Y_\nu^\dagger L A_\nu + A_e Y_\nu^\dagger L Y_\nu\right), \tag{2.117}$$

where

$$L_{ij} = \ln\left(\frac{M_{GUT}}{M_i}\right)\delta_{ij} \tag{2.118}$$

and the terms are evaluated at the M_{GUT} scale. Eqs. (2.115) and (2.117) can be written in terms of $\tilde{G}$MSB parameters, resulting in

$$\delta m_{\tilde{L}}^2 = -\frac{1}{8\pi^2}\tilde{M}_{1/2}^2\left(\frac{576}{15}S_2(t_C) + \left(\frac{96}{5}\right)^2 S_1^2(t_C)\right)Y_\nu^\dagger L Y_\nu \tag{2.119}$$

$$\delta A_e = \frac{9}{2\pi^2}\tilde{M}_{1/2}S_1(t_C)Y_e Y_\nu^\dagger L Y_\nu. \tag{2.120}$$

Chapter 3

Phenomenological implications

In this chapter analytical results and useful approximations for both radiative leptonic processes at low energies and the parameters of leptogenesis are discussed. The dependence on the relevant parameters is analyzed and relations between observables in different processes are outlined.

3.1 Lepton-flavor violating radiative decays $l_j \to l_i \gamma$

The effective Lagrangian for the decay $l_j^- \to l_i^- \gamma$ can be written in the form [38]

$$\mathcal{L}_{eff} = -\frac{e}{2} m_{l_j} \bar{l}_i \sigma^{\alpha\beta} F_{\alpha\beta} \left(A_L^{ij} P_L + A_R^{ij} P_R \right) l_j, \tag{3.1}$$

where $F^{\alpha\beta}$ is the electromagnetic field strength tensor, $\sigma_{\alpha\beta} = \frac{i}{2} [\gamma_\alpha, \gamma_\beta]$, i and j are flavor indices and $P_{R,L} = \frac{1}{2}(1 \pm \gamma_5)$ are the chiral projection operators. Eq. (3.1) has the form of an electromagnetic dipole operator. The electric and magnetic dipole operators couple left-handed and right-handed leptons, thus requiring a chirality flip which can be diagrammatically depicted by a mass insertion [37].
The amplitude for the $l_j^- \to l_i^- \gamma$ transition can be written as [31]

$$\mathcal{M}^{ij} = e m_{l_j} \bar{u}_i(p') i \epsilon_\alpha^* \sigma^{\alpha\beta} q_\beta \left(A_L^{ij} P_L + A_R^{ij} P_R \right) u_j(p). \tag{3.2}$$

In the limit of a massless final lepton, $m_{l_i} = 0$, the decay rate [31] is

$$\Gamma^{ij} = \frac{e^2}{16\pi} m_{l_j}^5 \left(\left| A_L^{ij} \right|^2 + \left| A_R^{ij} \right|^2 \right), \tag{3.3}$$

whereas for non-vanishing lepton masses the decay rate is determined as [52]

$$\Gamma^{ij} = \frac{e^2}{16\pi} \frac{\left(m_{l_j}^2 - m_{l_i}^2 \right)^3}{m_{l_j}} \left(\left| A_L^{ij} \right|^2 + \left| A_R^{ij} \right|^2 \right). \tag{3.4}$$

We show exact analytical one-loop expressions for A_L^{ij} and A_R^{ij} in appendix F, taking into account all leptonic masses, see eqs. (F.33) and (F.34). If the mass of the lighter lepton is neglected and the mass of l_j is neglected in the loop integrals, the well-known results [31] for the coefficients A_L^{ij} and A_R^{ij} are obtained,

$$
\begin{aligned}
A_L^{ij} &= \frac{1}{32\pi^2} \frac{1}{m_{\tilde{l}_x}^2} \left(N_{iax}^{L(l)} N_{jax}^{L(l)*} \frac{1 - 6r_{ax}^N + 3\left(r_{ax}^N\right)^2 + 2\left(r_{ax}^N\right)^3 - 6\left(r_{ax}^N\right)^2 \ln r_{ax}^N}{6\left(1 - r_{ax}^N\right)^4} \right. \\
&\quad \left. + \frac{m_{\tilde{\chi}_a^0}}{m_{l_j}} N_{iax}^{L(l)} N_{jax}^{R(l)*} \frac{1 - \left(r_{ax}^N\right)^2 + 2r_{ax}^N \ln r_{ax}^N}{\left(1 - r_{ax}^N\right)^3} \right) \\
&\quad - \frac{1}{32\pi^2} \frac{1}{m_{\tilde{\nu}_x}^2} \left(C_{iax}^{L(l)} C_{jax}^{L(l)*} \frac{2 + 3r_{ax}^C - 6\left(r_{ax}^C\right)^2 + \left(r_{ax}^C\right)^3 + 6r_{ax}^C \ln r_{ax}^C}{6\left(1 - r_{ax}^C\right)^4} \right. \\
&\quad \left. + \frac{m_{\tilde{\chi}_a^-}}{m_{l_j}} C_{iax}^{L(l)} C_{jax}^{R(l)*} \frac{-3 + 4r_{ax}^C - \left(r_{ax}^C\right)^2 - 2\ln r_{ax}^C}{\left(1 - r_{ax}^C\right)^3} \right)
\end{aligned}
\tag{3.5}
$$

$$
A_R^{ij} = A_L^{ij}\big|_{L \leftrightarrow R}
\tag{3.6}
$$

$$
r_{ax}^N = \frac{m_{\tilde{\chi}_a^0}^2}{m_{\tilde{l}_x}^2}, \qquad r_{ax}^C = \frac{m_{\tilde{\chi}_a^-}^2}{m_{\tilde{\nu}_x}^2},
\tag{3.7}
$$

where a summation over x and a indices is understood.

It should be noted that the decay rate for the charge conjugated mode, i. e. $l_j^+ \to l_i^+ \gamma$ is exactly as eq. (3.4) at the one-loop level. More precisely, in the decay $l_j^+ \to l_i^+ \gamma$ the coefficients $A_{L,R}$ are complex conjugated with respect to $l_j^- \to l_i^- \gamma$. This can be seen if one considers the effective Lagrangian for $l_j^+ \to l_i^+ \gamma$ [51],

$$
\mathcal{L}'_{eff} = -\frac{e}{2} m_{l_j} \bar{l}_j \sigma^{\alpha\beta} F_{\alpha\beta} \left(A_R^{ij\prime} P_L + A_L^{ij\prime} P_R \right) l_i.
\tag{3.8}
$$

By comparing L_{eff} with $L'^{\dagger}_{eff}$, one finds $A_{L,R} = A'^*_{L,R}$ using Dirac algebra, see appendix D. Eq. (3.3) or (3.4) then imply that at the one-loop level, there is no CP violation in the decays $Br\left(l_j^\pm \to l_i^\pm \gamma\right)$ [51, 38].

The polarization P_{l_i} $(-1 \leq P_{l_i} \leq 1)$ of the outgoing lepton with respect to the polarization direction of the incoming lepton P_{l_j} depends on the relative magnitudes of the coefficients A_L^{ij} and A_R^{ij}. The angular distribution shows a $\left(1 + A_{LR} P_{l_j} \cos\theta_i\right)$ dependence [53], see also [51] and [35], where

$$
A_{LR} = \frac{\left|A_L^{ij}\right|^2 - \left|A_R^{ij}\right|^2}{\left|A_L^{ij}\right|^2 + \left|A_R^{ij}\right|^2},
\tag{3.9}
$$

and θ_i is defined as the angle between the momentum of the outgoing lepton and the spin polarization direction of the incoming lepton. Neglecting the mass m_{l_i} of the outgoing lepton in the coefficients A_R^{ij} in eq. (F.34) and A_L^{ij} in eq. (F.33), one can see the dominance of A_R^{ij} over A_L^{ij} as follows: The chargino vertex factors $C_{iax}^{R(l)}$ eq. (B.7) and $C_{iax}^{L(l)}$ eq. (B.8),
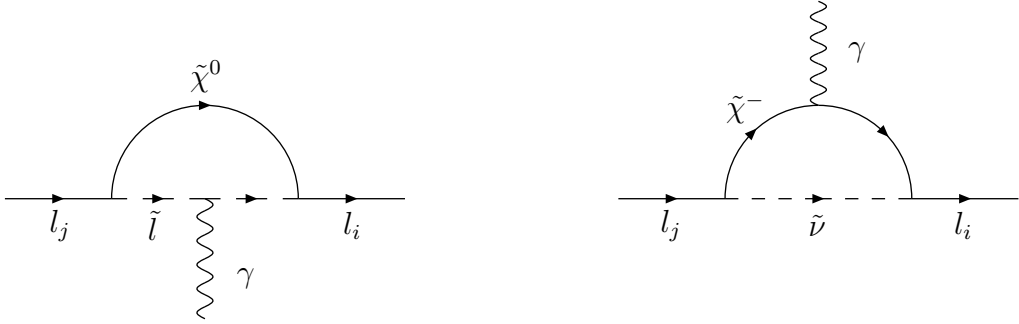
Figure 3.1: Diagrams for $l_j^- \to l_i^- \gamma$ in the MSSM
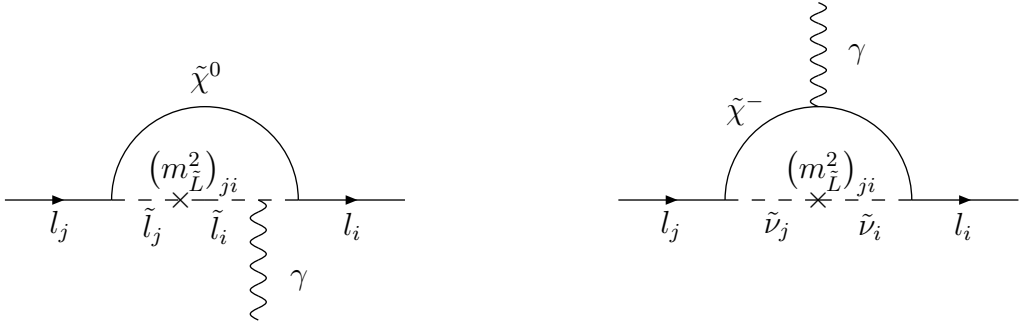
Figure 3.2: Dominant diagrams for $l_j^- \to l_i^- \gamma$ in the mass-insertion approximation.

where $C_{iax}^{R(l)} \gg C_{iax}^{L(l)}$ appear mainly in A_R^{ij} and A_L^{ij}, respectively. Likewise, for neutralino vertex factors in A_R^{ij} and A_L^{ij} one expects $N_{iax}^{R(l)} \gg N_{iax}^{L(l)}$, taking into account eqs. (B.13) and (B.14) and the fact that lepton-flavor violating slepton mixing arises dominantly in the left-handed slepton sector in the SUSY seesaw model. Therefore, in the SUSY seesaw model the relation $A_L^{ij} \ll A_R^{ij}$ is predicted, implying a characteristic $\left(1 - P_{l_j} \cos\theta_i\right)$ distribution for l_i. It is interesting to note that this angular distribution is expected to be different in SUSY $SU(5)$ or $SO(10)$ models [51]: In the $SU(5)$ GUT model, lepton-flavor violating terms arise in the right-handed slepton sector through the mixing of quark doublets and lepton singlets in the **5** representation. In the case of a $SO(10)$ GUT symmetry, all matter multiplets are embedded in the **16** representation, so that quark mixing and also lepton mixing induces lepton-flavor violating terms in the left-handed and right-handed part of the charged slepton mass matrix. These different mixing patterns provide a possibility to distinguish between the seesaw model and GUT based approaches by measuring the angular distribution of l_i.

It should be emphasized that in the SM with additional massive neutrinos, the branching ratios for $Br\left(l_j \to l_i\gamma\right)$ are extremely small and cannot be expected to be observed, see

[17] and [54]. For example, $Br\left(\mu \to e\gamma\right)$ would be many orders of magnitude below any planned experimental sensitivity due to the tiny neutrino masses compared to the W-boson mass and due to the very small admixture of heavy Majorana neutrinos in the light neutrino eigenstates.

In the mass insertion approximation, the branching ratio $Br\left(l_j \to l_i\gamma\right)$ is estimated [31], [35] as

$$Br\left(l_j \to l_i\gamma\right) \sim \frac{\alpha^3 \tan^2\beta}{\tilde{m}^8} \frac{m_{l_j}^5}{\Gamma_j} \left|\left(\delta m_{\tilde{L}}^2\right)_{ji}\right|^2, \tag{3.10}$$

see also Fig. 3.2. This implies the following pattern for branching ratios,

$$\frac{Br\left(l_j \to l_i\gamma\right)}{Br\left(l_{j'} \to l_{i'}\gamma\right)} \sim \frac{m_{l_j}^5 \Gamma_{j'}}{m_{l_j'}^5 \Gamma_j} \frac{\left|\left(\delta m_{\tilde{L}}^2\right)_{ji}\right|^2}{\left|\left(\delta m_{\tilde{L}}^2\right)_{j'i'}\right|^2}. \tag{3.11}$$

The mass $\tilde{m}$ in eq. (3.10) denotes the typical mass scale of the sleptons in the loop.

As the RG induced mass terms in the slepton mass matrices $\left(\delta m_{\tilde{L}}^2\right)_{ji}$ are proportional to $\left(Y_\nu^\dagger L Y_\nu\right)_{ji}$, we show some approximate results for $Y_\nu^\dagger L Y_\nu$ that will be useful for later discussion:

Under the assumption of real R and degenerate $M_i \equiv M_R$, i. e. $L_{ij} = \ln\frac{M_{GUT}}{M_R}\delta_{ij}$, one obtains

$$\left(Y_\nu^\dagger L Y_\nu\right)_{ji} \approx \frac{M_R}{v^2 \sin^2\beta} \ln\frac{M_{GUT}}{M_R} \left(m_1 U_{j1} U_{i1}^* + m_2 U_{j2} U_{i2}^* + m_3 U_{j3} U_{i3}^*\right). \tag{3.12}$$

Assuming in addition hierarchical light neutrinos, i. e. $m_1 \ll m_2 \ll m_3$, leads to [55]

$$\left(Y_\nu^\dagger L Y_\nu\right)_{ji} \approx \frac{M_R}{v^2 \sin^2\beta} \ln\frac{M_{GUT}}{M_R} \left(\sqrt{\Delta m_{21}^2} U_{j2} U_{i2}^* + \sqrt{\Delta m_{31}^2} U_{j3} U_{i3}^*\right). \tag{3.13}$$

On the other hand, in the case of quasi-degenerate light neutrinos one has $m_1 \gg \sqrt{\Delta m_{21}^2}$, $\sqrt{\Delta m_{31}^2}$ or, more specifically $m_2 \approx m_1 + \frac{1}{2m_1}\Delta m_{21}^2, m_3 \approx m_1 + \frac{1}{2m_1}\Delta m_{31}^2$, so that one can derive [55]

$$\left(Y_\nu^\dagger L Y_\nu\right)_{ji} \approx \frac{M_R}{v^2 \sin^2\beta} \ln\frac{M_{GUT}}{M_R} \left(m_1\delta_{ji} + \left(\frac{\Delta m_{21}^2}{2m_1}U_{j2}U_{i2}^* + \frac{\Delta m_{31}^2}{2m_1}U_{j3}U_{i3}^*\right)\right). \tag{3.14}$$

Assuming $R = \mathbf{1}$ and non-degenerate heavy neutrinos leads to

$$\left(Y_\nu^\dagger L Y_\nu\right)_{ji} \approx \frac{1}{v^2 \sin^2\beta} \sum_{k=1}^{3} m_k M_k \ln\frac{M_{GUT}}{M_k} U_{jk} U_{ik}^*. \tag{3.15}$$

In the limit of $y_1 = y_2 = y_3 \equiv y \ll 1$, degenerate $M_i \equiv M_R$ and $\kappa_1 = 0$, $x_i = 0$, $\delta = \varphi_1 = \varphi_2 = 0$ we obtain

$$\begin{aligned}\left(Y_\nu^\dagger L Y_\nu\right)_{ji} \simeq\ & M_R \ln\frac{M_{GUT}}{M_R} \left(\kappa_2 U_{j2} U_{i2}^* \left(1 + 4y^2\right) + \sqrt{\kappa_2\kappa_3} U_{j2} U_{i3}^* \left(2y^2 - 2iy\right)\right.\\ & \left.+ \sqrt{\kappa_2\kappa_3} U_{j3} U_{i2}^* \left(2y^2 + 2iy\right) + \kappa_3 U_{j3} U_{i3}^* \left(1 + 4y^2\right)\right). \end{aligned} \tag{3.16}$$

The quantity relevant for the decay rates is $\left|\left(Y_\nu^\dagger L Y_\nu\right)_{ji}\right|^2$ which in this case can be evaluated to be

$$
\begin{aligned}
\left|\left(Y_\nu^\dagger L Y_\nu\right)_{ji}\right|^2 \simeq\ & M_R^2\left(\ln\frac{M_{GUT}}{M_R}\right)^2\left(\left|\kappa_2 U_{j2}U_{i2}^* + \kappa_3 U_{j3}U_{i3}^*\right|^2\left(1+8y^2\right)\right. \\
& +4\kappa_2\kappa_3\left(\left|U_{j2}U_{i3}^*\right|^2 + \left|U_{j3}U_{i2}^*\right|^2\right)y^2 \\
& +4\sqrt{\kappa_2\kappa_3}Re\left(\left(\kappa_2 U_{j2}U_{i2}^* + \kappa_3 U_{j3}U_{i3}^*\right)U_{j2}^*U_{i3}\left(y^2+iy\right)\right) \\
& +4\sqrt{\kappa_2\kappa_3}Re\left(\left(\kappa_2 U_{j2}U_{i2}^* + \kappa_3 U_{j3}U_{i3}^*\right)U_{j3}^*U_{i2}\left(y^2-iy\right)\right) \\
& \left.-8\kappa_2\kappa_3 Re\left(U_{j2}U_{i3}^*U_{j3}^*U_{i2}\right)y^2\right).
\end{aligned}
\tag{3.17}
$$

Another interesting limit is given by non-degenerate M_i and real R, so that the dependence on the real mixing angles in R becomes important. For $\kappa_1 = 0$ and $y_i = 0$, we obtain

$$
\begin{aligned}
\left(Y_\nu^\dagger L Y_\nu\right)_{ji} \simeq\ & \kappa_2 U_{j2}U_{i2}^*\left(R^T D_M L R\right)_{22} + \kappa_3 U_{j3}U_{i3}^*\left(R^T D_M L R\right)_{33} \\
& +\sqrt{\kappa_2\kappa_3}\left(R^T D_M L R\right)_{23}\left(U_{j2}U_{i3}^* + U_{j3}U_{i2}^*\right).
\end{aligned}
\tag{3.18}
$$

If only x_1 is non-vanishing (cf. (2.36)), the relevant terms $\left(R^T D_M L R\right)$ in eq. (3.18) are given by

$$
\left(R^T D_M L R\right)_{22} = M_2\ln\frac{M_{GUT}}{M_2}c_1^2 + M_3\ln\frac{M_{GUT}}{M_3}s_1^2
\tag{3.19}
$$

$$
\left(R^T D_M L R\right)_{23} = -M_2\ln\frac{M_{GUT}}{M_2}s_1c_1 + M_3\ln\frac{M_{GUT}}{M_3}s_1c_1
\tag{3.20}
$$

$$
\left(R^T D_M L R\right)_{33} = M_2\ln\frac{M_{GUT}}{M_2}s_1^2 + M_3\ln\frac{M_{GUT}}{M_3}c_1^2.
\tag{3.21}
$$

Assuming that only x_2 is non-vanishing (cf. (2.37)) yields

$$
\left(R^T D_M L R\right)_{22} = M_2\ln\frac{M_{GUT}}{M_2}
\tag{3.22}
$$

$$
\left(R^T D_M L R\right)_{23} = 0
\tag{3.23}
$$

$$
\left(R^T D_M L R\right)_{33} = M_1\ln\frac{M_{GUT}}{M_1}s_2^2 + M_3\ln\frac{M_{GUT}}{M_3}c_2^2.
\tag{3.24}
$$

For non-vanishing x_3 (cf. (2.38)), the relevant combinations of $\left(R^T D_M L R\right)$ in eq. (3.18) are given by

$$
\left(R^T D_M L R\right)_{22} = M_2\ln\frac{M_{GUT}}{M_2}c_3^2 + M_1\ln\frac{M_{GUT}}{M_1}s_3^2
\tag{3.25}
$$

$$
\left(R^T D_M L R\right)_{23} = 0
\tag{3.26}
$$

$$
\left(R^T D_M L R\right)_{33} = M_3\ln\frac{M_{GUT}}{M_3}.
\tag{3.27}
$$

Here we use the abbreviation $s_i \equiv \sin x_i$ and $c_i \equiv \cos x_i$.

3.2   Magnetic and electric dipole moments of leptons

Magnetic dipole moments   The supersymmetric contribution to the leptonic $(g-2)_i$ arising from the diagrams of Fig. 3.1 with $l_i = l_j$ or the effective Lagrangian (3.1) is defined by the amplitude [31]

$$\mathcal{M}^i_{MDM} = e\overline{u}_i(p') \left(\frac{1}{4m_i}(g-2)_i \right) i\epsilon^*_\alpha \sigma^{\alpha\beta} q_\beta u_i(p). \tag{3.28}$$

In this work we will only consider the SUSY contribution and use the notation

$$\delta a_i \equiv \frac{(g-2)_i}{2}. \tag{3.29}$$

The definition of $A^{ij}_{L,R}$ in eq. (3.2) leads to the result

$$\delta a_i = m^2_{l_i} \left(A^{ii}_L + A^{ii}_R \right)|_{m_{l_i}=m_{l_j}}, \tag{3.30}$$

see also [56]. Making use of (3.3), the relation between $|\delta a_k|^2$ and $Br\,(l_j \to l_i\gamma)$ is as follows

$$\frac{Br\,(l_j \to l_i\gamma)}{|\delta a_k|^2} = \frac{1}{\Gamma_j} \frac{\alpha}{4} \frac{m^5_{l_j}}{m^4_{l_k}} \left| \frac{A^{ij}_R}{A^{kk}_L + A^{kk}_R} \right|^2, \tag{3.31}$$

where the dominance of A^{ij}_R over A^{ij}_L in the SUSY seesaw model has been used. It is therefore natural to expect that both $|\delta a_k|^2$ and $Br\,(l_j \to l_i\gamma)$ are related in a similar way to the SUSY masses involved in the loops [57].

The natural mass scale for the mass insertion describing the necessary chirality flip in the magnetic dipole moment (MDM) interaction is given by the lepton mass involved. Due to the extra m_{l_i} denominator in eq. (3.28) one therefore expects that the leptonic MDMs scale as

$$\frac{\delta a_i}{\delta a_j} \sim \left(\frac{m_i}{m_j} \right)^2, \tag{3.32}$$

which is also referred to as "naive scaling" [56].

The current discrepancy [18] between the measurement of $(g-2)_\mu$ [19] and the Standard Model prediction [18] is

$$\delta a_\mu \;=\; \begin{array}{ll} (22 \pm 7.2 \pm 3.5 \pm 8.0) \cdot 10^{-10} & [e^+e^- \text{ based estimate]} \qquad (3.33) \\[2mm] (7.4 \pm 5.8 \pm 3.5 \pm 8.0) \cdot 10^{-10} & [\tau \text{ based estimate]}. \qquad (3.34) \end{array}$$

In appendix F we derive a complete one-loop expression for the coefficients A^{ii}_L and A^{ii}_R, see eqs. (F.33) and (F.34), taking also into account the lepton masses in the corresponding

loop integrals. If the leptonic masses are neglected in the loop integrals, we obtain the well-known result for δa_i [31],

$$
\begin{aligned}
\delta a_i &= -\frac{1}{96\pi^2} \frac{m_{l_i}^2}{m_{\tilde{l}_x}^2} \frac{1 - 6r_{ax}^N + 3\left(r_{ax}^N\right)^2 + 2\left(r_{ax}^N\right)^3 - 6\left(r_{ax}^N\right)^2 \ln r_{ax}^N}{(1 - r_{ax}^N)^4} \left(\left| N_{iax}^{L(l)} \right|^2 + \left| N_{iax}^{R(l)} \right|^2 \right) \\
&\quad - \frac{1}{16\pi^2} \frac{m_{\tilde{\chi}_a^0} m_{l_i}}{m_{\tilde{l}_x}^2} \frac{1 - \left(r_{ax}^N\right)^2 + 2r_{ax}^N \ln r_{ax}^N}{(1 - r_{ax}^N)^3} Re\left(N_{iax}^{L(l)} N_{iax}^{R(l)*} \right) \\
&\quad + \frac{1}{96\pi^2} \frac{m_{l_i}^2}{m_{\tilde{\nu}_x}^2} \frac{2 + 3r_{ax}^C - 6\left(r_{ax}^C\right)^2 + \left(r_{ax}^C\right)^3 + 6r_{ax}^C \ln r_{ax}^C}{(1 - r_{ax}^C)^4} \left(\left| C_{iax}^{L(l)} \right|^2 + \left| C_{iax}^{R(l)} \right|^2 \right) \\
&\quad + \frac{1}{16\pi^2} \frac{m_{\tilde{\chi}_a^-} m_{l_i}}{m_{\tilde{\nu}_x}^2} \frac{-3 + 4r_{ax}^C - \left(r_{ax}^C\right)^2 - 2\ln r_{ax}^C}{(1 - r_{ax}^C)^3} Re\left(C_{iax}^{L(l)} C_{iax}^{R(l)*} \right).
\end{aligned}
\tag{3.35}
$$

We want to approximate the deviations of the MSSM prediction for $(g-2)_\mu$ if one includes LFV. For simplicity and illustrative purposes, we approximate the loop integrals in the limit of $m_{\tilde{\chi}_a^-} = m_{\tilde{\nu}_x}$ and $m_{\tilde{\chi}_a^0} = m_{\tilde{l}_x}$. Assuming a real mixing matrix of charginos, see appendix C, the contribution from the chargino-sneutrino diagram yields approximately

$$
\begin{aligned}
\delta a_\mu^c &\simeq \frac{g^2}{284\pi^2} \frac{m_\mu^4}{m_W^2 \cos^2\beta} \sum_{a=1}^2 [(O_L)_{a2}]^2 \sum_{x=1}^3 \frac{|(U_{\tilde{\nu}})_{x2}|^2}{m_{\tilde{\nu}_x}^2} + \frac{g^2 m_\mu^2}{192\pi^2} \sum_{a=1}^2 [(O_R)_{a1}]^2 \sum_{x=1}^3 \frac{|(U_{\tilde{\nu}})_{x2}|^2}{m_{\tilde{\nu}_x}^2} \\
&\quad - \frac{g^2}{24\sqrt{2}\pi^2} \frac{m_\mu^2}{m_W \cos\beta} \sum_{a=1}^2 (O_L)_{a2} (O_R)_{a1} \sum_{x=1}^3 \frac{|(U_{\tilde{\nu}})_{x2}|^2}{m_{\tilde{\nu}_x}^2}.
\end{aligned}
\tag{3.36}
$$

The basic dependence on lepton-flavor violating parameters shall be illustrated in a simple two generation model, where the relevant sneutrino (mass)^2 matrix is

$$
\left(m_{\tilde{\nu}}^2 \right)_{LFV} = \begin{pmatrix} m^2 & \delta m^2 \\ \delta m^2 & m^2 + \Delta m^2 \end{pmatrix}.
\tag{3.37}
$$

The mass eigenvalues are chosen such that the lighter state is equal to $\tilde{\nu}_\mu$ in the non-LFV case. The mass eigenvalues corresponding to eq. (3.37) are

$$
\left(m_{\tilde{\nu}}^2 \right)_{1,2} = \frac{1}{2} \left(2m^2 + \Delta m^2 \mp \sqrt{(\Delta m^2)^2 + 4\left(\delta m^2\right)^2} \right).
\tag{3.38}
$$

In this approach, the sneutrino mixing matrix takes the form

$$
U_{\tilde{\nu}} = \begin{pmatrix} \cos\theta^{\tilde{\nu}} & -\sin\theta^{\tilde{\nu}} \\ \sin\theta^{\tilde{\nu}} & \cos\theta^{\tilde{\nu}} \end{pmatrix},
\tag{3.39}
$$

where the mixing angle is given by

$$
\theta^{\tilde{\nu}} = \frac{1}{2} \arctan \frac{2\delta m^2}{\Delta m^2}.
\tag{3.40}
$$

The contribution of sneutrino-chargino loops to the magnetic dipole moment of the muon can then be expressed as follows,

$$\delta a_\mu^c \;\simeq\; \frac{g^2}{284\pi^2}\frac{m_\mu^4}{m_W^2\cos^2\beta}\sum_{a=1}^{2}[(O_L)_{a2}]^2\,s_1^{\tilde\nu}$$

$$+\frac{g^2}{192\pi^2}m_\mu^2\sum_{a=1}^{2}[(O_R)_{a1}]^2\,s_1^{\tilde\nu}$$

$$-\frac{g^2}{24\sqrt{2}\pi^2}\frac{m_\mu^2}{m_W\cos\beta}\sum_{a=1}^{2}(O_L)_{a2}\,(O_R)_{a1}\,s_2^{\tilde\nu}. \tag{3.41}$$

The terms $s_1^{\tilde\nu}$ and $s_2^{\tilde\nu}$ result from the sum over sneutrinos and can be given approximately,

$$s_1^{\tilde\nu} \;\simeq\; \frac{1}{m^2}\left(1-\frac{\sqrt{(\Delta m^2)^2+4\,(\delta m^2)^2}}{2m^2}\left(1-2\sin^2\theta^{\tilde\nu}\right)\right) \tag{3.42}$$

$$s_2^{\tilde\nu} \;\simeq\; \frac{1}{m}\left(1-\frac{\sqrt{(\Delta m^2)^2+4\,(\delta m^2)^2}}{m^2}\left(1-2\sin^2\theta^{\tilde\nu}\right)\right), \tag{3.43}$$

where the assumptions $\Delta m^2\ll m^2$ and $\delta m^2\ll m^2$ are made. This shows that in this case the relative shift due to LFV is determined by the terms in brackets. In particular, this shift vanishes for maximal mixing, i. e. $\theta^{\tilde\nu}=\frac{\pi}{4}$. In the case of $\delta m^2=0$, i. e. $U_{\tilde\nu}=\mathbf{1}$, the sum over sneutrino states breaks down to the state of $\tilde\nu_\mu$.

Keeping only the dominant terms of the neutralino charged slepton contribution to δa_μ and assuming for simplicity that the lepton-flavor violating 2×2 sub-matrix in the left-handed sector of $m_{\tilde l}^2$ is

$$\left(m_{\tilde l}^2\right)_{LFV}\simeq\left(\begin{array}{cc}m^2 & \delta m^2\\ \delta m^2 & m^2+\Delta m^2\end{array}\right), \tag{3.44}$$

we obtain

$$\delta a_\mu^n \;\simeq\; -\frac{g^2 m_\mu^2}{96\pi^2}\left(\frac{\tan^2\theta_W}{m_{\tilde\mu_R}^2}\sum_{a=1}^{4}((O_N)_{a1})^2+\frac{2}{m_W\cos\beta\,m_{\tilde\mu_R}}\sum_{a=1}^{4}(O_N)_{a1}\,(O_N)_{a3}\right)$$

$$-\frac{g^2 m_\mu^2}{284\pi^2}\sum_{a=1}^{4}((O_N)_{a2}+(O_N)_{a1}\tan\theta_W)^2\,s_1^{\tilde\nu}$$

$$+\frac{g^2 m_\mu^2}{96\pi^2}\frac{1}{m_W\cos\beta}\sum_{a=1}^{4}(O_N)_{a3}\,((O_N)_{a2}+(O_N)_{a1}\tan\theta_W)\,s_2^{\tilde\nu}. \tag{3.45}$$

The first line in eq. (3.45) corresponds to lepton-flavor conserving contributions from the right-handed smuon sector. The modifications in eqs. (3.42) and (3.43) due to lepton-flavor violating mixing turn out to be rather small, e. g. they are of the order of 10^{-2} if the terms δm^2 or Δm^2 are roughly one percent of m^2 in eq. (3.37).

Electric dipole moments   Electric dipole moments (EDMs) d_i of charged leptons are defined by the Lagrangian [38]

$$\mathcal{L}_{EDM} = -\frac{i}{2} d_i \bar{l}_i \sigma^{\alpha\beta} F_{\alpha\beta} \gamma_5 l_i, \tag{3.46}$$

corresponding to an amplitude of the form

$$\mathcal{M}^i_{EDM} = \bar{u}_i(p') i \epsilon_\alpha^* \sigma^{\alpha\beta} q_\beta \left(d_i \gamma_5 \right) u_i(p). \tag{3.47}$$

By comparison to eq. (3.2), this type of leptonic dipole operator can also be directly related to $A^{ij}_{L,R}$,

$$d_i = \frac{e}{2} m_{l_i} \left(A^{ii}_R - A^{ii}_L \right) \big|_{m_{l_i} = m_{l_j}}. \tag{3.48}$$

From the results of appendix F, see eqs. (F.33), (F.34), one obtains a complete one-loop expression for the SUSY contribution to leptonic EDMs. Neglecting the leptonic masses in the loop integrals yields the well-known result,

$$
\begin{aligned}
d_i &= -\frac{e}{32\pi^2} Im \left(C^{L(l)}_{iax} C^{R(l)*}_{iax} \right) \frac{m_{\tilde{\chi}_a^-}}{m_{\tilde{\nu}_x}^2} \frac{3 - 4r^C_{ax} + \left(r^C_{ax}\right)^2 + 2\ln r^C_{ax}}{\left(1 - r^C_{ax}\right)^3} \\
&\quad - \frac{e}{32\pi^2} Im \left(N^{L(l)}_{iax} N^{R(l)*}_{iax} \right) \frac{m_{\tilde{\chi}_a^0}}{m_{\tilde{l}_x}^2} \frac{1 - \left(r^N_{ax}\right)^2 + 2r^N_{ax} \ln r^N_{ax}}{\left(1 - r^N_{ax}\right)^3},
\end{aligned} \tag{3.49}
$$

see e. g. [38]. This clearly demonstrates that EDMs are a measure for complex, or more specifically CP-violating parts of the slepton mixing matrices.

The natural mass scale for the mass insertion describing the chirality flip in the EDM interaction is given by the lepton mass involved. One therefore expects that the leptonic EDMs are proportional to the corresponding lepton masses, leading to the the so-called naive scaling relation [58]

$$d_i \sim \frac{m_{l_i}}{m_{l_j}} d_j. \tag{3.50}$$

The authors of [58] have pointed out that in general LFV terms lead to a violation of naive scaling. In this case new contributions arise, e. g. $\frac{m_\tau}{m_\mu}$ enhanced contributions to d_μ in the mass insertion approximation, see [58]. Due to the smallness of m_e, contributions from m_μ and/or m_τ are even more important for the electron EDM, so that large deviations from naive EDM scaling are possible [56].

If no other sources of SUSY phases exist, leptonic EDMs are generated through RGE effects from complex parts in $Y_\nu^\dagger Y_\nu$ in the SUSY seesaw model. In this context, it has been noted in [38] that leptonic EDMs can be strongly enhanced if there is a large hierarchy among the M_i. For strongly hierarchical right-handed Majorana neutrino masses, electron and muon EDMs can be in the range of future experimental searches, because $d_\mu \simeq 10^{-26}$ ecm or $d_e \simeq 10^{-31}$ ecm are possible, as has been shown in [38]. In that analysis it has been pointed out that a step-function-like enhancement of EDMs is expected when going from the degenerate to the non-degenerate M_i case. Effects from non-degenerate
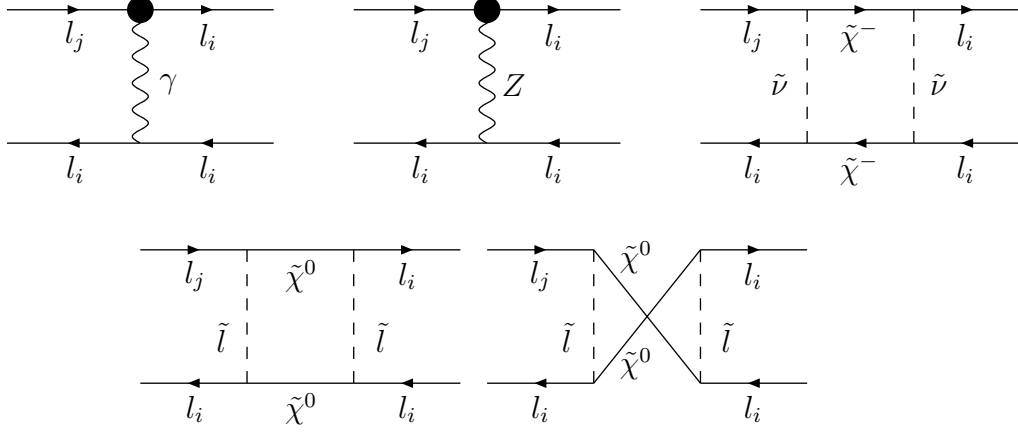
Figure 3.3: Generic diagrams for $l_j^- \to l_i^- l_i^+ l_i^-$ in the MSSM with LFV; the blob indicates a $l_j l_i \gamma$-vertex as in Fig. 3.1 or a $l_j l_i Z$-vertex where the Z-boson is external.

M_i induce additional imaginary contributions being proportional to diagonal elements of trilinear A-terms. This also implies that in the SUSY seesaw model with non-degenerate M_i, the leptonic EDMs depend strongly on the magnitude of A-terms.

3.3   Other rare lepton-flavor violating processes

Processes of the type $l_j \to l_i \bar{l}_i l_i$ are generated by photon penguin diagrams, Z-penguin diagrams and box diagrams (see Fig. 3.3). The photon penguin diagrams to $l_j \to l_i \bar{l}_i l_i$ give rise to the amplitude [31]

$$
\begin{aligned}
\mathcal{M}_\gamma =\ & \overline{u}_i \left(p_1 \right) \left(q^2 \gamma_\alpha \left(A_1^L P_L + A_1^R P_R \right) + m_{l_j} i \sigma_{\alpha\beta} q^\beta \left(A_2^L P_L + A_2^R P_R \right) \right) u_j(p) \\
& \times \frac{e^2}{q^2} \overline{u}_i \left(p_2 \right) \gamma^\alpha v_i \left(p_3 \right) - \left(p_1 \leftrightarrow p_2 \right) .
\end{aligned}
\tag{3.51}
$$

The term proportional to m_{l_j} corresponds to on-shell photon penguin diagrams, whereas the terms involving A_1 correspond to off-shell photon contributions. The minus sign indicates an antisymmetrization due to the exchange of identical external fermions in $l_j \to l_i \bar{l}_i l_i$. Analogously, the Z-penguin diagrams for $l_j \to l_i \bar{l}_i l_i$ lead to an amplitude of the form [31]

$$
\begin{aligned}
\mathcal{M}_Z =\ & \frac{g_Z^2}{m_Z^2} \overline{u}_i \left(p_1 \right) \gamma_\alpha \left(F_L P_L + F_R P_R \right) u_j(p) \\
& \times \overline{u}_i \left(p_2 \right) \gamma^\alpha \left(Z_L^l P_L + Z_R^l P_R \right) v_i \left(p_3 \right) - \left(p_1 \leftrightarrow p_2 \right) .
\end{aligned}
\tag{3.52}
$$
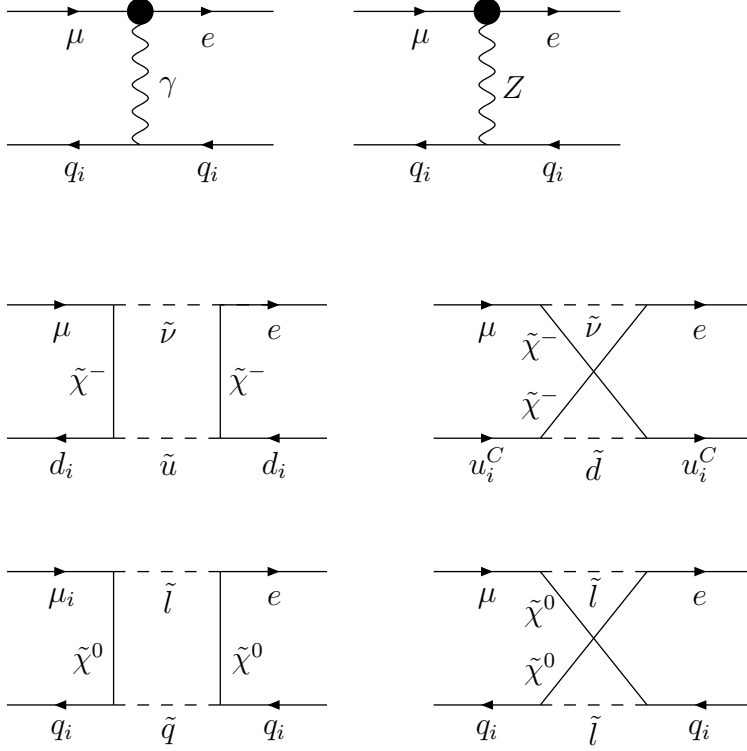
Figure 3.4: Generic diagrams for $\mu - e$ conversion processes on nuclei at the quark level in the MSSM with LFV; the blob indicates a $l_j l_i \gamma$-vertex as in Fig. 3.1 or a $l_j l_i Z$-vertex where the Z-boson is external.

The coefficients of the couplings of the Z-boson to left(right)-handed fermions are

$$Z^f_{L(R)} = T^f_{3L(R)} - Q^f_{em} \sin^2 \theta_W, \tag{3.53}$$

where $T^f_{3L(R)}$ and Q^f_{em} represent weak isospin and electric charge, respectively. The amplitude for the box-type Feynman diagrams can be written in the form [31]

$$
\begin{aligned}
\mathcal{M}_{box} =\ & B_1^L e^2 \overline{u}_i(p_1)\gamma^\alpha P_L u_j(p)\overline{u}_i(p_2)\gamma_\alpha P_L v_i(p_3) + (L \leftrightarrow R) \\
& + B_2^L e^2 \left(\overline{u}_i(p_1)\gamma^\alpha P_L u_j(p)\overline{u}_i(p_2)\gamma_\alpha P_R v_i(p_3) - (p_1 \leftrightarrow p_2)\right) + (L \leftrightarrow R) \\
& + B_3^L e^2 \left(\overline{u}_i(p_1) P_L u_j(p)\overline{u}_i(p_2) P_L v_i(p_3) - (p_1 \leftrightarrow p_2)\right) + (L \leftrightarrow R) \\
& + B_4^L e^2 \left(\overline{u}_i(p_1)\sigma_{\alpha\beta} P_L u_j(p)\overline{u}_i(p_2)\sigma^{\alpha\beta} P_L v_i(p_3) - (p_1 \leftrightarrow p_2)\right) + (L \leftrightarrow R).
\end{aligned}
\tag{3.54}
$$

The abbreviation "$+ (L \leftrightarrow R)$" indicates a term that is equal to the preceding term when any index L is substituted by R and vice versa. For the complete form of the resulting

decay rate we refer to [31] and to the additional formulae given in appendix G,

$$
\begin{aligned}
\Gamma\left(l_j^- \to l_i^- l_i^+ l_i^-\right) &= \frac{e^4 m_{l_j}^5}{512\pi^3}\left(\left|A_1^L\right|^2 + \left|A_1^R\right|^2 - 2\left(A_1^L A_2^{R*} + A_2^L A_1^{R*} + h.c.\right)\right. \\
&\quad + \left(\left|A_2^L\right|^2 + \left|A_2^R\right|^2\right)\left(\frac{8}{3}\ln\frac{m_{l_j}^2}{m_{l_i}^2} - \frac{22}{3}\right) + \frac{1}{6}\left(\left|B_1^L\right|^2 + \left|B_1^R\right|^2\right) \\
&\quad + \frac{1}{3}\left(\left|B_2^L\right|^2 + \left|B_2^R\right|^2\right) + \frac{1}{24}\left(\left|B_3^L\right|^2 + \left|B_3^R\right|^2\right) + 6\left(\left|B_4^L\right|^2 + \left|B_4^R\right|^2\right) \\
&\quad - \frac{1}{2}\left(B_3^L B_4^{L*} + B_3^R B_4^{R*} + h.c.\right) \\
&\quad + \frac{1}{3}\left(A_1^L B_1^{L*} + A_1^R B_1^{R*} + A_1^L B_2^{L*} + A_1^R B_2^{R*} + h.c.\right) \\
&\quad - \frac{2}{3}\left(A_2^R B_1^{L*} + A_2^L B_1^{R*} + A_2^L B_2^{R*} + A_2^R B_2^{L*} + h.c.\right) \\
&\quad + \frac{1}{3}\left(\left(B_1^L F_{LL}^* + B_1^R F_{RR}^* + B_2^L F_{LR}^* + B_2^R F_{RL}^* + h.c.\right)\right. \\
&\quad + 2\left(A_1^L F_{LL}^* + A_1^R F_{RR}^* + h.c.\right) + \left(A_1^L F_{LR}^* + A_1^R F_{RL}^* + h.c.\right) \\
&\quad - 4\left(A_2^R F_{LL}^* + A_2^L F_{RR}^* + h.c.\right) - 2\left(A_2^L F_{RL}^* + A_2^R F_{LR}^* + h.c.\right) \\
&\quad \left. 2\left(\left|F_{LL}\right|^2 + \left|F_{RR}\right|^2\right) + \left|F_{LR}\right|^2 + \left|F_{RL}\right|^2\right)\right). \quad (3.55)
\end{aligned}
$$

Here the following coefficients involving Z-penguin contributions appear,

$$
\begin{aligned}
F_{LL} &= \frac{F_L Z_L^l}{m_Z^2 \sin^2\theta_W \cos^2\theta_W} \\
F_{RR} &= F_{LL}|_{L\leftrightarrow R} \\
F_{LR} &= \frac{F_L Z_R^l}{m_Z^2 \sin^2\theta_W \cos^2\theta_W} \\
F_{RL} &= F_{LR}|_{L\leftrightarrow R}. \quad (3.56)
\end{aligned}
$$

As in the case of $Br\left(l_j^\pm \to l_i^\pm \gamma\right)$, the decay rates for $Br\left(l_j^- \to l_i^- l_i^+ l_i^-\right)$ and its charge conjugated decay mode are the same which can be checked by inspection of the effective Lagrangian [51] of both processes.

The process of μ-e conversion in nuclei, i. e. the process $\mu + (A, Z) \to e + (A, Z)$ where A and Z denote the atomic and proton numbers in a nucleus, arises from diagrams depicted in Fig. 3.4. The effective Lagrangian relevant for this process at the quark level consists of penguin-type contributions and box-type contributions. The penguin-type contributions read as

$$
\begin{aligned}
\mathcal{L}_{eff}^{peng} &= -\frac{e^2}{q^2}\overline{e}\left(q^2\gamma_\alpha\left(A_1^L P_L + A_1^R P_R\right) + m_\mu i\sigma_{\alpha\beta}q^\beta\left(A_2^L P_L + A_2^R P_R\right)\right)\mu \\
&\quad \times \sum_{q=u,d} Q_{em}^q \overline{q}\gamma^\alpha q + \frac{g_Z^2}{m_Z^2}\sum_{q=u,d}\frac{Z_L^q + Z_R^q}{2}\overline{q}\gamma_\alpha q\,\overline{e}\gamma^\alpha\left(F_L P_L + F_R P_R\right)\mu, \quad (3.57)
\end{aligned}
$$

where the first term comes from photon penguin diagrams and the second from penguin diagrams with Z-boson exchange. For box-type contributions, one obtains

$$\mathcal{L}_{eff}^{box} = e^2 \sum_{q=u,d} \overline{q}\gamma_\alpha q \overline{e}\gamma^\alpha \left(D_q^L P_L + D_q^R P_R\right)\mu. \tag{3.58}$$

Normalizing to the total muon capture rate Γ_{cap}, the following rate for μ-e conversion on a nucleus C, can be obtained [31]

$$R(\mu^- C \to e^- C) = \frac{4\alpha^5 m_\mu^5}{\Gamma_{cap}} \frac{Z_{eff}^4}{Z} |F(q)|^2 \left(\left|Z\left(A_1^L - A_2^R\right) - (2Z+N)\overline{D}_u^L\right.\right.$$
$$\left.\left. -(Z+2N)\overline{D}_d^L\right|^2 + (L \leftrightarrow R)\right), \tag{3.59}$$

where N denotes the neutron number of the nucleus, Z_{eff} is the effective charge of the nucleus and $F(q^2)$ the nuclear form factor. For Ti$_{22}^{48}$, these quantities are given by $Z_{eff} = 17.6$ [59], $\Gamma_{cap} = 2.59 \cdot 10^6$ s^{-1} $\approx 1.7 \cdot 10^{-18}$ GeV [60] and $F\left(q^2 \simeq m_\mu^2\right) \simeq 0.54$ [59]. In the above equation (3.59) the terms $\overline{D}_{u,d}^{L,R}$ contain Z-boson penguin contributions and the box-type contributions, specified in [31],

$$\overline{D}_q^L = D_L^q + \frac{Z_L^q + Z_R^q}{2} \frac{F_L}{m_Z^2 \sin^2\theta_W \cos^2\theta_W} \tag{3.60}$$

$$\overline{D}_q^R = \overline{D}_q^L\big|_{L\leftrightarrow R} \qquad (q = u, d). \tag{3.61}$$

A few comments are in order: The evaluation of the nuclear effects in μ-e conversion is based on the Weinberg-Feinberg approximation [61], i. e. relativistic effects and the Coulomb distortion have been ignored. It should also be mentioned that recently there has been a more detailed approach to the evaluation of μ-e conversion taking into account relativistic overlap integrals of protons and neutrons in nuclei [62]. In the case of Titanium nuclei, the difference of the conversion rates in the two methods of calculation amounts to approximately 15%, leading to a slight reduction of the μ-e conversion rate calculated in the Weinberg-Feinberg approximation.

If R-parity is conserved, the main contribution to leptonic three-body decays is given by the on-shell photon penguin terms (see [63] and [51]),

$$\Gamma\left(l_j \to l_i \bar{l}_i l_i\right) \simeq \frac{8}{3} \frac{e^4}{512\pi^3} m_{l_j}^5 \left(|A_L|^2 + |A_R|^2\right)\left(\ln\frac{m_{l_j}^2}{m_{l_i}^2} - \frac{11}{4}\right). \tag{3.62}$$

Therefore one obtains the following ratios of branching ratios in the R-parity conserving case,

$$\frac{Br(\tau \to 3\mu)}{Br(\tau \to \mu\gamma)} \simeq \frac{\alpha}{3\pi}\left(\ln\frac{m_\tau^2}{m_\mu^2} - \frac{11}{4}\right) \approx \frac{1}{444}$$

$$\frac{Br(\tau \to 3e)}{Br(\tau \to e\gamma)} \simeq \frac{\alpha}{3\pi}\left(\ln\frac{m_\tau^2}{m_e^2} - \frac{11}{4}\right) \approx \frac{1}{95}$$

$$\frac{Br(\mu \to 3e)}{Br(\mu \to e\gamma)} \simeq \frac{\alpha}{3\pi}\left(\ln\frac{m_\mu^2}{m_e^2} - \frac{11}{4}\right) \approx \frac{1}{143}. \tag{3.63}$$
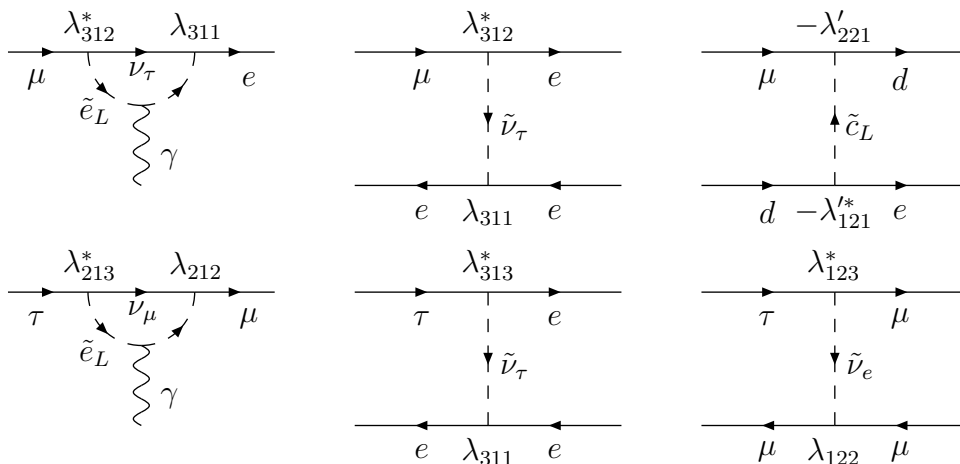
Figure 3.5: Examples of diagrams for LFV at low energies in the MSSM with trilinear R-parity violation; trilinear R-parity violating couplings are explicitly shown.

Analogously, the dominance of on-shell photon penguin contributions leads to

$$\frac{R(\mu^- C \to e^- C)}{Br(\mu \to e\gamma)} \approx \frac{\Gamma_\mu}{\Gamma_{cap}} 16\alpha^4 Z_{eff}^4 Z |F(q^2)|^2 \tag{3.64}$$

$$\approx 6 \cdot 10^{-3} \quad \text{for Titanium.} \tag{3.65}$$

These predictions are SUSY model-independent if R-parity conservation is assumed. Effects due to Higgs mediated LFV in these three-body decays have been extensively studied in [64]. It turns out that the Higgs mediated contributions to these decays are subleading compared to the photonic penguin ones, in particular for low or medium values of $\tan \beta$. It should be mentioned that our numerical results on $Br\left(l_i \to l_i \bar{l}_i l_i\right)$ and μ-e conversion were obtained according to the results of [31] with the additional calculations summarized in appendix G.

LFV at low energies and
trilinear R-parity violation It has been demonstrated in [65] that in models with trilinear R-parity violation ($\not{R}$), $\frac{Br(\mu \to 3e)}{Br(\mu \to e\gamma)}$ can be in the range from 1 to 10^4, in contrast to the predictions of the SUSY seesaw model shown before, see eq. (3.63). Similarly the rate for μ-e conversion on nuclei can be strongly enhanced.
The R-parity violating superpotential with MSSM chiral superfields is given by [65]

$$\mathcal{W}_{\not{R}} = \frac{\lambda_{ijk}}{2} l_i l_j \overline{e}_k + \lambda'_{ijk} l_i q_j \overline{d}_k + \lambda''_{ijk} \overline{u}_i \overline{d}_j \overline{d}_k + \mu'_i l_i h_2. \tag{3.66}$$

For the study of LFV the λ''-couplings are not relevant at the one-loop level and we also assume that the bilinear μ'_i-couplings vanish. As the λ-couplings are antisymmetric in

the first two indices, this model has 9 couplings of λ type and 27 of λ' type. Under these assumptions, $\mathcal{W}_{\not{R}}$ leads to the following SSB Lagrangian [65],

$$
\begin{aligned}
\mathcal{L}_{\not{R}} \;=\; & \lambda_{ijk}\left(\overline{\nu}^{c}_{L_i}e_{L_j}\tilde{e}^{*}_{R_k} + \overline{e}_{R_k}\nu_{L_i}\tilde{e}_{L_j} + \overline{e}_{R_k}e_{L_j}\tilde{\nu}_{L_i}\right) \\
& +\lambda'_{ijk}V^{j\alpha}_{KM}\left(\overline{\nu}^{c}_{L_i}d_{L_\alpha}\tilde{d}^{*}_{R_k} + \overline{d}_{R_k}\nu_{L_i}\tilde{d}_{L_\alpha} + \overline{d}_{R_k}d_{L_\alpha}\tilde{\nu}_{L_i}\right) \\
& -\lambda'_{ijk}\left(\overline{u}^{c}_{L_j}e_{L_i}\tilde{d}^{*}_{R_k} + \overline{d}_{R_k}e_{L_i}\tilde{u}_{L_j} + \overline{d}_{R_k}u_{L_j}\tilde{e}_{L_i}\right) + h.c. \qquad (3.67)
\end{aligned}
$$

In the above equation, the Kobayashi-Maskawa quark mixing matrix is denoted by V_{KM}. It is assumed that there is no left-right mixing in the squark and slepton sectors which is a good approximation for studying generic predictions for ratios of rates for rare LFV processes. If R-parity is violated, tree-level contributions in rare leptonic three-body decays and μ-e conversion on nuclei arise [65], see also Fig. 3.5. Therefore the relation between $Br\left(l_j \to l_i\gamma\right)$ and $Br\left(l_j \to l_i\bar{l}_il_i\right)$ is expected to be essentially different in models with generic trilinear $\not{R}$ couplings, as compared to the seesaw predictions in eq. (3.63). Note that the ratios of $\frac{Br(\mu\to 3e)}{Br(\mu\to e\gamma)}$ and $\frac{R(\mu^-Ti\to e^-Ti)}{Br(\mu\to 3e)}$ in $\not{R}$ depend only on the SUSY spectrum, not on the values of the R-parity violating couplings, if one assumes that the processes are mediated by only two non-vanishing $\not{R}$ couplings [65], see also the diagrams for $\mu \to e\gamma$ and $\mu \to 3e$ in Fig. 3.5. It should be emphasized that in addition to rare muon decays studied in [65], there is also the possibility to distinguish LFV in R-parity conserving/violating models by comparing predictions for τ three-body decays to the respective two-body decays, as illustrated in Fig. 3.5.

3.4 Leptogenesis

The asymmetry in the numbers of baryons as compared to those of antibaryons in the universe has been confirmed e. g. by a the WMAP collaboration. They have measured the ratio of baryon number density to photon number density at the recombination time of photons [66],

$$\eta_B = \left(6.1^{+0.3}_{-0.2}\right) \times 10^{-10}. \qquad (3.68)$$

The three Sakharov conditions [67], necessary for the generation of a baryon asymmetry are:

1. Violation of baryon number B: B-violating interactions are necessary to generate an asymmetry in baryons over antibaryons.

2. Violation of C and CP: If CP was conserved, every reaction producing a particle would be accompanied by a process which produces its antiparticle at exactly the same rate. To generate a baryon asymmetry, CP and C have to be violated.

3. Departure from thermal equilibrium: Moreover, if B-violating interactions are in equilibrium, then the thermal average $\langle B \rangle$ vanishes. The B- and CP-violating processes should have interaction rates smaller than the expansion rate of the universe, so that $\langle B \rangle$ is not washed out by the inverse processes. In other words, the interactions must have an arrow of time.

According to the standard theory of cosmology in the early universe [68], a particle remains in thermal equilibrium, if the interaction rate Γ per particle is greater or at least comparable to the expansion rate H of the universe, $\Gamma \geq H$, where the Hubble constant is $H = \frac{\dot{R}}{R}$ and R denotes the scale factor of the universe.

In theories with heavy right-handed Majorana neutrinos, one can understand the generation of the baryon asymmetry of the universe (BAU) through the mechanism of leptogenesis [16]. In thermal leptogenesis the heavy right-handed Majorana neutrinos are produced thermally after inflation and they induce L-violating interactions at temperatures above their mass scales.

At lower temperatures, the generated $(B-L)$ asymmetry N_{B-L} is converted into a baryon asymmetry by sphaleron processes [69] being related to the non-trivial vacuum configurations of the electroweak theory. The vacuum structure of the $SU(2)_L$ theory leads to an anomalous non-conservation of $(B + L)$, so that transitions between different vacua are accompanied by a change in $(B + L)$. Since this process is non-perturbative, the rate for $(B + L)$ violation is proportional to $\exp\left(-1/g^2\right)$. Because $1/g^2 \gg 1$, such quantum tunneling is completely negligible today. At finite temperatures however, the transitions between different vacua can be driven by thermal effects. The analysis of Kuzmin et al. [69] has demonstrated that the barriers between different vacua can be surmounted at temperatures above the electroweak phase transition near 100 GeV. The sphaleron solution corresponds to the lowest barrier between two electroweak vacua states. Moreover

these transitions conserve $(B - L)$, so that an initial L asymmetry induces a B asymmetry through $(B + L)$ violating sphaleron processes which are in thermal equilibrium for temperatures between 100 GeV and 10^{12} GeV.

A necessary condition for successful thermal leptogenesis is that the masses of the heavy neutrinos are non-degenerate, see e. g. [70]; otherwise one could choose a basis where the mass matrix M and the Yukawa matrix Y_ν are both diagonal, so that no CP asymmetry would be generated, see also eq. (3.75) below. Therefore one often assumes hierarchical masses, i. e. $M_3 \gg M_2 \gg M_1$ or at least $M_3 - M_2 \simeq \mathcal{O}(M_2)$, $M_2 - M_1 \simeq \mathcal{O}(M_1)$. In this case the $(B - L)$ asymmetries produced by the heavier neutrinos will be washed out by processes involving the lightest right-handed neutrino which are in thermal equilibrium for temperatures above the M_1-threshold [71]. The authors of [71] have also demonstrated that the final $(B - L)$ asymmetry is independent of initial conditions, e. g. a large initial asymmetry if the effective neutrino mass is $\tilde{m}_1 \gtrsim 5 \cdot 10^{-3}$ eV. The latter is defined as $\tilde{m}_1 = \frac{(m_D m_D^\dagger)_{11}}{M_1}$, see also discussion on p. 48.

The Boltzmann equations [71] specify the time evolution of the numbers N_{N_1} and N_{B-L} for the lightest singlet Majorana neutrino N_1 and the $B - L$ asymmetry in the comoving volume element. Taking the effects of the interactions of the lightest right-handed Majorana neutrino into account, they can formally be given in a compact form [71]. The notation N_i corresponds to the three heavy Majorana neutrinos [70]

$$N_i = \nu_{R_i} + \nu_{R_i}^c. \tag{3.69}$$

Then the Boltzmann equations are given by

$$\begin{aligned} \frac{dN_{N_1}}{dz} &= -(D + S)\left(N_{N_1} - N_{N_1}^{eq}\right) \\ \frac{dN_{B-L}}{dz} &= -\epsilon_1 D \left(N_{N_1} - N_{N_1}^{eq}\right) - W N_{B-L}. \end{aligned} \tag{3.70}$$

It is convenient to express the time dependence through the variable $z = \frac{M_1}{T}$ in eq. (3.70). The Boltzmann equations above show explicitly that a difference $\left(N_{N_1} - N_{N_1}^{eq}\right)$ in the numbers of lightest right-handed Majorana neutrinos N_{N_1} and their numbers in thermal equilibrium $N_{N_1}^{eq}$ is necessary to generate an asymmetry in $(B - L)$. Four classes of processes contribute to the Boltzmann equations [71]:

- Decays of N_1 into leptons and Higgs bosons $N_1 \rightarrow l h_2$ and into antileptons and anti-Higgs bosons $N_1 \rightarrow \bar{l} h_2^\dagger$

- Inverse decays of N_1, i. e. $h_2 l \rightarrow N_1$ and $h_2^\dagger \bar{l} \rightarrow N_1$

- $\Delta L = 1$ processes mediated by Higgs particles, i. e. $N_1 l(\bar{l}) \leftrightarrow \bar{t}(t) q(\bar{q})$ and $N_1 t(\bar{t}) \leftrightarrow \bar{l}(l) q(\bar{q})$

- $\Delta L = 2$ scatterings with intermediate singlet Majorana neutrinos, i. e. $l h_2 \leftrightarrow \bar{l} h_2^\dagger$, $ll \leftrightarrow h_2^\dagger h_2^\dagger$ and $\bar{l}\,\bar{l} \leftrightarrow h_2 h_2$

In the above Boltzmann equations (3.70), the thermally averaged $\Delta L = 1$ reaction rate per particle Γ_S enters through the quantity $S = \frac{\Gamma_S}{Hz}$. The rescaled quantity $D = \frac{\Gamma_D}{Hz}$ accounts for decays and inverse decays of N_1 and the rescaled washout rate $W = \frac{\Gamma_W}{Hz}$ gets contributions from inverse decays, $\Delta L = 1$ and $\Delta L = 2$ scatterings.

A formal solution to the asymmetry N_{B-L} in the Boltzmann equations (3.70) is given by [71]

$$N_{B-L}(z) = N_{B-L}(z_{in}) \exp\left(-\int_{z_{in}}^{z} dz' W(z')\right) - \frac{3}{4}\epsilon_1 \kappa_f(z), \qquad (3.71)$$

where the efficiency factor κ_f is given by

$$\kappa_f(z) = \frac{4}{3}\int_{z_{in}}^{z} dz' D(z')\left(N_{N_1}(z') - N_{N_1}^{eq}(z')\right)\exp\left(-\int_{z'}^{z} dz'' W(z'')\right), \qquad (3.72)$$

and initial values are defined at z_{in}. We assume that the initial $(B-L)$ asymmetry is zero, so that $N_{B-L}(z)$ is proportional to the CP asymmetry and the efficiency factor,

$$N_{B-L} = -\frac{3}{4}\epsilon_1 \kappa_f. \qquad (3.73)$$

The efficiency factor κ_f takes into account the effects of the washout rate W on an initial $(B-L)$ asymmetry by inverse decays, $\Delta L = 1$ and $\Delta L = 2$ processes. Thus the washout of the $(B-L)$ asymmetry does not depend on the decay rate of N_1 or on the CP asymmetry ϵ_1 in N_1 decays. The latter is defined as [70]

$$\epsilon_1 = \frac{\Gamma(N_1 \rightarrow h_2 + l) - \Gamma(N_1 \rightarrow h_2^\dagger + \bar{l})}{\Gamma(N_1 \rightarrow h_2 + l) + \Gamma(N_1 \rightarrow h_2^\dagger + \bar{l})}. \qquad (3.74)$$

Note that the aforementioned scattering and decay processes are shown for illustrative purposes. In the SUSY seesaw model one also has to consider supersymmetric versions of these interactions involving e. g. heavy right-handed sneutrinos, see for e. g. [70] for a detailed analysis. The CP-violation in the decays of N_i is given by [72],

$$\epsilon_i \simeq -\frac{1}{8\pi}\frac{1}{\left(Y_\nu Y_\nu^\dagger\right)_{ii}}\sum_{j\neq i} Im\left(\left(Y_\nu Y_\nu^\dagger\right)_{ij}\left(Y_\nu Y_\nu^\dagger\right)_{ij}\right) f\left(\frac{M_j^2}{M_i^2}\right), \qquad (3.75)$$

$$f(x) = \sqrt{x}\left(\frac{2}{x-1} + \ln\frac{1+x}{x}\right). \qquad (3.76)$$

The CP asymmetry ϵ_i arises from the interference of the tree-level decay diagrams with vertex and self-energy corrections, see Fig. 3.6, where the diagrams are shown generically. A quantitative analysis, see e. g. the reviews in [73] and [72], taking into account the chemical potentials of all particle species in the high-temperature phase, shows that the sphaleron conversion factor a_{Sph} for an initial $(B-L)$ asymmetry is

$$N_B = a_{Sph}N_{B-L} = \frac{8n_F + 4n_H}{22n_F + 13n_H}N_{B-L}. \qquad (3.77)$$

For three generations of fermions ($n_F = 3$) and two Higgs doublets ($n_H = 2$), this leads to a conversion factor

$$a_{Sph} = \frac{8}{23} \tag{3.78}$$

in the case of the MSSM. Note that this factor of roughly one third also arises in the SM with one Higgs doublet.

For the measured baryon asymmetry η_B one also has to take into account the dilution of the asymmetry due to standard photon production from the onset of leptogenesis until the recombination of photons [71]. This is done by the dilution factor

$$f_{dil} = \frac{N_\gamma(T \simeq M_1)}{N_\gamma(T_0)} \simeq \frac{g_{*s}(T_0)}{g_{*s}(T \simeq M_1)} \sim 0.017, \tag{3.79}$$

where T_0 is the recombination temperature of the universe. This dilution factor can be understood as follows [68]: The number of effectively massless degrees of freedom, i. e. of those species with mass $m_i \ll T$ that are relevant for the entropy density of the universe, is given by

$$g_{*s} = \sum_{i=\text{bosons}} g_i \left(\frac{T_i}{T_\gamma}\right)^3 + \frac{7}{8} \sum_{i=\text{fermions}} g_i \left(\frac{T_i}{T_\gamma}\right)^3, \tag{3.80}$$

where the factor $\frac{7}{8}$ is due to the difference in Bose and Fermi statistics and g_i represents the internal degrees of freedom of a particle. Moreover the temperature T_i takes into account that a particle i may have a thermal distribution different from the photon temperature T_γ. The conservation of the entropy per comoving volume in thermal equilibrium implies that $g_{*s}T^3R^3$ remains constant during the expansion of the universe. At temperatures below 1 MeV, the interaction rates for electron-neutrino processes, $\bar{\nu}_e\nu_e \leftrightarrow e^+e^-$ and $\nu_e e \leftrightarrow \nu_e e$ fall below the expansion rate and neutrino interactions are too weak to keep them in equilibrium, so that the light neutrino species decouple from the plasma. Shortly after neutrino decoupling the temperature drops below the mass of the electron, and entropy in $e^\pm$ pairs is transferred to the photons, but not to the neutrinos. As mentioned above, for particles in thermal equilibrium, $g_{*s}(RT)^3$ remains constant. Therefore the value of T_γ after electron decoupling must be larger than T_ν before $e^\pm$ annihilation, leading to

$$\frac{T_\gamma}{T_\nu} = \left(\frac{11}{4}\right)^{1/3} \approx 1.4. \tag{3.81}$$

This in turn yields

$$g_{*s}(T_0) = 2 + \frac{7}{8} \times 2 \times 3 \times \frac{4}{11} \approx 3.91. \tag{3.82}$$

On the other hand, at the time of decoupling of the lightest right-handed (s)neutrinos, all lighter MSSM particles are active degrees of freedom ($g_{*s} = 228.75$ in the MSSM, see [70]), so that at $T \simeq M_1$

$$g_{*s}(M_1) = 228.75 + 2 + \frac{7}{8} \times 2 = 232.5. \tag{3.83}$$
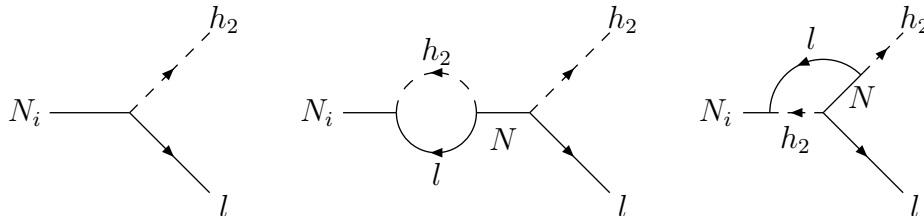
Figure 3.6: Tree-level diagram, self-energy diagram and vertex correction for the decay of singlet Majorana neutrinos.

Taking into account the sphaleron conversion factor eq. (3.78) and the dilution factor eq. (3.79) finally yields the following form for the observed baryon asymmetry,

$$\eta_B \approx -0.0044\epsilon_1\kappa_f. \tag{3.84}$$

For hierarchical heavy Majorana neutrinos $\frac{M_j^2}{M_1^2} \gg 1$, one obtains $f\left(\frac{M_j^2}{M_1^2}\right) \simeq 3\frac{M_1}{M_j}$, leading to [72, 74]

$$\epsilon_1 \simeq -\frac{3}{8\pi}\frac{1}{\left(Y_\nu Y_\nu^\dagger\right)_{11}}\sum_{j\neq 1} Im\left(\left(Y_\nu Y_\nu^\dagger\right)_{1j}\left(Y_\nu Y_\nu^\dagger\right)_{1j}\right)\frac{M_1}{M_j}.$$

Summarizing, extensive studies of thermal leptogenesis [71] have revealed that the generated $(B-L)$ asymmetry depends on the following quantities:

1. The CP asymmetry ϵ_1 in decays of N_1

2. The mass M_1 of N_1

3. The effective neutrino mass $\tilde{m}_1 = \frac{\left(m_D m_D^\dagger\right)_{11}}{M_1}$, which is constrained to be $m_1 \leq \tilde{m}_1 \lesssim m_3$

4. The sum of all neutrino masses squared, $\overline{m}^2 = m_1^2 + m_2^2 + m_3^2$, which controls an important class of washout processes.

In the limit of hierarchical light neutrinos, i. e. $\kappa_1 = 0$, one can express the effective neutrino mass $\tilde{m}_1$ in terms of R-matrix elements and $\kappa_{2,3}$ as follows,

$$\kappa_2 \left|R_{12}\right|^2 + \kappa_3 \left|R_{13}\right|^2 = \frac{\tilde{m}_1}{v^2 \sin^2\beta}. \tag{3.86}$$

For quasi-degenerate light neutrinos of mass scale m_1, the analogous equation is given by

$$\left|R_{11}\right|^2 + \left|R_{12}\right|^2 + \left|R_{13}\right|^2 = \frac{\tilde{m}_1}{m_1}. \tag{3.87}$$

This relation can be interpreted as a sphere of radius $\sqrt{\frac{\tilde{m}_1}{m_1}}$ in $|R_{11}|$, $|R_{12}|$, $|R_{13}|$ space. A numerical fit for κ_f for hierarchical light neutrinos and $M_1 < 10^{14}$ GeV is given by [71]

$$\kappa_f(\tilde{m}_1) \simeq 0.24 \left(x_- e^{-x_-} + x_+ e^{-x_+} \right), \qquad x_{\pm} = \left(\frac{\tilde{m}_1}{\tilde{m}_{\pm}} \right)^{\mp 1 - \alpha}, \qquad (3.88)$$

where $\tilde{m}_- = 3.5 \cdot 10^{-4}$ eV, $\tilde{m}_+ = 8.3 \cdot 10^{-4}$ eV and $\alpha = 0.1$. Note that this fit has been obtained in the non-supersymmetric seesaw model. However it is expected that in the case of thermal leptogenesis in the SUSY seesaw model, the efficiency factor is approximately as in eq. (3.88), see also [70] and [75]. The efficiency factor eq. (3.88) increases for $\tilde{m}_1 \lesssim 1$ meV roughly as $\tilde{m}_1$ due to the first term in (3.88). Since $\tilde{m}_1$ is a measure of the coupling of right-handed neutrinos to the thermal bath, the efficiency factor grows in the region of small $\tilde{m}_1 \ll \tilde{m}_-$, where out of equilibrium decays lead to a strong dependence on the number of N_1 [76]. The decrease of κ_f, $\kappa_f \propto \frac{1}{\tilde{m}_1}$, for large $\tilde{m}_1 \gtrsim 1$ meV is controlled by the second term. For large $\tilde{m}_1 \gg 1$ meV, the lightest right-handed neutrinos are rapidly produced and their number approaches the thermal equilibrium value. Then the washout processes dominate over the production processes, diluting a generated asymmetry more effectively [76].

For hierarchical right-handed Majorana neutrinos, the CP asymmetry in the decays of N_1 is given by

$$\epsilon_1 = -\frac{3}{8\pi v_2^2} \frac{M_1}{\left(Y_\nu Y_\nu^\dagger \right)_{11}} Im \left[(Y_\nu m_\nu^\dagger Y_\nu^T)_{11} \right] \qquad (3.89)$$

$$= -\frac{3}{8\pi} \frac{M_1}{\left(Y_\nu Y_\nu^\dagger \right)_{11}} Im \left[\left(Y_\nu Y_\nu^\dagger \frac{1}{M} Y_\nu^* Y_\nu^T \right)_{11} \right] \qquad (3.90)$$

$$= -\frac{3}{8\pi} \frac{M_1}{\left(Y_\nu Y_\nu^\dagger \right)_{11}} Im \left[(D_{\sqrt{M}} R D_{\kappa^2} R^T D_{\sqrt{M}})_{11} \right]. \qquad (3.91)$$

Note that the approximation (3.85) for ϵ_1 is obtained by inserting the seesaw formula $m_\nu = v_2^2 Y_\nu^T \frac{1}{M} Y_\nu$ in (3.89). From the above equation (3.91), one can also conclude that [74]

$$\epsilon_1 \simeq -\frac{3}{8\pi} \frac{M_1}{v_2^2} \frac{\sum_i m_i^2 Im(R_{1i}^2)}{\sum_i m_i |R_{1i}|^2}. \qquad (3.92)$$

Using the orthogonality condition $\sum_i R_{1i}^2 = 1$, the authors of [74] have shown that

$$|\epsilon_1| \lesssim \frac{3}{8\pi} \frac{M_1}{v_2^2} (m_3 - m_1). \qquad (3.93)$$

Assuming a hierarchical spectrum of light neutrinos, this corresponds to an upper bound on the CP asymmetry ϵ_1. On the other hand this also implies a lower bound on the M_1-scale, e. g. if $\epsilon_1 < 10^{-6}$, then $M_1 > 4 \cdot 10^9$ GeV, see also the discussion in [74].

Writing the terms contributing to eq. (3.90) explicitly, the expression for the CP asymmetry becomes

$$\epsilon_1 = -\frac{3}{8\pi} \frac{M_1}{\left(Y_\nu Y_\nu^\dagger\right)_{11}} Im \left(\sum_{k,l=1}^{3} (Y_\nu)_{1k} (Y_\nu^*)_{2k} \frac{1}{M_2} (Y_\nu^*)_{2l} (Y_\nu)_{1l} \right.$$

$$\left. + \sum_{k,l=1}^{3} (Y_\nu)_{1k} (Y_\nu^*)_{3k} \frac{1}{M_3} (Y_\nu^*)_{3l} (Y_\nu)_{1l} \right). \qquad (3.94)$$

In the above equation, the terms involving M_2 are from interference processes in the decays of ν_{R_1} involving ν_{R_2}, while those involving M_3 are from interference processes in the decays of ν_{R_1} involving ν_{R_3}. For numerical results, these terms are evaluated at the scales of M_2 and M_3 [77], respectively. On the other hand, $\left(Y_\nu Y_\nu^\dagger\right)_{11}$ being relevant for the effective neutrino mass $\tilde{m}_1$ is evaluated at the scale of M_1 in eq. (3.94).

As the MNS matrix U drops out in ϵ_1, it is clear from eq. (3.91) that non-zero imaginary parts of the R-matrix elements are necessary to generate a CP asymmetry. We will study a minimal model, where the real parts of the angles in the R matrix are vanishing, i. e. $x_{1,2,3} = 0$. For small imaginary parts, i. e. $y_{1,2,3} \simeq 10^{-2}$, the form of the R-matrix has been derived in eq. (2.39). In this limit one obtains the following approximate results:

$$\frac{\tilde{m}_1}{v_2^2} \simeq \left(\kappa_1 \left(1 + y_2^2 + y_3^2\right) + \kappa_2 y_3^2 + \kappa_3 y_2^2 \right) \qquad (3.95)$$

$$Im \left(\left((Y_\nu Y_\nu^\dagger)_{12}\right)^2 \right) \simeq -2 M_1 M_2 \left(\kappa_1 + \kappa_2\right) \left(\kappa_2 + \kappa_3\right) y_1 y_2 y_3 \qquad (3.96)$$

$$Im \left(\left((Y_\nu Y_\nu^\dagger)_{13}\right)^2 \right) \simeq 2 M_1 M_3 \left(\kappa_1 + \kappa_3\right) \left(\kappa_2 + \kappa_3\right) y_1 y_2 y_3 \qquad (3.97)$$

In the above equations, terms of higher order in y_i have been neglected. This shows that successful leptogenesis is possible if $y_1 y_2 y_3 \neq 0$. Therefore the minimal choice is $y_1 = y_2 = y_3 \equiv y$. If one further assumes hierarchical light neutrinos, i. e. $\kappa_1 = 0$, the baryon asymmetry is determined through eq. (3.84) by the parameters

$$\epsilon_1 \simeq -\frac{3 M_1}{4\pi} \left(-\kappa_2 + \kappa_3\right) y \qquad (3.98)$$

$$\kappa_f \simeq 0.24 \, x_- e^{-x_-}$$

$$\simeq 0.24 \left(\frac{v_2^2}{\tilde{m}_-} \left(\kappa_2 + \kappa_3\right) \right)^{0.9} y^{1.8} \left(1 - \left(\frac{v_2^2}{\tilde{m}_-} \left(\kappa_2 + \kappa_3\right) \right)^{0.9} y^{1.8} \right). \qquad (3.99)$$

Summarizing, in this model the sign of $y_1 y_2 y_3$ is fixed to be positive, and the baryon asymmetry depends on a common $y \equiv y_i \lesssim 10^{-2}$ as $\eta_B \propto y^{2.8}$, in the limit of hierarchical light neutrino masses and $\tilde{m}_1 \ll \tilde{m}_-$.

It has been noted that an overabundance of gravitinos can cause serious cosmological problems [78]. For example, the abundances of light elements as explained by big-bang nucleosynthesis (BBN) may be modified by gravitino decays: Since the couplings of the

gravitino to ordinary matter are strongly suppressed by the gravitational scale, it has a very long lifetime. However, if it is heavier than the LSP, it can decay e. g. radiatively into a photon and photino. These decays will occur after the big-bang nucleosynthesis, unless the gravitino is heavier than ~ 10 GeV [41]. Among the gravitino decay products are energetic photons which induce electromagnetic cascade processes, thereby spoiling successful BBN. Since the number of gravitinos produced during the reheating epoch is approximately proportional to the reheating temperature T_R, one can obtain upper bounds on T_R depending on the gravitino mass $m_{3/2}$. According to the analysis [79], the upper bounds corresponding to a heavy, i.e unstable gravitino are given by $T_R \lesssim 10^7$, 10^9 and 10^{12} GeV for $m_{3/2} = 100$ GeV, 1 TeV and 3 TeV, respectively. Assuming that the right-handed neutrinos are produced thermally after inflation results in a constraint on M_1, i. e. $M_1 < T_R$. This potential problem of thermal leptogenesis can be overcome e. g. in AMSB, as has been realized in [44]. In anomaly mediated SUSY-breaking, $m_{3/2}$ is typically of the order of 10-100 TeV, so that bounds obtained from $m_{3/2}$ are less severe. This is due to the fact that for $m_{3/2} \gtrsim 60$ TeV, the gravitinos decay well before the start of nucleosynthesis, see also [44] for details. Another way to solve the gravitino problem has been proposed recently by the authors of [80]. It has been noticed that in gaugino mediated supersymmetry breaking, gauge couplings decrease above a critical temperature T_* which depends on the SUSY breaking mass scale. In this scenario, the gravitino is the LSP and therefore the dark matter candidate. The decrease of the gauge couplings crucially affects the production of gravitinos after inflation. The authors of [80] have shown that this mechanism leads to a relic gravitino density which is compatible with the WMAP results and which becomes independent of the reheating temperature for $T_R > T_*$.

Since an analysis of the gravitino problem is beyond the scope of this work, we will not consider the related constraints which are also model dependent in the following.

Chapter 4

Numerical results

4.1 Input parameters

4.1.1 Neutrino parameters

For numerical results we use the global fits in a three neutrino framework performed in [3] including data from KamLAND, CHOOZ, MACRO and Super-Kamiokande, and also the recently improved measurement of the neutral currents at SNO as well as the first spectral data from the K2K long baseline accelerator experiment, see references in [3]. The neutrino oscillation parameters corresponding to the highly-favored large mixing angle solution of the solar neutrino problem are summarized in Tab. 4.1.

Parameter	best fit	error (3σ)
$\sin^2\theta_{23}$	0.52	$^{+0.20}_{-0.21}$
$\sin^2\theta_{13}$	0.006	$^{+0.048}_{-0.006}$
$\sin^2\theta_{12}$	0.30	$^{+0.09}_{-0.07}$
$\Delta m^2_{21}/10^{-5}$ eV^2	6.9	$^{+2.6}_{-1.5}$
$\Delta m^2_{31}/10^{-3}$ eV^2	2.6	$^{+1.1}_{-1.2}$

Table 4.1: Best-fit values and 3σ confidence level (CL) intervals for the present uncertainties of neutrino oscillation parameters corresponding to [3].

For the Dirac phase δ of (2.19) and the two Majorana phases ϕ and ϕ' introduced in (2.18), no experimental limits exist.
Upper bounds on the absolute mass scale of neutrinos can be obtained from tritium beta decay experiments, neutrinoless double beta decay searches and the neutrino hot dark matter contribution to the cosmological large scale structure and the cosmic microwave background, see [81] for details. Assuming that thermal leptogenesis in the decays of N_1 provides the solution to the BAU yields a very strong constraint on the mass scale of the lightest neutrino [71],

$$m_1 < 0.11 \text{ eV.} \tag{4.1}$$

SPS 1a				
m_0/GeV	$\tilde{M}_{1/2}/\text{GeV}$	A_0/GeV	$\tan\beta$	$\text{sign}(\mu)$
100	250	-100	10	1
$m_0 = -A_0 = 0.4\ \tilde{M}_{1/2}$, $\tilde{M}_{1/2}$ varies				

Table 4.2: Input parameters and parameter line of the SPS 1a mSUGRA scenario.

SPS 9			
m_0/GeV	$m_{3/2}/\text{TeV}$	$\tan\beta$	$\text{sign}(\mu)$
450	60	10	1
$m_0 = 0.0075\ m_{3/2}$, $m_{3/2}$ varies			

Table 4.3: Input parameters and parameter line of the SPS 9 AMSB scenario.

Note also that a positive signal at the final sensitivity of the tritium beta decay experiment KATRIN would imply $m_1 = 0.3 \pm 0.1$ eV [82].

4.1.2 SUSY parameters

The fundamental SUSY input parameters should be chosen such that they are consistent with all experimental and cosmological constraints. These include

- direct sparticle searches;

- $b \to s\gamma$;

- cosmological relic density, with the lightest neutralino as LSP and dark matter candidate;

- Higgs searches.

In the following, we specify the numerical values of the fundamental input parameters of the SUSY models and also show the resulting sparticle spectra in Tab. 4.6.

mSUGRA There have been several proposals for mSUGRA benchmark scenarios, e. g. [39] and [83]. The so-called Snowmass Points and Slopes (SPS) benchmark scenarios [39] propose single points in mSUGRA parameter space, including parameter lines along which dimensionfull input parameters are varied. The mSUGRA scenario SPS 1a studied in this work is specified in Tab. 4.2. Note that SPS 1a is similar to scenario B of [83].

AMSB parameters For the input parameters in the AMSB scenario we refer to SPS 9 of [39], see Tab. 4.3.

$\tilde{G}$MSB			
$\tilde{M}_{1/2}/\text{GeV}$	$\frac{M_C}{M_{GUT}}$	$\tan\beta$	$\text{sign}(\mu)$
500	2	12	1

Table 4.4: Parameters of the $\tilde{G}$MSB scenario.

GMSB				
F_S/GeV^2	M_m/GeV	N_m	$\tan\beta$	$\text{sign}(\mu)$
10^{19}	10^{14}	1	15	1

Table 4.5: Parameters of the GMSB scenario.

$\tilde{G}$MSB parameters   We choose the parameters of the $\tilde{G}$MSB model according to the so-called "heavy MGM" scenario of [46], specified in Tab. 4.4, for simplicity referred to as "$\tilde{G}$MSB" in the following.

GMSB parameters   The fundamental input parameters of the GMSB scenario considered here are specified in Tab. 4.5. As mentioned earlier, for sizeable LFV effects in the SUSY seesaw model, the messenger mass scale has to be larger than the Majorana mass scales. The other parameters, in particular F_S are chosen such that they lead to sparticle masses comparable to the other scenarios.

4.2   Leptogenesis

Effective neutrino mass $\tilde{m}_1$ as a function of elements of R   The effective neutrino mass $\tilde{m}_1$ is displayed in Fig. 4.1 as a function of a common $y \equiv y_i$ and vanishing x_i, showing an increase proportional to y^2, as expected from eq. (3.95) for $y \ll 1$ in the limit $\kappa_1 = 0$. In order to demonstrate effects when this restriction is relaxed, we show in Fig. 4.5 $\tilde{m}_1$ when y_i are non-equal and x_i are small. It turns out that in this case $\tilde{m}_1$ is approximately proportional to $(y_1 y_2 y_3)^{2/3}$ although the correlation is weaker in comparison to the previous case.
For definiteness, we choose $\tan\beta = 10$ and a SUSY-scale of $M_{SUSY} = 467$ GeV, corresponding to the scenario SPS 1a. Note, however, that the results concerning leptogenesis are virtually independent of the choice of a low-energy SUSY-scale. This also implies that the results for the leptogenesis parameters would be almost identical in the other models of SSB considered here.

Efficiency factor κ_f as a function of elements of R   As mentioned in section 3.4 on p. 49, for hierarchical light and heavy neutrinos with $M_1 < 10^{14}$ GeV, the efficiency factor κ_f for the generated $(B-L)$ asymmetry is to a good approximation only a function of $\tilde{m}_1$. Using the numerical fit of eq. (3.88) for the efficiency factor, we plot in Figs. 4.2 and 4.6

Parameter	SPS 1a	$\tilde{G}$MSB	SPS 9	GMSB
$m_{\tilde{\chi}_1^0}/\text{GeV}$	96	211	164	207
$m_{\tilde{\chi}_2^0}/\text{GeV}$	177	406	551	221
$m_{\tilde{\chi}_3^0}/\text{GeV}$	359	739	986	428
$m_{\tilde{\chi}_4^0}/\text{GeV}$	378	750	991	444
$m_{\tilde{\chi}_1^-}/\text{GeV}$	176	406	164	213
$m_{\tilde{\chi}_2^-}/\text{GeV}$	378	750	990	444
$m_{\tilde{e}_R}/\text{GeV}$	143	235	383	310
$m_{\tilde{\tau}_1}/\text{GeV}$	133	224	355	298
$m_{\tilde{\nu}_e}/\text{GeV}$	186	364	382	393
$m_{\tilde{e}_L}/\text{GeV}$	202	373	390	401
$m_{\tilde{\tau}_2}/\text{GeV}$	206	375	400	400
$m_{\tilde{\nu}_\tau}/\text{GeV}$	185	364	377	390
$m_{\tilde{b}_1}/\text{GeV}$	492	1121	1087	668
$m_{\tilde{t}_1}/\text{GeV}$	379	906	906	533
$m_{\tilde{b}_2}/\text{GeV}$	525	1195	1251	701
$m_{\tilde{t}_2}/\text{GeV}$	575	1117	1118	721

Table 4.6: Sparticle masses in the scenarios under consideration; in an obvious notation, the slepton masses of the first two generations are displayed with an "e" index, i. e. $m_{\tilde{\mu}_R} = m_{\tilde{e}_R}$ etc.

κ_f as a function of y and $\sqrt[3]{y_1 y_2 y_3}$, where the relevant parameters are as in Figs. 4.1 and 4.5, respectively. As discussed before, the efficiency factor scales roughly as $\tilde{m}_1$ or $1/\tilde{m}_1$ for $\tilde{m}_1 \ll 0.1$ meV or $\tilde{m}_1 \gg 0.1$ meV, respectively. Therefore a maximal κ_f near 0.1 meV can be expected in Fig. 4.2. Moreover, the increase of the efficiency factor proportional to $y^{1.8}$ for $y \ll 1$ is explained in eq. (3.99). The scattering of κ_f in Fig. 4.6 follows from the variation of $\tilde{m}_1$ for different y_i and small x_i.

CP asymmetry ϵ_1 as a function of elements of R   The CP asymmetry ϵ_1 generated in the decays of N_1 also depends on M_1 in the case of hierarchical right-handed neutrinos. We present ϵ_1 as a function of y in Fig. 4.3 when M_1 is varied in the range $10^{10} - 10^{12}$ GeV. As expected from eq. (3.98), in the case of small $y_i \equiv y$ and $y > 0$, real mixing angles set to zero and scattering of M_1 around 10^{11} GeV, the resulting CP asymmetry is negative resulting in a correct sign of η_B. The fact that $-\epsilon_1$ scales linear with both M_1 and y for $y \ll 1$ is explained in eq. (3.98). We also show results for the "less constrained" choices of R in Fig. 4.7. Note, however that in this case some choices of x_i and y_i, especially for large $\sqrt[3]{y_1 y_2 y_3}$, yield the wrong sign of ϵ_1, in which case the points do not appear in Fig. 4.7.
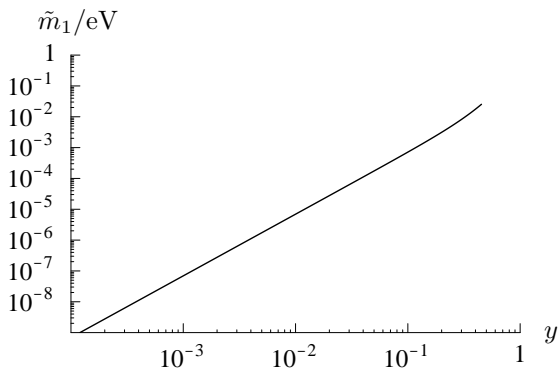
Figure 4.1: Effective neutrino mass parameter $\tilde{m}_1$ as a function of $y_i \equiv y > 0$, real mixing angles x_i set to zero.
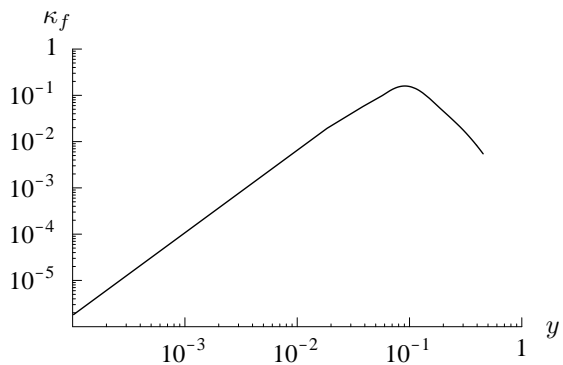
Figure 4.2: Efficiency factor κ_f as a function of $y_i \equiv y > 0$, real mixing angles x_i set to zero.
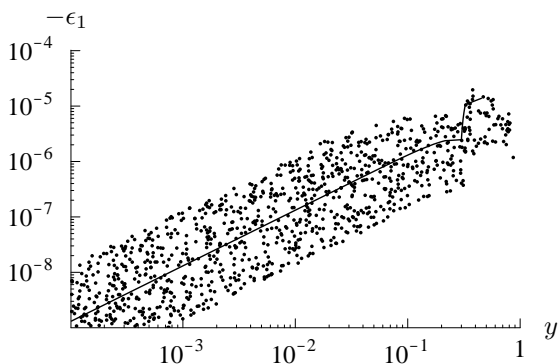
Figure 4.3: CP asymmetry $-\epsilon_1$ as a function of $y_i \equiv y > 0$, real mixing angles x_i set to zero; scattering of M_1 around 10^{11} GeV (inner line) between 10^{10} GeV and 10^{12} GeV, $M_{2(3)} = 10(100)M_1$.
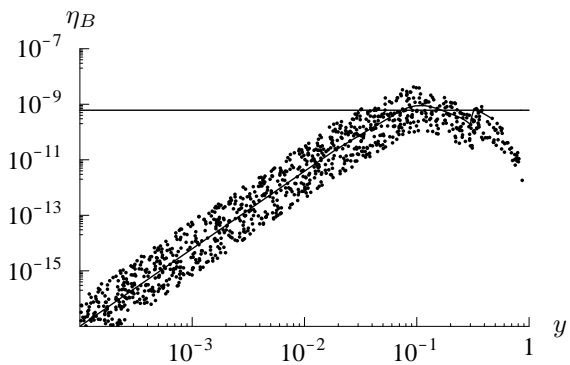
Figure 4.4: Baryon asymmetry η_B as a function of $y_i \equiv y > 0$, real mixing angles x_i set to zero; scattering of M_1 around 10^{11} GeV (inner line) between 10^{10} GeV and 10^{12} GeV, $M_{2(3)} = 10(100)M_1$; straight line corresponds to eq. (3.68).

Baryon asymmetry η_B as a function of elements of R   The predictions for the final baryon asymmetry η_B in the case of a variation of y or y_i and x_i are shown in Figs. 4.4 and 4.8, respectively. As η_B is proportional to $-\epsilon_1$, it is clear that it also scales linearly with the mass scale M_1 corresponding to the spread of points in Fig. 4.4 for a variation of M_1 in the interval $10^{10} - 10^{12}$ GeV. As expected from eqs. (3.84), (3.99) and (3.98), η_B strongly increases proportional to $y^{2.8}$ in the range $y \ll 10^{-1}$. The maximal baryon asymmetry is reached near the maximal efficiency factor, i. e. for $y \simeq 0.1$ corresponding to $\tilde{m}_1 \simeq 0.1$ meV. Comparing the values of maximal baryon asymmetry to the measured one, see eq. (3.68), we conclude that for this "minimal" choice of the R-matrix, M_1 should be roughly 10^{11} GeV or larger. Fig. 4.8 shows that η_B is only weakly dependent on $\sqrt[3]{y_1 y_2 y_3}$
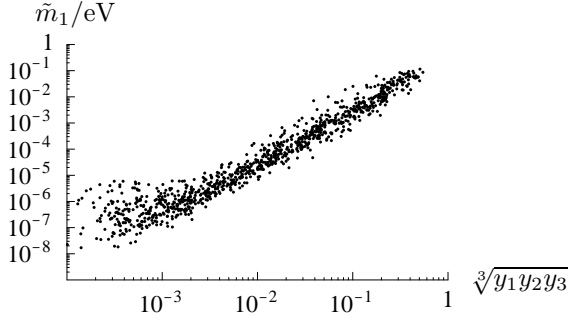
Figure 4.5: Correlation of $\tilde{m}_1$ and $\sqrt[3]{y_1 y_2 y_3} > 0$, random variation of y_1, $y_2 = [0.1; 10]y_1$, $y_3 = [0.1; 10]y_1$, x_i scattered between 10^{-4} and 10^{-2}.
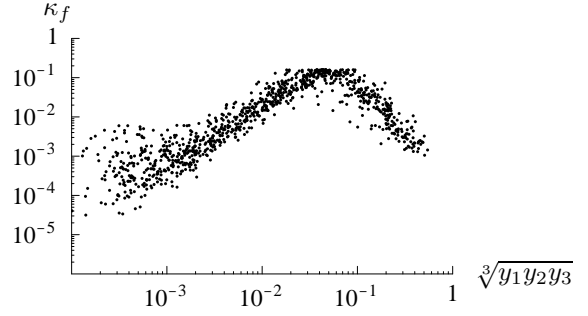
Figure 4.6: Correlation of κ_f and $\sqrt[3]{y_1 y_2 y_3} > 0$, random variation of y_1, $y_2 = [0.1; 10]y_1$, $y_3 = [0.1; 10]y_1$, x_i scattered between 10^{-4} and 10^{-2}.
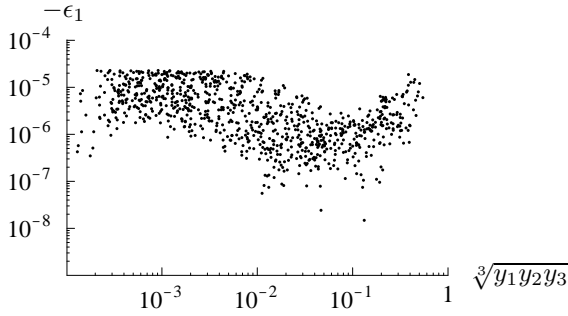
Figure 4.7: Correlation of $-\epsilon_1$ and $\sqrt[3]{y_1 y_2 y_3} > 0$, random variation of y_1, $y_2 = [0.1; 10]y_1$, $y_3 = [0.1; 10]y_1$, x_i scattered between 10^{-4} and 10^{-2}; $M_1 = 10^{11}$ GeV.
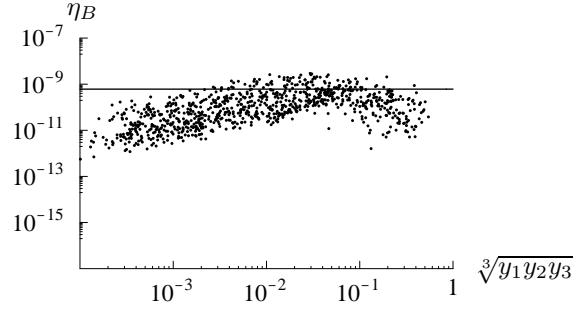
Figure 4.8: Correlation of η_B and $\sqrt[3]{y_1 y_2 y_3} > 0$, random variation of y_1, $y_2 = [0.1; 10]y_1$, $y_3 = [0.1; 10]y_1$, x_i scattered between 10^{-4} and 10^{-2}; $M_1 = 10^{11}$ GeV; straight line corresponds to eq. (3.68).

when considering the "less constrained" form of the R-matrix. This is a consequence of the weaker correlation of ϵ_1 and $\sqrt[3]{y_1 y_2 y_3}$, see Fig. 4.3.

4.3 Leptonic processes at low energies

In this section we discuss effects of various parameters on $Br\,(l_j \to l_i \gamma)$ and also on electric and magnetic dipole moments. In order to illustrate the results, they are displayed for each of the different SSB scenarios, performing the full one-loop RGE evolution numerically, see also appendix H.

Earlier works   Before discussing the numerical results on $Br\,(l_j \to l_i \gamma)$ of this analysis in detail, we want to summarize some of our results obtained in former studies on LFV in

low-energy and high-energy processes in the SUSY seesaw model with mSUGRA universality conditions: In [55] we have analyzed the possibility to probe the scale M_R of degenerate heavy Majorana neutrinos under the assumption of a real R-matrix. To this end, we have studied $Br\,(\mu \to e\gamma)$ and $Br\,(\tau \to \mu\gamma)$ in various mSUGRA benchmark scenarios proposed in [83]. Varying simultaneously over all neutrino oscillation parameters, we have derived upper bounds on M_R in these scenarios, if the rare decay $Br\,(\mu \to e\gamma)$ is not observed by future experiments. Moreover we have obtained intervals for the sensitivity on M_R provided that future measurements of $Br\,(\mu \to e\gamma)$ and/or $Br\,(\tau \to \mu\gamma)$ are successful. It turned out that for very light neutrino masses corresponding to $m_1 < 0.03$ eV, the measurement of $Br\,(\mu \to e\gamma) \approx 10^{-14}$ would probe M_R in the range $5 \cdot 10^{12}$ GeV to $5 \cdot 10^{14}$ GeV, depending on the mSUGRA scenario. On the other hand, a future measurement of $Br\,(\tau \to \mu\gamma)$ at a level of 10^{-9} will determine M_R in the range above $5 \cdot 10^{13}$ GeV with an accuracy of a factor of 2 for a specific scenario. In the case of quasi-degenerate light neutrinos, i. e. $m_1 \simeq 0.3$ eV, the upper bound from $Br\,(\mu \to e\gamma) < 10^{-14}$ is shifted to $(1-3) \cdot 10^{14}$ GeV, independently of the mSUGRA scenario.

Another interesting possibility is to search for LFV at a future e^+e^- linear collider, see references in [84]. We have studied in [84] possible signal cross-sections for lepton-flavor violating slepton production and decay $e^{\pm}e^- \to \sum_{i,j} \tilde{l}_j^{\pm}\tilde{l}_i^- \to l_{\beta}^{\pm}l_{\alpha}^- \tilde{\chi}_1^0\tilde{\chi}_1^0$, $\alpha \neq \beta$. The numerical results have been obtained in the context of the SUSY seesaw model under the assumptions explained before, i. e. real R-matrix and degenerate right-handed Majorana masses. We have considered those scenarios proposed in [83] leading to left-handed sleptons that can be pair-produced in the cms energy range (500-800) GeV. The cross-sections can in principle be as large as (1-10) fb, although they depend strongly on the SUSY parameters and on neutrino masses and mixings. On the other hand, the correlations between high-energy cross-sections and the branching ratios for the corresponding rare radiative decays are less influenced by experimental uncertainties in the neutrino parameters. It turns out that present bounds on $\mu \to e\gamma$ and $\tau \to \mu\gamma$ still allow sizeable signal rates at a LC. If the result from the PSI experiment would be $Br\,(\mu \to e\gamma) \lesssim 10^{-14}$, the cross-sections are constrained to be below 10^{-1} fb in these mSUGRA scenarios thus making it very challenging to search for such a signal. For more details of these works, the reader is referred to [55] and [84].

$Br\,(l_j \to l_i\gamma)$ **as a function of** M_R According to the leading logarithmic approximations eqs. (2.50), (2.63), (2.88), (2.115) and the mass insertion approximation eq. (3.10), we expect that $Br\,(l_j \to l_i\gamma)$ should be proportional to M_R^2 in the case of degenerate heavy Majorana masses, because of the form of $Y_{\nu}^{\dagger}LY_{\nu}$ in eq. (2.55). Figs. 4.9 to 4.12 show that this approximation is valid for a wide range of values of M_R assuming hierarchical light neutrino masses, vanishing phases and real R. As can be seen from eq. (3.11), the ratios of branching ratios are expected to remain approximately constant in the various scenarios if only M_R is varied. Numerically, this expectation is fulfilled in SPS 1a, $\tilde{G}$MSB, GMSB and also for $M_R \leq 10^{13}$ GeV in SPS 9 which can be seen in Figs. 4.9 to 4.12. In Tab. 4.7 the detailed ranges of the branching ratios resulting from a variation of M_R are shown, together with results based on the LL approximations where the parameters are
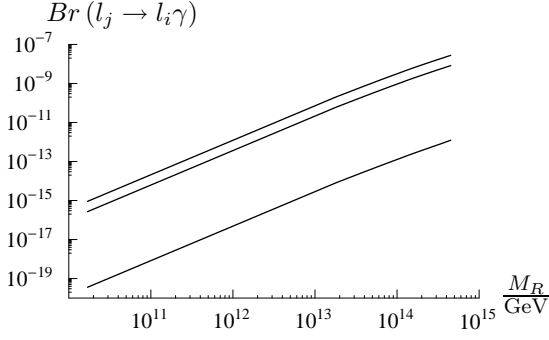
Figure 4.9: $Br\,(\tau \to \mu\gamma)$ (upper curve), $Br\,(\mu \to e\gamma)$ (middle curve), $Br\,(\tau \to e\gamma)$ (lower curve) as a function of $M_i \equiv M_R$, $\kappa_1 = 0$, scenario SPS 1a.
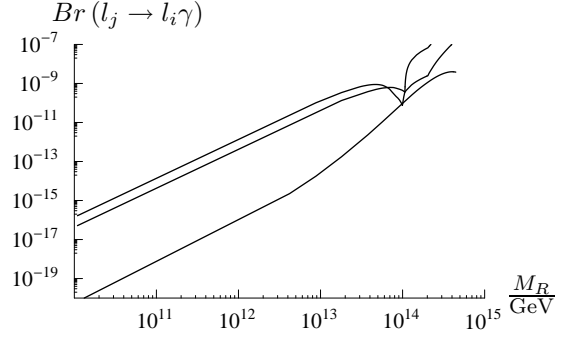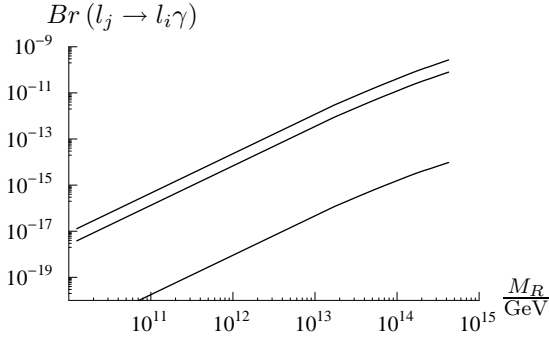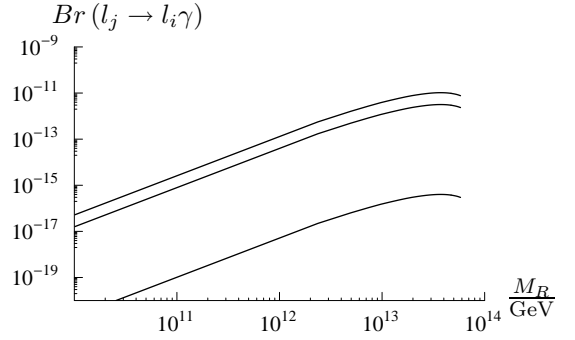
Figure 4.10: $Br\,(\tau \to \mu\gamma)$ (upper curve), $Br\,(\mu \to e\gamma)$ (middle curve), $Br\,(\tau \to e\gamma)$ (lower curve) as a function of $M_i \equiv M_R$, $\kappa_1 = 0$, scenario SPS 9.

Figure 4.11: $Br\,(\tau \to \mu\gamma)$ (upper curve), $Br\,(\mu \to e\gamma)$ (middle curve), $Br\,(\tau \to e\gamma)$ (lower curve) as a function of $M_i \equiv M_R$, $\kappa_1 = 0$, $\tilde{G}$MSB scenario.

Figure 4.12: $Br\,(\tau \to \mu\gamma)$ (upper curve), $Br\,(\mu \to e\gamma)$ (middle curve), $Br\,(\tau \to e\gamma)$ (lower curve) as a function of $M_i \equiv M_R$, $\kappa_1 = 0$, GMSB scenario.

evaluated at the GUT-scale for SPS 1a, SPS 9 and $\tilde{G}$MSB or at the messenger scale in the case of the GMSB scenario, respectively.

For hierarchical light neutrinos, vanishing phases, real R matrix and best-fit neutrino oscillation parameters according to Tab. 4.1 one obtains the generic results

$$\frac{Br\,(\tau \to \mu\gamma)}{Br\,(\mu \to e\gamma)} \;\approx\; 3 \tag{4.2}$$

$$\frac{Br\,(\mu \to e\gamma)}{Br\,(\tau \to e\gamma)} \;\approx\; 8 \cdot 10^3. \tag{4.3}$$

For these ratios, RGE evolution effects are not important, i. e. inserting the input values for the seesaw parameters would lead to the same approximate ratios as in eqs. (4.2) and (4.3). However as mentioned below eq. (2.93), for large values of neutrino Yukawa cou-

plings corresponding to $M_R > 10^{13}$ GeV, effects from additional contributions of neutrino Yukawa couplings become important in AMSB, leading to the deviations from the simple M_R^2 dependence in Fig. 4.10 for large M_R.

Non-degeneracy of M_i In order to demonstrate effects of non-degenerate heavy Majorana masses, we compare predictions for rare decays for degenerate Majorana masses, i. e. $M_i \equiv M_R$ and non-degenerate mass spectra in Tab. 4.8. Inserting the best-fit neutrino oscillation parameters and assuming a real R-matrix, $\kappa_1 = 0$ and vanishing phases, $Y_\nu^\dagger L Y_\nu$ at $\tan \beta = 10$ becomes

$$
\begin{aligned}
\left(Y_\nu^\dagger L Y_\nu\right)_{21} &\approx 8 \cdot 10^{-17} \frac{M_2}{\text{GeV}} \ln \frac{M_{GUT}}{M_2} + 9 \cdot 10^{-17} \frac{M_3}{\text{GeV}} \ln \frac{M_{GUT}}{M_3} \\
\left(Y_\nu^\dagger L Y_\nu\right)_{31} &\approx -1 \cdot 10^{-16} \frac{M_2}{\text{GeV}} \ln \frac{M_{GUT}}{M_2} + 9 \cdot 10^{-17} \frac{M_3}{\text{GeV}} \ln \frac{M_{GUT}}{M_3} \\
\left(Y_\nu^\dagger L Y_\nu\right)_{32} &\approx -1 \cdot 10^{-16} \frac{M_2}{\text{GeV}} \ln \frac{M_{GUT}}{M_2} + 8 \cdot 10^{-16} \frac{M_3}{\text{GeV}} \ln \frac{M_{GUT}}{M_3}.
\end{aligned} \tag{4.4}
$$

The form of eq. (4.4) shows that $Br(\tau \to e\gamma)$ is strongly suppressed in the case of degenerate M_i due to the approximate cancellation of the terms involving M_2 and M_3 in $\left(Y_\nu^\dagger L Y_\nu\right)_{31}$. For $Br(\mu \to e\gamma)$ the contributions from M_2 and M_3 in $\left(Y_\nu^\dagger L Y_\nu\right)_{21}$ are roughly of the same size, whereas for $Br(\tau \to \mu\gamma)$ the term proportional to M_3 is dominant. By increasing M_3 with respect to M_2 one therefore expects that particularly $Br(\tau \to e\gamma)$ is strongly enhanced, whereas $Br(\mu \to e\gamma)$ is suppressed compared to the other two decay modes. Moreover $Br(\tau \to \mu\gamma)$ is only weakly affected by a different hierarchy among M_2 and M_3. Numerically, a spectrum of $M_1 : M_2 : M_3 = 1 : 2 : 3$ leads to typical ratios such as

$$
\begin{aligned}
\frac{Br\left(\tau \to \mu\gamma\right)}{Br\left(\mu \to e\gamma\right)} &\approx 5 \\
\frac{Br\left(\mu \to e\gamma\right)}{Br\left(\tau \to e\gamma\right)} &\approx 2 \cdot 10^2.
\end{aligned} \tag{4.5}
$$

These ratios are roughly as expected from eq. (3.11), when eq. (4.4) is inserted in the LL approximations.

A hierarchical spectrum of right-handed neutrinos, i. e. $M_1 : M_2 : M_3 = 1 : 10 : 100$, leads to the numerical results

$$
\begin{aligned}
\frac{Br\left(\tau \to \mu\gamma\right)}{Br\left(\mu \to e\gamma\right)} &\approx 11 \\
\frac{Br\left(\mu \to e\gamma\right)}{Br\left(\tau \to e\gamma\right)} &\approx 10,
\end{aligned} \tag{4.6}
$$

which is also expected from eq. (4.4). It should be noted that the values given in eqs. (4.5) and (4.6) should be understood as typical values of these ratios for the parameter space considered. There are however some exceptional regions, to be discussed below, especially

SPS 1a			
	M_R	$y_i \equiv y$	m_1
$Br\left(\tau \to \mu\gamma\right)$	$9 \cdot 10^{-16}; 3 \cdot 10^{-8}$	$7.5 \cdot 10^{-11}; 5.4 \cdot 10^{-10}$	$8 \cdot 10^{-13}; 8 \cdot 10^{-11}$
$\dfrac{\left\|(\delta m_{\tilde{L}}^2)_{32}\right\|^2_{min}}{\left\|(\delta m_{\tilde{L}}^2)_{32}\right\|^2_{max}}$	$1 \cdot 10^{-8}$	0.14	0.01
$Br\left(\mu \to e\gamma\right)$	$3 \cdot 10^{-16}; 8 \cdot 10^{-9}$	$2.0 \cdot 10^{-11}; 3.1 \cdot 10^{-11}$	$7 \cdot 10^{-14}; 2 \cdot 10^{-11}$
$\dfrac{\left\|(\delta m_{\tilde{L}}^2)_{21}\right\|^2_{min}}{\left\|(\delta m_{\tilde{L}}^2)_{21}\right\|^2_{max}}$	$2 \cdot 10^{-8}$	0.64	0.004
SPS 9			
	M_R	$y_i \equiv y$	m_1
$Br\left(\tau \to \mu\gamma\right)$	$2 \cdot 10^{-16}; 1 \cdot 10^{-6}$	$1.3 \cdot 10^{-10}; 6.0 \cdot 10^{-10}$	$9 \cdot 10^{-14}; 1 \cdot 10^{-10}$
$\dfrac{\left\|(\delta m_{\tilde{L}}^2)_{32}\right\|^2_{min}}{\left\|(\delta m_{\tilde{L}}^2)_{32}\right\|^2_{max}}$	$6 \cdot 10^{-10}$	0.14	0.02
$Br\left(\mu \to e\gamma\right)$	$5 \cdot 10^{-17}; 2 \cdot 10^{-7}$	$3.7 \cdot 10^{-11}; 5.5 \cdot 10^{-11}$	$1 \cdot 10^{-14}; 4 \cdot 10^{-11}$
$\dfrac{\left\|(\delta m_{\tilde{L}}^2)_{21}\right\|^2_{min}}{\left\|(\delta m_{\tilde{L}}^2)_{21}\right\|^2_{max}}$	$2 \cdot 10^{-9}$	0.64	0.006
$\tilde{G}$MSB			
	M_R	$y_i \equiv y$	m_1
$Br\left(\tau \to \mu\gamma\right)$	$1 \cdot 10^{-17}; 3 \cdot 10^{-10}$	$1.3 \cdot 10^{-12}; 8.4 \cdot 10^{-12}$	$1 \cdot 10^{-14}; 1 \cdot 10^{-12}$
$\dfrac{\left\|(\delta m_{\tilde{L}}^2)_{32}\right\|^2_{min}}{\left\|(\delta m_{\tilde{L}}^2)_{32}\right\|^2_{max}}$	$9 \cdot 10^{-9}$	0.15	0.01
$Br\left(\mu \to e\gamma\right)$	$4 \cdot 10^{-18}; 8 \cdot 10^{-11}$	$3.4 \cdot 10^{-13}; 5.1 \cdot 10^{-13}$	$1 \cdot 10^{-15}; 4 \cdot 10^{-13}$
$\dfrac{\left\|(\delta m_{\tilde{L}}^2)_{21}\right\|^2_{min}}{\left\|(\delta m_{\tilde{L}}^2)_{21}\right\|^2_{max}}$	$1 \cdot 10^{-8}$	0.66	0.004
GMSB			
	M_R	$y_i \equiv y$	m_1
$Br\left(\tau \to \mu\gamma\right)$	$5 \cdot 10^{-17}; 1 \cdot 10^{-11}$	$3.9 \cdot 10^{-12}; 2.4 \cdot 10^{-11}$	$4 \cdot 10^{-14}; 4 \cdot 10^{-12}$
$\dfrac{\left\|(\delta m_{\tilde{L}}^2)_{32}\right\|^2_{min}}{\left\|(\delta m_{\tilde{L}}^2)_{32}\right\|^2_{max}}$	$6 \cdot 10^{-6}$	0.16	0.01
$Br\left(\mu \to e\gamma\right)$	$2 \cdot 10^{-17}; 3 \cdot 10^{-12}$	$1.1 \cdot 10^{-12}; 1.7 \cdot 10^{-12}$	$4 \cdot 10^{-15}; 1 \cdot 10^{-12}$
$\dfrac{\left\|(\delta m_{\tilde{L}}^2)_{21}\right\|^2_{min}}{\left\|(\delta m_{\tilde{L}}^2)_{21}\right\|^2_{max}}$	$6 \cdot 10^{-6}$	0.65	0.004

Table 4.7: Ranges of $Br\left(l_j \to l_i\gamma\right)$ that correspond to the variation of the corresponding parameter in the case of SPS 1a, SPS 9, $\tilde{G}$MSB and GMSB. Additional rows show the estimate of the effects of these variations based on the LL approximations eqs. (2.50), (2.63), (2.88) and (2.115).

SPS 1a			
	$M_i \equiv M_R$	$M_1\text{Diag}(1,2,3)$	$M_1\text{Diag}(1,10,100)$
$\frac{Br(\tau\to\mu\gamma)}{Br(\mu\to e\gamma)}$	3.36; 3.37	4.7; 5.0	11.0; 11.9
$\frac{m_\tau^5\Gamma_\mu}{m_\mu^5\Gamma_\tau}\frac{\left|\left(\delta m_{\tilde L}^2\right)_{32}\right|^2}{\left|\left(\delta m_{\tilde L}^2\right)_{21}\right|^2}$	3.2	4.7	11.0
$\frac{Br(\mu\to e\gamma)}{Br(\tau\to e\gamma)}$	$7.3\cdot10^3$; $7.5\cdot10^3$	191; 302	9.4; 11.3
$\frac{m_\mu^5\Gamma_\tau}{m_\tau^5\Gamma_\mu}\frac{\left|\left(\delta m_{\tilde L}^2\right)_{21}\right|^2}{\left|\left(\delta m_{\tilde L}^2\right)_{31}\right|^2}$	$1\cdot10^4$	216	10.3
SPS 9			
	$M_i \equiv M_R$	$M_1\text{Diag}(1,2,3)$	$M_1\text{Diag}(1,10,100)$
$\frac{Br(\tau\to\mu\gamma)}{Br(\mu\to e\gamma)}$	0.16; 27	2.6; 938	9.6; 16.6
$\frac{m_\tau^5\Gamma_\mu}{m_\mu^5\Gamma_\tau}\frac{\left|\left(\delta m_{\tilde L}^2\right)_{32}\right|^2}{\left|\left(\delta m_{\tilde L}^2\right)_{21}\right|^2}$	4.3	4.8	11.1
$\frac{Br(\mu\to e\gamma)}{Br(\tau\to e\gamma)}$	2.2; $7.7\cdot10^3$	0.02; $9\cdot10^3$	4.9; 14.1
$\frac{m_\mu^5\Gamma_\tau}{m_\tau^5\Gamma_\mu}\frac{\left|\left(\delta m_{\tilde L}^2\right)_{21}\right|^2}{\left|\left(\delta m_{\tilde L}^2\right)_{31}\right|^2}$	$3.2\cdot10^3$	227	10.2
$\tilde{\text{GMSB}}$			
	$M_i \equiv M_R$	$M_1\text{Diag}(1,2,3)$	$M_1\text{Diag}(1,10,100)$
$\frac{Br(\tau\to\mu\gamma)}{Br(\mu\to e\gamma)}$	3.37; 3.38	4.5; 5.0	10.4; 11.8
$\frac{m_\tau^5\Gamma_\mu}{m_\mu^5\Gamma_\tau}\frac{\left|\left(\delta m_{\tilde L}^2\right)_{32}\right|^2}{\left|\left(\delta m_{\tilde L}^2\right)_{21}\right|^2}$	3.2	4.7	11.0
$\frac{Br(\mu\to e\gamma)}{Br(\tau\to e\gamma)}$	$7.4\cdot10^3$; $8.1\cdot10^3$	204; 475	9.8; 13.0
$\frac{m_\mu^5\Gamma_\tau}{m_\tau^5\Gamma_\mu}\frac{\left|\left(\delta m_{\tilde L}^2\right)_{21}\right|^2}{\left|\left(\delta m_{\tilde L}^2\right)_{31}\right|^2}$	$2\cdot10^4$	216	10.4
GMSB			
	$M_i \equiv M_R$	$M_1\text{Diag}(1,2,3)$	$M_1\text{Diag}(1,10,100)$
$\frac{Br(\tau\to\mu\gamma)}{Br(\mu\to e\gamma)}$	3.268; 3.271	2.8; 4.8	5.0; 11.1
$\frac{m_\tau^5\Gamma_\mu}{m_\mu^5\Gamma_\tau}\frac{\left|\left(\delta m_{\tilde L}^2\right)_{32}\right|^2}{\left|\left(\delta m_{\tilde L}^2\right)_{21}\right|^2}$	3.16	4.3	9.0
$\frac{Br(\mu\to e\gamma)}{Br(\tau\to e\gamma)}$	$7.7\cdot10^3$; $7.9\cdot10^3$	$2\cdot10^2$; $8\cdot10^3$	10.5; 163
$\frac{m_\mu^5\Gamma_\tau}{m_\tau^5\Gamma_\mu}\frac{\left|\left(\delta m_{\tilde L}^2\right)_{21}\right|^2}{\left|\left(\delta m_{\tilde L}^2\right)_{31}\right|^2}$	$8\cdot10^3$	$1\cdot10^3$	30

Table 4.8: Minimal (maximal) ratios of $Br\left(l_j \to l_i\gamma\right)$ that correspond to a variation of the Majorana mass scales in different M_i mass spectra. Also the averaged estimates for these variations based on the LL eqs. (2.50), (2.63), (2.88) and (2.115) are shown.
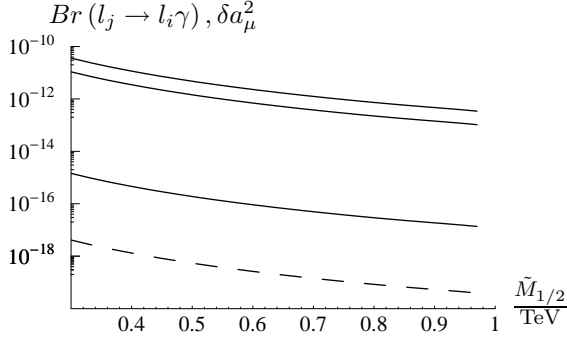
Figure 4.13: Curves of $Br\,(l_j \to l_i\gamma)$ as in Fig. 4.9 and δa_μ^2 (dashed) as a function of $\tilde{M}_{1/2}$, $M_i \equiv M_R = 10^{13}$ GeV, $\kappa_1 = 0$, scenario SPS 1a.
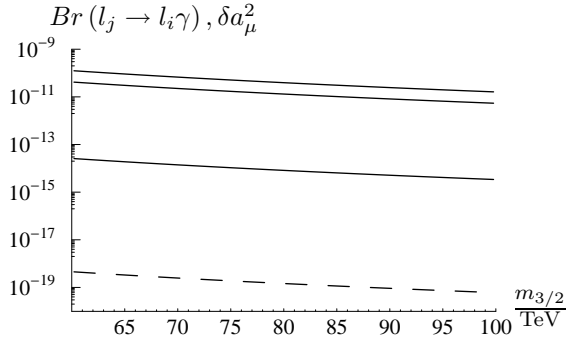
Figure 4.14: Curves of $Br\,(l_j \to l_i\gamma)$ as in Fig. 4.10 and δa_μ^2 (dashed) as a function of $m_{3/2}$, $M_i \equiv M_R = 10^{13}$ GeV, $\kappa_1 = 0$, scenario SPS 9.
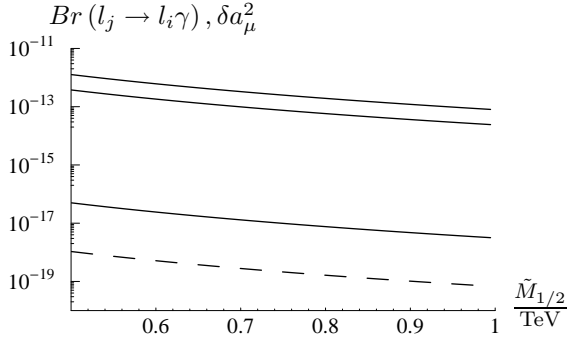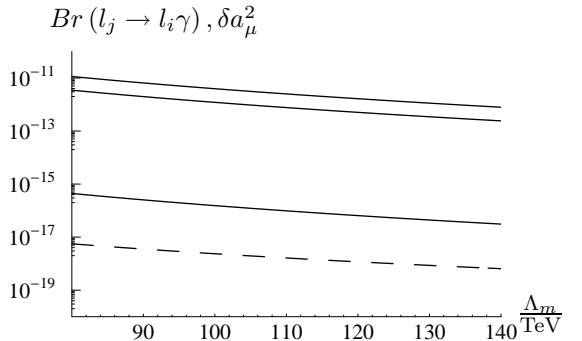
Figure 4.15: Curves of $Br\,(l_j \to l_i\gamma)$ as in Fig. 4.11 and δa_μ^2 (dashed) as a function of $\tilde{M}_{1/2}$, $M_i \equiv M_R = 10^{13}$ GeV, $\kappa_1 = 0$, $\tilde{G}$MSB scenario.

Figure 4.16: Curves of $Br\,(l_j \to l_i\gamma)$ as in Fig. 4.12 and δa_μ^2 (dashed) as a function of Λ_m, $M_i \equiv M_R = 10^{13}$ GeV, $\kappa_1 = 0$, GMSB scenario.

in SPS 9 and GMSB scenarios, where large deviations from eqs. (4.5) and (4.6) arise which are included in the ranges of Tab. 4.7. In the AMSB scenario SPS 9 the predictions from eqs. (4.5) and (4.6) hold well for $M_R < 10^{13}$ GeV, before effects from additional contributions of neutrino Yukawa couplings become important. In the case of GMSB, sizeable LFV rates are only possible if the messenger scale M_m is larger than the corresponding heavy Majorana neutrino scale. If $M_m \lesssim M_i$, the different LFV rates are damped and the ratios based on the leading logarithmic approximations eqs. (4.5) and (4.6) differ from the numerical results.

Differences between different SUSY breaking models The branching ratios $Br\,(l_j \to l_i\gamma)$ generically depend on the mass scales of the sleptons, neutralinos and charginos in the loops and are enhanced by $\tan^2\beta$. From eq. (3.10) it is also obvious
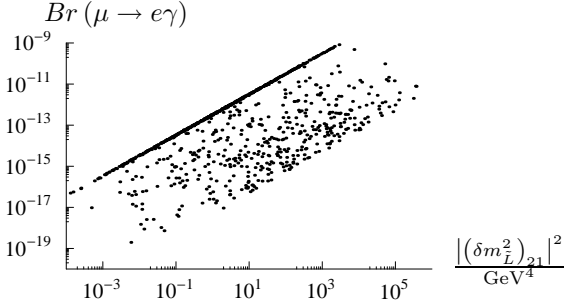
Figure 4.17: Correlation of $Br\left(\mu \to e\gamma\right)$ and $\left|\left(\delta m_{\tilde{L}}^2\right)_{21}\right|^2$, scattering over all parameters, scenario SPS 1a; thick line corresponds to $(\tilde{M}_{1/2}, m_0) = (250, 100)$ GeV.
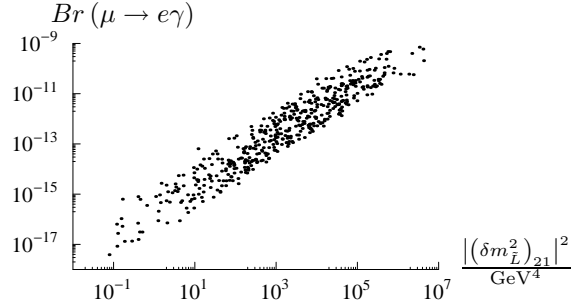
Figure 4.18: Correlation of $Br\left(\mu \to e\gamma\right)$ and $\left|\left(\delta m_{\tilde{L}}^2\right)_{21}\right|^2$, scattering over all parameters, scenario SPS 9.
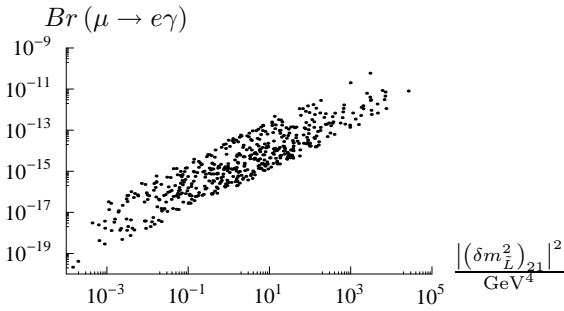
Figure 4.19: Correlation of $Br\left(\mu \to e\gamma\right)$ and $\left|\left(\delta m_{\tilde{L}}^2\right)_{21}\right|^2$, scattering over all parameters, $\tilde{G}$MSB scenario.
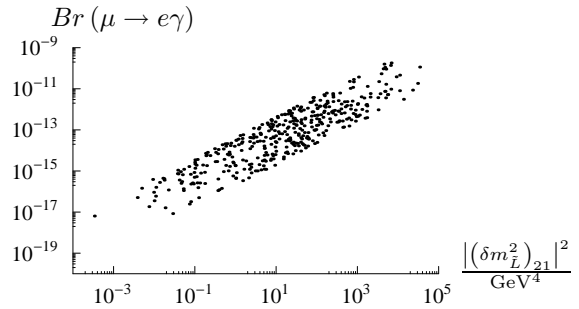
Figure 4.20: Correlation of $Br\left(\mu \to e\gamma\right)$ and $\left|\left(\delta m_{\tilde{L}}^2\right)_{21}\right|^2$, scattering over all parameters, GMSB scenario.

that the size of the off-diagonal mass terms $\delta m_{\tilde{L}}^2$ is very important. By comparison of the approximate form of $\left|\delta m_{\tilde{L}}^2\right|^2$ in eqs. (2.50), (2.63), (2.88), (2.115), one can deduce that these terms are expected to be largest in the case of mSUGRA and AMSB. Assuming similar size of the high-energy SSB terms and neglecting trilinear terms, we expect from these LL approximations that the branching ratios in $\tilde{G}$MSB and GMSB models should be suppressed by roughly a factor of 0.5. In principle one also has to consider effects from trilinear terms and also terms involving $m_{3/2}^2$ in AMSB that modify this naive estimate. For a rough understanding of the quantitative differences in $Br\left(l_j \to l_i\gamma\right)$ of the models, the effects of sparticle masses in the loop and $\tan\beta$ have also to be taken into account.

In order to illustrate the ranges of slepton and gaugino masses that correspond to a variation of the SUSY-scale, we show the mass of heaviest slepton and of the wino for

light and heavy SUSY-scales in the different scenarios:

- SPS 1a: $m_{\tilde{l}_6} = (206; 779)$ GeV, $\tilde{M}_2 = (188; 765)$ GeV

$$\tilde{M}_{1/2} = (0.25; 1) \text{ TeV}, \qquad m_0 = -A_0 = 0.4 \, \tilde{M}_{1/2} \tag{4.7}$$

- SPS 9: $m_{\tilde{l}_6} = (400; 651)$ GeV, $\tilde{M}_2 = (167; 274)$ GeV

$$m_{3/2} = (60; 100) \text{ TeV} \tag{4.8}$$

- $\tilde{G}$MSB: $m_{\tilde{l}_6} = (375; 700)$ GeV, $\tilde{M}_2 = (386; 782)$ GeV

$$\tilde{M}_{1/2} = (0.5; 1) \text{ TeV} \tag{4.9}$$

- GMSB: $m_{\tilde{l}_6} = (306; 590)$ GeV, $\tilde{M}_2 = (170; 337)$ GeV

$$\Lambda_m = (80; 140) \text{ TeV}, \qquad M_m = (0.66; 1.33) \cdot 10^{14} \text{ GeV} \tag{4.10}$$

The mass $m_{\tilde{l}_6}$ is a measure of the masses of left-handed sleptons and the wino mass is a typical mass scale for gaugino masses in both diagrams of Fig. 3.1. Increasing the scale of SUSY breaking typically leads to a reduction of leptonic dipole moments, because for heavier slepton and gaugino masses, the loop contributions are more suppressed. In order to demonstrate this behavior, we show in Figs. 4.13 to 4.16 both branching ratios and δa_μ^2 when the SUSY-scale is increased. This is done along the model lines in the case of SPS 1a and SPS 9, whereas for $\tilde{G}$MSB we varied $\tilde{M}_{1/2}$ within a factor of 2, as specified in eqs. (4.7) to (4.9). In the case of GMSB, the SSB masses increase with Λ_m which is varied in the interval (80-140) TeV. It can be seen that for a variation of the SUSY-scale, δa_μ^2 scales in the same way as the branching ratios, as expected from eq. (3.31). In Figs. 4.17 to 4.20 we show the correlation of $Br(\mu \to e\gamma)$ to the RG-induced slepton mass terms $\left|\left(\delta m_{\tilde{L}}^2\right)_{21}\right|^2$. From the mass-insertion approximation eq. (3.10), we expect $Br(\mu \to e\gamma)$ to scale as $\left|\left(\delta m_{\tilde{L}}^2\right)_{21}\right|^2$ which can also be seen in Figs. 4.17 to 4.20, apart from scattering effects. In these figures, we have scattered simultaneously over the following parameters:

- Neutrino oscillation parameters are varied in their 3σ CL interval, phases are scattered in the interval $[0; 2\pi]$.

- The real parts x_i of the mixing angles of the R-matrix are also varied in $[0; 2\pi]$.

- The imaginary parts y_i of the mixing angles of the R-matrix are scattered in the range $[0.0001; 1]$.

- M_1 is in the interval $[10^{10} - 10^{13}]$ GeV, the other heavy Majorana masses are randomly chosen in the ranges $M_2 = [1; 10] \, M_1$, $M_3 = [1; 10] \, M_2$.

- m_1 varies in the interval $[0.0001; 0.3]$ eV.

- The SUSY-scales are varied in the ranges corresponding to eqs. (4.7) to (4.10).

Note that these ranges of variation are referred to as "scattering over all parameters" in the following. The different ranges of scattering around an ideal correlation stems from the different variation of the SUSY-scales and therefore different ranges for the mass scales in the loops. The largest range of scattering is thus understandable in SPS 1a, where slepton masses and gaugino masses increase by roughly a factor of 4 through the variation of the SUSY-scale along the model line, see eq. (4.7). In order to make this point clear we also show in Fig. 4.17 the corresponding correlation when all seesaw parameters are simultaneously varied and the SUSY-scale is kept fixed in SPS 1a. This leads to the narrow line in Fig. 4.17, demonstrating that the variation of the SUSY-scale is indeed the reason for the spread in the correlation of Figs. 4.17 to 4.20 which also implies that the scaling of $Br\left(l_j \to l_i\gamma\right)$ with $\left|\left(\delta m_{\tilde{L}}^2\right)_{21}\right|^2$ holds even for the most general choices of seesaw parameters. If all lepton-flavor conserving masses are fixed, results on $Br\left(\mu \to e\gamma\right)$ lead to bounds on $\left(\delta m_{\tilde{L}}^2\right)_{21}$, e. g. $Br\left(\mu \to e\gamma\right) < 10^{-11}$ implies $\left|\left(\delta m_{\tilde{L}}^2\right)_{21}\right|^2 <$ (a few) GeV^2 in SPS 1a.

Effects of m_1 on $Br\left(l_j \to l_i\gamma\right)$ We show the dependence on the mass scale m_1 of the lightest neutrino in Figs. 4.21 to 4.24 in the case of SPS 1a, SPS 9, $\tilde{G}$MSB and GMSB, respectively. These results have been obtained assuming degenerate $M_i \equiv M_R = 10^{13}$ GeV, real R-matrix and vanishing phases. It can be seen that there is a strong suppression of all branching ratios if $m_1 \gtrsim \sqrt{m_{31}^2}$. A suppression of $Br\left(l_j \to l_i\gamma\right)$ with increasing m_1 is expected by comparing eqs. (3.13) and (3.14): In the limit of quasi-degenerate light neutrinos, the branching ratios $Br\left(l_j \to l_i\gamma\right)$ are then suppressed by $\frac{\sqrt{\Delta m_{21}^2}}{2m_1}$ and $\frac{\sqrt{\Delta m_{31}^2}}{2m_1}$ as compared to the hierarchical case. The ranges of the branching ratios resulting from a variation of m_1 can be seen in Tab. 4.7, together with results based on the LL approximations. In order to demonstrate the effect of a varying m_1-scale, we show its effect in $Y_\nu^\dagger L Y_\nu$ explicitly,

$$\left(Y_\nu^\dagger L Y_\nu\right)_{21} \approx 10^{-14}\frac{M_R}{\mathrm{GeV}}\frac{m_1}{\mathrm{eV}}\ln\frac{M_{GUT}}{M_R}\left(-1 + \sqrt{1 + \frac{\Delta m_{21}^2}{m_1^2}} + 0.2\sqrt{1 + \frac{\Delta m_{31}^2}{m_1^2}}\right) \quad (4.11)$$

$$\left(Y_\nu^\dagger L Y_\nu\right)_{31} \approx 10^{-14}\frac{M_R}{\mathrm{GeV}}\frac{m_1}{\mathrm{eV}}\ln\frac{M_{GUT}}{M_R}\left(1 - \sqrt{1 + \frac{\Delta m_{21}^2}{m_1^2}} + 0.2\sqrt{1 + \frac{\Delta m_{31}^2}{m_1^2}}\right) \quad (4.12)$$

$$\left(Y_\nu^\dagger L Y_\nu\right)_{32} \approx 10^{-14}\frac{M_R}{\mathrm{GeV}}\frac{m_1}{\mathrm{eV}}\ln\frac{M_{GUT}}{M_R}\left(-0.5 - \sqrt{1 + \frac{\Delta m_{21}^2}{m_1^2}} + 2\sqrt{1 + \frac{\Delta m_{31}^2}{m_1^2}}\right). \quad (4.13)$$

Evaluating eq. (4.12) we see that $\left(Y_\nu^\dagger L Y_\nu\right)_{31}$ increases up to $m_1 \approx 0.01$ eV, before the decrease for quasi-degenerate light neutrinos sets in. Note also that suppression factors of
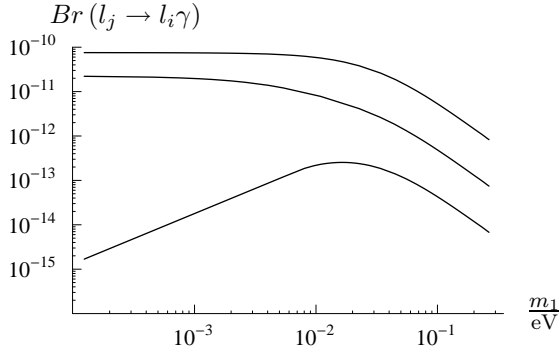
Figure 4.21: Curves of $Br\,(l_j \to l_i\gamma)$ as a function of m_1, $M_i \equiv M_R = 10^{13}$ GeV, scenario SPS 1a.
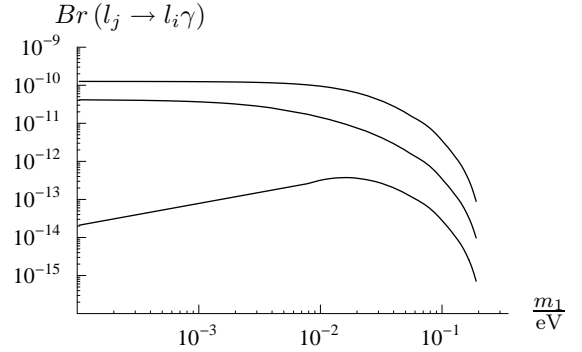
Figure 4.22: Curves of $Br\,(l_j \to l_i\gamma)$ as a function of m_1, $M_i \equiv M_R = 10^{13}$ GeV, scenario SPS 9.
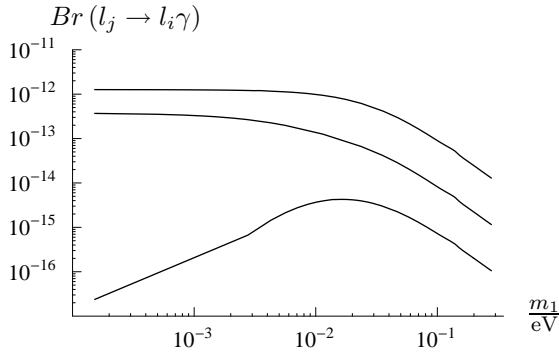
Figure 4.23: Curves of $Br\,(l_j \to l_i\gamma)$ as a function of m_1, $M_i \equiv M_R = 10^{13}$ GeV, $\tilde{G}$MSB scenario.
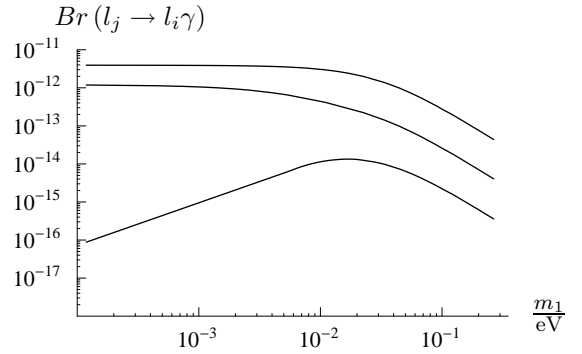
Figure 4.24: Curves of $Br\,(l_j \to l_i\gamma)$ as a function of m_1, $M_i \equiv M_R = 10^{13}$ GeV, GMSB scenario.

roughly $3\cdot 10^{-3}$ and $9\cdot 10^{-3}$ are obtained from eqs. (4.11) and (4.13), when m_1 is increased from 0 to 0.3 eV in $\left|\left(Y_\nu^\dagger L Y_\nu\right)_{21}\right|^2$ and $\left|\left(Y_\nu^\dagger L Y_\nu\right)_{32}\right|^2$, respectively. On the other hand, $\left|\left(Y_\nu^\dagger L Y_\nu\right)_{31}\right|^2$ is enhanced by a factor of 2. The different m_1-dependence of $\left|\left(Y_\nu^\dagger L Y_\nu\right)_{32}\right|^2$ or $\left|\left(Y_\nu^\dagger L Y_\nu\right)_{21}\right|^2$ as compared to $\left|\left(Y_\nu^\dagger L Y_\nu\right)_{31}\right|^2$ for $m_1 \ll \sqrt{\Delta m_{31}^2}$ can be understood as follows: In the region of small m_1, the effect of m_1 mainly comes from the "interference" of terms proportional to $m_1 \times \sqrt{\Delta m_{31}^2}$. This term obtains a negative sign in eqs. (4.11) and (4.13), as opposed to eq. (4.12). The order of magnitude of the suppression factor can also be seen in Fig. 4.21 or in Tab. 4.7. For accurate numerical predictions one has to include the full one-loop RG running.

The authors of [85] have analyzed the RG running of neutrino masses, mixing angles and phases. It has been demonstrated that the RGE effects are generically enhanced in the case of very large $\tan\beta$ or in the case of quasi-degenerate light neutrinos. More specifically, the enhancement of RGE effects of τ Yukawa couplings for neutrino parameters scales as
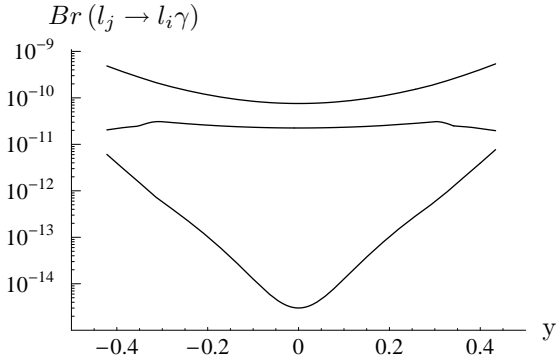
Figure 4.25: $Br\left(l_j \to l_i\gamma\right)$ as a function of $y_i \equiv y$, $M_i \equiv M_R = 10^{13}$ GeV, $\kappa_1 = 0$, scenario SPS 1a.
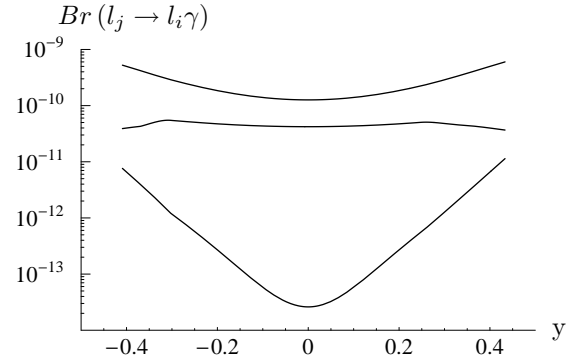
Figure 4.26: $Br\left(l_j \to l_\gamma\right)$ as a function of $y_i \equiv y$, $M_i \equiv M_R = 10^{13}$ GeV, $\kappa_1 = 0$, scenario SPS 9.
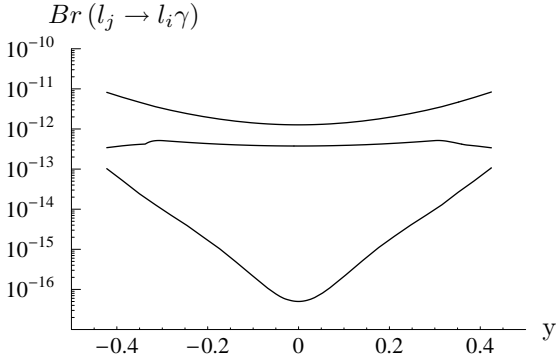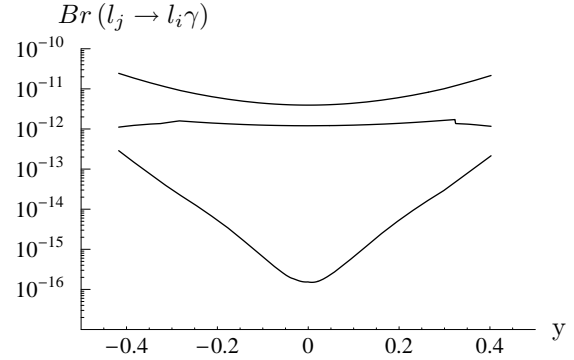

Figure 4.27: $Br\left(l_j \to l_\gamma\right)$ as a function of $y_i \equiv y$, $M_i \equiv M_R = 10^{13}$ GeV, $\kappa_1 = 0$, $\tilde{G}$MSB scenario.

Figure 4.28: $Br\left(l_j \to l_i\gamma\right)$ as a function of $y_i \equiv y$, $M_i \equiv M_R = 10^{13}$ GeV, $\kappa_1 = 0$, GMSB scenario.

$\tan^2\beta$ and the RGE effects of neutrino Yukawa couplings increase for quasi-degenerate light neutrino states. Apart from the effects of quasi-degenerate neutrinos discussed here, we work in the limit of hierarchical light neutrinos and small or moderate values of $\tan\beta$, so that RG effects for the neutrino masses and mixings are less pronounced, though we include them in our numerical predictions.

Effects of y on $Br\left(l_j \to l_i\gamma\right)$ The effect of a variation of the imaginary part $y \equiv y_i$ in the R-matrix is shown in Figs. 4.25, 4.26, 4.27 and 4.28 assuming degenerate $M_i = 10^{13}$ GeV, hierarchical light neutrinos, vanishing x_i and phases. The detailed ranges of the branching ratios resulting from a variation of y can be seen in Tab. 4.7, together with results based on the LL approximations eqs. (2.50), (2.63), (2.88), (2.115). The basic y-dependence for small y is estimated in eq. (3.17). Using the input values of the neutrino parameters

according to Figs. 4.25 to 4.28 in this approximation yields

$$
\begin{aligned}
\left| \left(Y_\nu^\dagger L Y_\nu \right)_{21} \right|^2 &\approx 2 \cdot 10^{-4} + 4 \cdot 10^{-3} y^2 \\
\left| \left(Y_\nu^\dagger L Y_\nu \right)_{31} \right|^2 &\approx 1 \cdot 10^{-7} + 2 \cdot 10^{-3} y^2 \\
\left| \left(Y_\nu^\dagger L Y_\nu \right)_{32} \right|^2 &\approx 3 \cdot 10^{-3} + 3 \cdot 10^{-2} y^2,
\end{aligned}
\tag{4.14}
$$

where higher powers of y have been neglected. Eq. (4.14) clearly shows that we expect a strong increase of $Br(\tau \to e\gamma)$ with increasing y. In Figs. 4.25, 4.26, 4.27 and 4.28 we actually see the increase of $Br(\tau \to e\gamma)$ over roughly two orders of magnitude. As has been mentioned before, we cannot consider arbitrarily large y-values, because Y_ν has to stay perturbative. For $M_R = 10^{13}$ GeV, this corresponds approximately to $y \lesssim 0.4$.
From eqs. (4.14) one expects a much smaller y-dependence in the decay modes $Br(\tau \to \mu\gamma)$ and $Br(\mu \to e\gamma)$. This behavior is confirmed in Figs. 4.25 to 4.28. Moreover, numerically it turns out that $Br(\tau \to \mu\gamma)$ has a stronger y-dependence than $Br(\mu \to e\gamma)$, a conclusion that could not be drawn from the simple approximations in eqs. (4.14). It should be emphasized that for a lower M_R scale, perturbativity allows larger values of y, e. g. $y \lesssim 1$ for $M_R \simeq 10^{11}$ GeV. Then the effects of y can be strongly enhanced, as compared to a Majorana mass scale of 10^{13} GeV.

Effects of x_i on $Br(\mu \to e\gamma)$ We study effects of the real mixing angles x_i of the R-matrix for vanishing imaginary angles $y_i = 0$ and phases, hierarchical light and heavy neutrinos in the case of $Br(\mu \to e\gamma)$. The corresponding Figures 4.29 to 4.32 show the dependence of $Br(\mu \to e\gamma)$ on a single x_i, assuming $M_1 = 10^{11}$ GeV and $M_1 : M_2 : M_3 = 1 : 10 : 100$, also referred to as "spectrum I" for the heavy Majorana masses. In this case the approximations based on eq. (3.18) are relevant, leading to

$$
\begin{aligned}
\left(Y_\nu^\dagger L Y_\nu \right)_{21} &\simeq \sqrt{\kappa_3} U_{13}^* \left(M_3 \ln \frac{M_{GUT}}{M_3} c_1 \left(U_{22} s_1 \sqrt{\kappa_2} + U_{23} c_1 \sqrt{\kappa_3} \right) \right. \\
&\qquad \left. - M_2 \ln \frac{M_{GUT}}{M_2} s_1 \left(U_{22} c_1 \sqrt{\kappa_2} - U_{23} s_1 \sqrt{\kappa_3} \right) \right) \\
&\quad + \sqrt{\kappa_2} U_{12}^* \left(M_2 \ln \frac{M_{GUT}}{M_2} c_1 \left(U_{22} c_1 \sqrt{\kappa_2} - U_{23} s_1 \sqrt{\kappa_3} \right) \right. \\
&\qquad \left. + M_3 \ln \frac{M_{GUT}}{M_3} s_1 \left(U_{22} s_1 \sqrt{\kappa_2} + U_{23} c_1 \sqrt{\kappa_3} \right) \right)
\end{aligned}
\tag{4.15}
$$

$$
\begin{aligned}
\left(Y_\nu^\dagger L Y_\nu \right)_{21} &\simeq \kappa_2 M_2 \ln \frac{M_{GUT}}{M_2} U_{12}^* U_{22} \\
&\quad + \kappa_3 U_{13}^* U_{23} \left(M_3 \ln \frac{M_{GUT}}{M_3} c_2^2 + M_1 \ln \frac{M_{GUT}}{M_1} s_2^2 \right)
\end{aligned}
\tag{4.16}
$$

$$
\begin{aligned}
\left(Y_\nu^\dagger L Y_\nu \right)_{21} &\simeq \kappa_3 M_3 \ln \frac{M_{GUT}}{M_3} U_{13}^* U_{23} \\
&\quad + \kappa_2 U_{12}^* U_{22} \left(M_2 \ln \frac{M_{GUT}}{M_2} c_3^2 + M_1 \ln \frac{M_{GUT}}{M_1} s_3^2 \right),
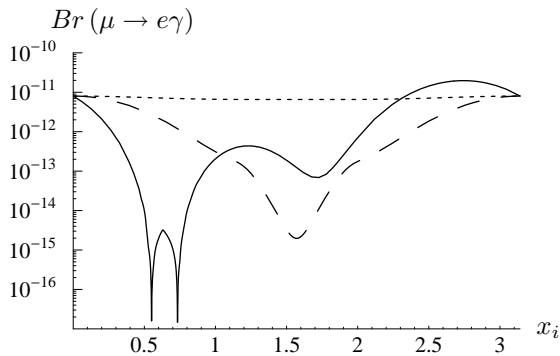\end{aligned}
\tag{4.17}
$$

$Br\,(\mu \to e\gamma)$

Figure 4.29: $Br\,(\mu \to e\gamma)$ as a function of x_1(full curve), x_2 (long-dashed curve), x_3 (short-dashed curve), $y = 0$, spectrum I, $\kappa_1 = 0$, scenario SPS 1a.
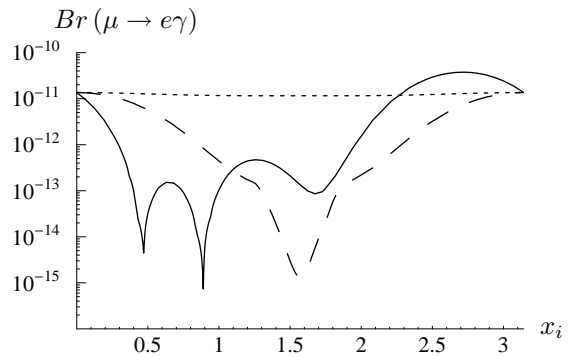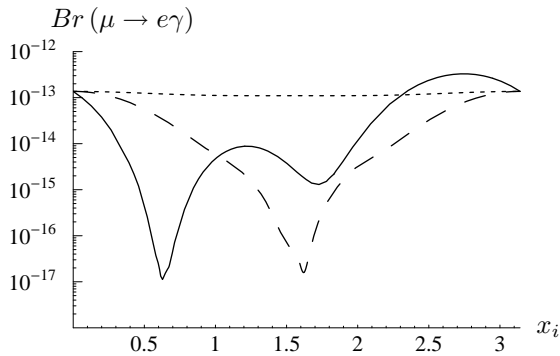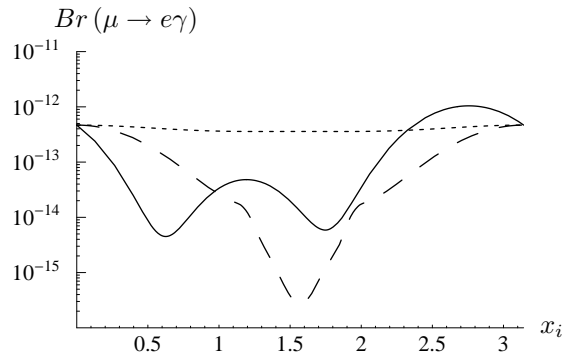
Figure 4.30: $Br\,(\mu \to e\gamma)$ as a function of x_1(full curve), x_2 (long-dashed curve), x_3 (short-dashed curve), $y = 0$, spectrum I, $\kappa_1 = 0$, scenario SPS 9.

Figure 4.31: $Br\,(\mu \to e\gamma)$ as a function of x_1(full curve), x_2 (long-dashed curve), x_3 (short-dashed curve), $y = 0$, spectrum I, $\kappa_1 = 0$, $\tilde{G}$MSB scenario.

Figure 4.32: $Br\,(\mu \to e\gamma)$ as a function of x_1(full curve), x_2 (long-dashed curve), x_3 (short-dashed curve), $y = 0$, spectrum I, $\kappa_1 = 0$, GMSB scenario.

in the case where only x_1, x_2 or x_3 are non-vanishing. In the above equations, the abbreviation $s_i(c_i) \equiv \sin x_i(\cos x_i)$, $i = 1, 2, 3$ is used.

From eq. (4.15) we see that cancellations in terms proportional to M_3 are possible if

$$\tan x_1 \;\; = \;\; -\sqrt{\frac{\kappa_3}{\kappa_2}}\frac{U_{23}}{U_{22}}, \quad x_1 \approx -1.3 \tag{4.18}$$

$$\tan x_1 \;\; = \;\; -\sqrt{\frac{\kappa_3}{\kappa_2}}\frac{U_{13}^*}{U_{12}^*}, \quad x_1 \approx -0.3, \tag{4.19}$$

as has also been discussed in [35]. It is clear from the above that in the limit of $\theta_{13} = 0$, the cancellation corresponding to eq. (4.18) occurs at $x_1 = 0$, whereas the best fit value for
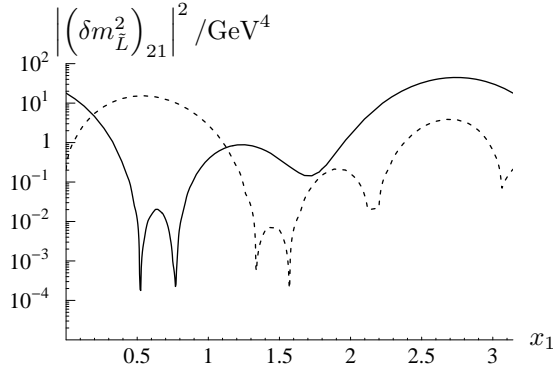
PSfrag replacements

Figure 4.33: $\left|\left(m_{\tilde{L}}^2\right)_{21}\right|^2/\mathrm{GeV}^4$ acc. to LL eq. (2.50) as a function of x_1. Full (short-dashed) curve corresponds to $\sin^2\theta_{13} = 0.006\ (0)$, $y = 0$, spectrum I, $\kappa_1 = 0$, scenario SPS 1a.

$\theta_{13} = 0$ moves this kink towards negative x_1. Due to the periodicity of the trigonometric functions this corresponds to a kink near $x_1 = 2.8$. The other cancellation then occurs near $x_1 = 1.9$. For the precise values of these cancellations one has to take into account the RG evolution of the neutrino parameters, as has been done numerically. The different cancellations already occur in the LL terms $\left|\left(\delta m_{\tilde{L}}^2\right)_{21}\right|^2$, as can be seen from Fig. 4.33. In order to demonstrate the large impact of θ_{13}, we show curves for its best-fit value and also for vanishing θ_{13}. Notice that the kinks in both curves are shifted and that for $\theta_{13} = 0$ the rate $Br\,(\mu \to e\gamma)$ is suppressed near $x_1 = 0$, as is obvious from eq. (4.19), see also [35]. From eq. (4.15) it follows that cancellations arise for $\cos x_1 = 0$, i. e. $x_1 = \frac{\pi}{2} \approx 1.6$. Moreover, cancellations in terms proportional to M_2 are possible for

$$\tan x_1 = \sqrt{\frac{\kappa_2}{\kappa_3}}\frac{U_{22}}{U_{23}}, \qquad x_1 \approx 0.3, \qquad (4.20)$$

and also between contributions involving M_2 and M_3.

In the case of non-vanishing x_2 and the best-fit values for neutrino parameters, it turns out that the the coefficient of c_2^2 is the dominant term, so that for $Br\,(\mu \to e\gamma)$ we expect a dependence similar to c_2^4, i. e. being minimal around $x_2 = \frac{\pi}{2}$.

If only x_3 is non-vanishing, the term proportional to $\kappa_3 M_3$ is clearly dominating and independent of x_3, so that there is virtually no x_3-dependence in $Br\,(\mu \to e\gamma)$.

Effects on δa_μ and EDMs   Recently, there has been a work on magnetic and electric dipole moments in the SPS 1a scenario [56]. The authors have taken into account all possible SUSY phases and generic LFV mass terms and have shown that in the most general case SUSY phases can be large and still be consistent with experimental bounds. Moreover a variation of δa_μ by a factor of up to 3 has been reported together with EDMs
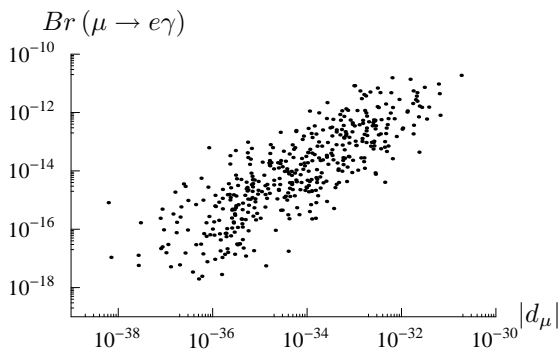
Figure 4.34: Correlation of $|d_\mu|/$ecm and $Br\,(\mu \to e\gamma)$, scattering over all parameters, scenario SPS 1a.
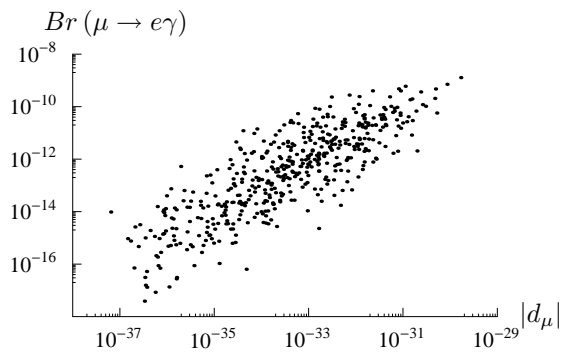

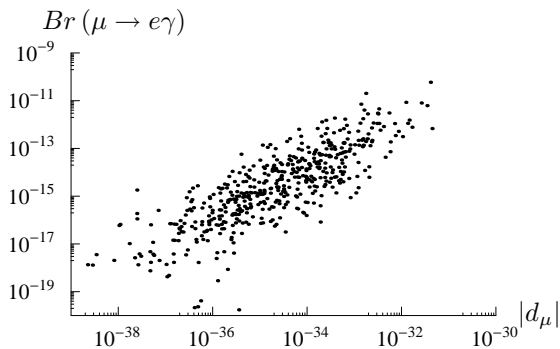Figure 4.35: Correlation of $|d_\mu|/$ecm and $Br\,(\mu \to e\gamma)$, scattering over all parameters, scenario SPS 9.

Figure 4.36: Correlation of $|d_\mu|/$ecm and $Br\,(\mu \to e\gamma)$, scattering over all parameters, $\tilde{G}$MSB scenario.

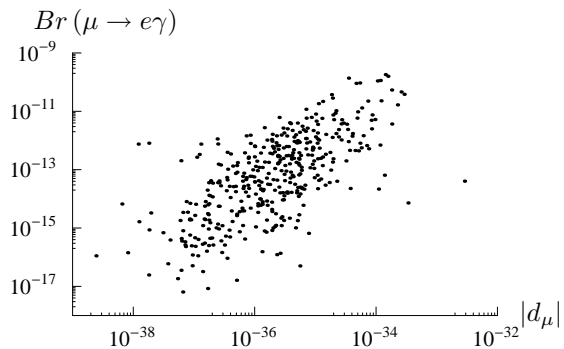Figure 4.37: Correlation of $|d_\mu|/$ecm and $Br\,(\mu \to e\gamma)$, scattering over all parameters, GMSB scenario.

that can be expected to be measured. In [86] the authors have analyzed the impact of a large mixing of smuons and staus on the muon anomalous magnetic moment in the decoupling solution, i. e. sfermion masses of the third generation are assumed to be below 1 TeV, while those of the first two generations should be a heavier, e. g. 10 TeV. In this case it has been demonstrated that LFV mixings between relatively light sleptons of the third generation and heavy second generation sleptons can significantly enhance δa_μ. We have studied effects on δa_μ and EDMs in the SUSY seesaw model and have found that, even in for the most general cases of seesaw parameters the effects on the muon magnetic dipole moment are tiny. This can be expected from the approximate results in section 3.2 implying that relatively small off-diagonal slepton mass terms, i. e. relatively small mixing angles only correspond to tiny shifts in δa_μ.

Imaginary parts in the combination $Y_\nu^\dagger Y_\nu$ of neutrino Yukawa couplings generate leptonic EDMs in the SUSY seesaw model, so that for the most general choices of Y_ν and allowing complex entries, an increase in the magnitude and/or the imaginary parts in Y_ν leads

to larger EDMs. This also implies that leptonic EDMs and lepton-flavor violating decay rates should be approximately correlated when the seesaw parameters are varied simultaneously. The correlation between $|d_\mu|/$ecm and $Br\,(\mu \to e\gamma)$ is shown in Figs. 4.34 to 4.37 for the different scenarios, demonstrating that this correlation is rather weak for a simultaneous variation of all parameters. In principle constraints from a measurement of $Br\,(\mu \to e\gamma)$ on the muon electric dipole moment are possible. However the maximal values of $|d_\mu|/$ecm are below the sensitivities of future experiments for the parameters considered here. Nevertheless the work of [38] has shown that leptonic EDMs strongly increase for large hierarchies among M_i masses and also specific textures in Y_ν or larger values of trilinear terms A_e can enhance EDMs to a level that can be tested in future experiments. As has been also pointed out in [38], particularly for non-degenerate M_i, no strong correlation is expected between d_μ and d_e, because of additional contributions to A_e that violate naive scaling of the form eq. (3.50). We show the correlation between $|d_\mu|/$ecm and $|d_e|/$ecm for a simultaneous variation of all parameters in Figs. 4.38 to 4.41. Both leptonic EDMs are typically far below future experimental sensitivities, however as mentioned above, a strong enhancement is possible. As expected, $|d_\mu|$ and $|d_e|$ are only weakly correlated for the simultaneous variation of all parameters considered.

Effects of non-vanishing lepton masses in loop integrals   The difference between the results for branching ratios using exact one-loop results presented in appendix F and the well-known results from [31] for $Br\,(l_j \to l_i\gamma)$ are mainly due to the phase space factor in eq. (3.4). Taking into account the non-vanishing lepton masses in the two-body decay phase space corresponds to a factor of $\frac{\left(m_{l_j}^2 - m_{l_i}^2\right)^3}{m_{l_j}}$, as compared to $m_{l_j}^5$ in the standard approximation. This factor yields a reduction of the exact one-loop result by a factor of 0.989 in $Br\,(\tau \to \mu\gamma)$, while for $Br\,(\tau \to \mu\gamma)$ and $Br\,(\tau \to e\gamma)$, small relative deviations at a level of 10^{-5} and 10^{-7} are obtained from non-vanishing lepton masses in the decay phase space. Scattering over the whole parameter space, we find that these predictions for $Br\,(l_j \to l_i\gamma)$ are accurately fulfilled in SPS 1a, i. e. the relative changes with respect to the standard formulae are at the level of one percent, 10^{-5} and 10^{-6} in the above cases. This also implies that the modifications for the MDMs and EDMs in SPS 1a are tiny, because then only the corrections in the loop integrals enter, leading to a relative modification of δa_μ at a level of 10^{-7} and for the EDMs of e and μ at the level of 10^{-4}, respectively.

We emphasize that the relative shifts in leptonic electric dipole moments below the level of 0.1 percent when taking into account all lepton masses are generic for slepton masses and gaugino masses of the order of 100 GeV. Such tiny effects from m_{l_i} masses are expected from the exact denominators eqs. (F.17) and (F.32) of the loop integrals, see eqs. (F.14), (F.15), (F.16), (F.29), (F.30) and (F.31), where lepton and sparticle masses enter quadratically.
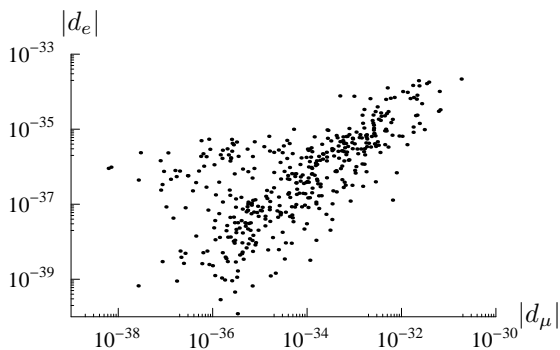
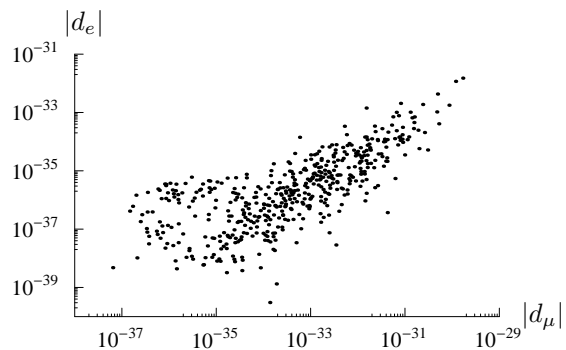Figure 4.38: Correlation of $|d_\mu|$/ecm and $|d_e|$/ecm, scattering over all parameters, scenario SPS 1a.

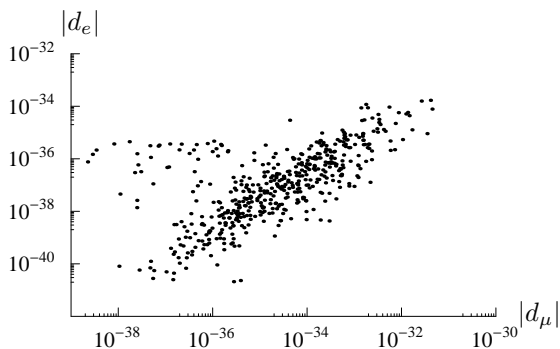Figure 4.39: Correlation of $|d_\mu|$/ecm and $|d_e|$/ecm, scattering over all parameters, scenario SPS 9.

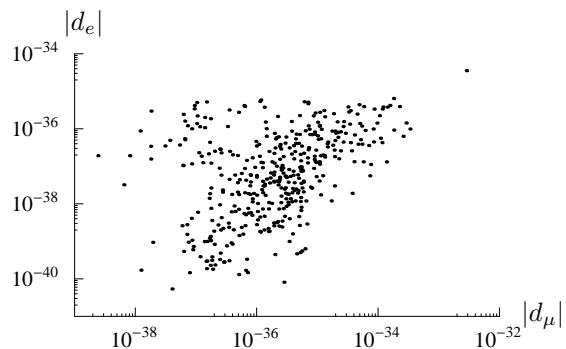Figure 4.40: Correlation of $|d_\mu|$/ecm and $|d_e|$/ecm, scattering over all parameters, $\tilde{G}$MSB scenario.

Figure 4.41: Correlation of $|d_\mu|$/ecm and $|d_e|$/ecm, scattering over all parameters, GMSB scenario.

Relations of $Br\left(l_j \to l_i\gamma\right)$ to $Br\left(l_j \to l_i\bar{l}_i l_i\right)$ and μ-e conversion   We have examined the approximations eqs. (3.63) and (3.65) obtained under the assumption of dominance of on-shell photon penguin diagrams numerically by varying over the whole parameter space of the models. Using complete analytic expressions as specified in [31] and appendix G, we have found the results of Tab. 4.9. It can be seen that in the models considered, the approximations eqs. (3.63) hold with good accuracy, even for a simultaneous variation of all parameters. Therefore these correlations among different lepton-flavor violating processes provide predictions that can probe the SUSY seesaw model in the future. One can e. g. conclude that a measurement of $Br\left(\mu \to e\gamma\right) \simeq 1.5 \cdot 10^{-13}$ corresponds roughly to a value of $1 \cdot 10^{-15}$ for $R\left(\mu^- Ti \to e^- Ti\right)$ or $Br\left(\mu \to 3e\right)$. Taking into account the different future sensitivities for these processes mentioned in the introduction, a measurement of $R\left(\mu^- Ti \to e^- Ti\right)$ at a level of 10^{-16} would correspond to a sensitivity of $1.7 \cdot 10^{-14}$ in $Br\left(\mu \to e\gamma\right)$.

Ratio	SPS 1a	SPS 9	$\tilde{G}$MSB	GMSB
$\frac{Br(\mu \to 3e)}{Br(\mu \to e\gamma)}/10^{-3}$	6.2	6.2	6.2	6.1
$\frac{Br(\tau \to 3\mu)}{Br(\tau \to \mu\gamma)}/10^{-3}$	2.3	2.3	2.3	2.3
$\frac{Br(\tau \to 3e)}{Br(\tau \to e\gamma)}/10^{-2}$	1.05	1.05	1.05	1.05
$\frac{R(\mu^- Ti \to e^- Ti)}{Br(\mu \to e\gamma)}/10^{-3}$	$(4.3 - 4.7)$	$(7.1 - 7.2)$	$(4.3 - 4.4)$	$(5.0 - 5.1)$

Table 4.9: Ranges obtained by scattering over the whole parameter space of the models. We display only one value if the variation is less than one percent.

Effects of oscillation parameters and phases on $Br(l_j \to l_i\gamma)$ The detailed ranges of the branching ratios resulting from a variation of a single neutrino oscillation parameter including the Dirac phase δ can be seen in Tab. 4.10, together with results based on the LL approximations. Comparing the predictions for the variations based on the LL approximations eqs. (2.50), (2.63), (2.88), (2.115) evaluated at the GUT-scale or messenger scale and the numerical ranges of $Br(l_j \to l_i\gamma)$, one sees that the LL approximations are rather accurate for an estimate of the effect of a single parameter.

In the following we will briefly discuss these effects, keeping in mind that they can be approximately understood by inserting numerical values in eq. (3.13). It turns out that variations in the parameters θ_{12}, θ_{23} and Δm_{21}^2 within their 3σ CL intervals have a small impact on $Br(\mu \to e\gamma)$ and $Br(\tau \to \mu\gamma)$, while a variation of θ_{13} and δ causes significant changes in $Br(\mu \to e\gamma)$. The effects of the neutrino oscillation parameters on $Br(\tau \to e\gamma)$ will be discussed separately below.

Considering only the effect of a variation of θ_{12} on the rare decays, a numerical estimate based on eq. (3.13) shows that $Br(\mu \to e\gamma)$ and $Br(\tau \to \mu\gamma)$ both increase with θ_{12}, although the dependence on θ_{12} is rather weak corresponding to an increase of roughly 11% and 6%, respectively.

The angle θ_{13} has quite a large impact on $Br(\mu \to e\gamma)$, i. e. increasing θ_{13} from 0 to its maximal value at 3σ CL leads to a rise in $Br(\mu \to e\gamma)$ by approximately a factor of 15. On the other hand $Br(\tau \to \mu\gamma)$ slightly decreases by less than 10%, if θ_{13} is increased in its 3σ CL range.

Varying only θ_{23}, it turns out that $Br(\mu \to e\gamma)$ and $Br(\tau \to \mu\gamma)$ are both maximal for $\theta_{23} \approx 0.8$ with a stronger θ_{23} dependence of $Br(\tau \to \mu\gamma)$.

If the neutrino mass parameter Δm_{21}^2 is increased within the 3σ CL range, the rate of $\mu \to e\gamma$ also increases by roughly 23%, because $(Y_\nu^\dagger Y_\nu)_{21}$ scales linearly with $\sqrt{\Delta m_{21}^2}$, as can be seen from eq. (3.13). In $(Y_\nu^\dagger Y_\nu)_{32}$ there is a relative minus sign between the subdominant contribution from Δm_{21}^2 and the dominant term involving Δm_{31}^2, so that $Br(\tau \to \mu\gamma)$ decreases by about 7% for increasing Δm_{21}^2.

An increase of Δm_{31}^2 in its 3σ CL interval leads to a rise in both $Br(\mu \to e\gamma)$ and $Br(\tau \to \mu\gamma)$. The term proportional to Δm_{31}^2 is numerically dominant in $(Y_\nu^\dagger Y_\nu)_{32}$. The increase in $Br(\tau \to \mu\gamma)$ can be roughly approximated by $\frac{\max(\Delta m_{31}^2)}{\min(\Delta m_{31}^2)} \approx 2.6$. On the other

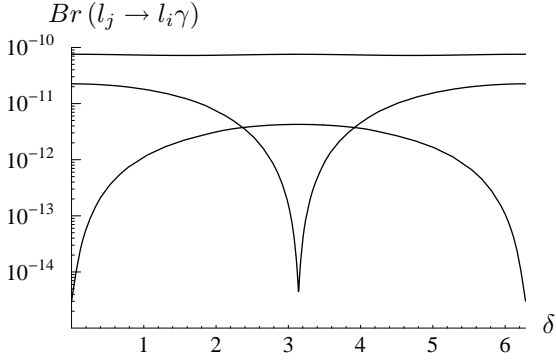$Br\left(l_j \to l_i\gamma\right)$

Figure 4.42: $Br\left(l_j \to l_i\gamma\right)$ as a function of the Dirac phase δ, $M_i \equiv M_R = 10^{13}$ GeV, real R, $\kappa_1 = 0$, scenario SPS 1a.

$Br\left(l_j \to l_i\gamma\right)$

Figure 4.43: $Br\left(l_j \to l_i\gamma\right)$ as a function of the Dirac phase δ, $M_i \equiv M_R = 10^{13}$ GeV, real R, $\kappa_1 = 0$, scenario SPS 9.
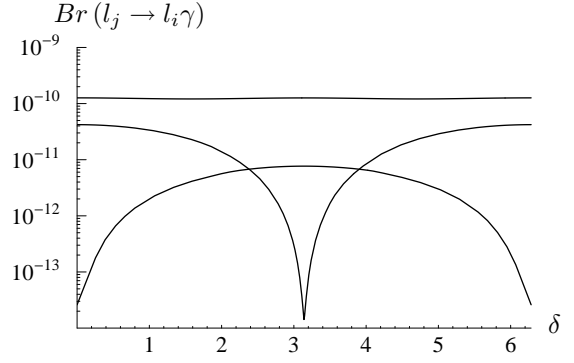
$Br\left(l_j \to l_i\gamma\right)$

Figure 4.44: $Br\left(l_j \to l_i\gamma\right)$ as a function of the Dirac phase δ, $M_i \equiv M_R = 10^{13}$ GeV, real R, $\kappa_1 = 0$, $\tilde{G}$MSB scenario.
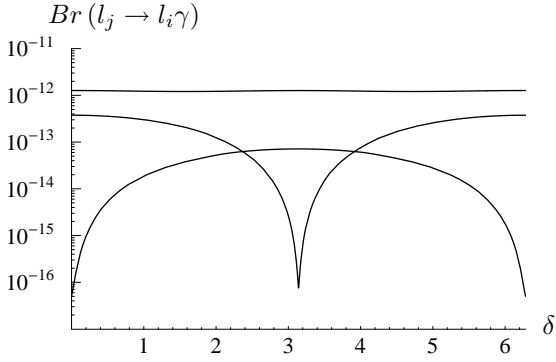
$Br\left(l_j \to l_i\gamma\right)$

Figure 4.45: $Br\left(l_j \to l_i\gamma\right)$ as a function of the Dirac phase δ, $M_i \equiv M_R = 10^{13}$ GeV, real R, $\kappa_1 = 0$, GMSB scenario.

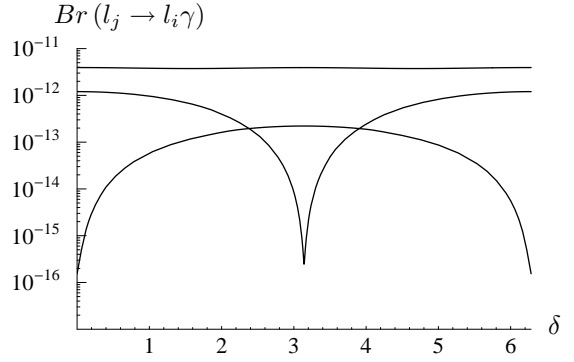hand, in $(Y_\nu^\dagger Y_\nu)_{21}$ the terms involving Δm_{31}^2 and Δm_{21}^2 have a relative plus sign and are of similar magnitude, leading to a variation of $Br\left(\mu \to e\gamma\right)$ by 40%.

The variation of a single parameter within its 3σ CL range can induce a large suppression in $Br\left(\tau \to e\gamma\right)$, implying cancellations in $(Y_\nu^\dagger Y_\nu)_{31}$. From eq. (3.13) it follows that

$$
\begin{aligned}
(Y_\nu^\dagger Y_\nu)_{31} \;\simeq\; & \frac{M_R}{v^2 \sin^2\beta} \ln\frac{M_{GUT}}{M_R}\left(\sqrt{\Delta m_{31}^2}\,\sin\theta_{13}\cos\theta_{23}\cos\theta_{13} \right. \\
& \left. -\sqrt{\Delta m_{21}^2}\,\cos\theta_{13}\sin\theta_{12}\left(\cos\theta_{12}\sin\theta_{23} + \cos\theta_{23}\sin\theta_{13}\sin\theta_{12}\right) \right).(4.21)
\end{aligned}
$$

Different cancellations can occur in the aforementioned equation (4.21). More specifically, inserting numerically the best-fit values from Tab. 4.1 where necessary, these cancellations are approximately at:

- $\theta_{12} \approx 0.53$

- $\theta_{13} \approx 0.08$

- $\theta_{23} \approx 0.78$

- $\sqrt{\Delta m_{21}^2} \approx 7.9$ meV

- $\sqrt{\Delta m_{31}^2} \approx 54$ meV

It is interesting to notice that the best-fit value for $\theta_{13} \approx 0.0775$ is very close to the cancellation value shown before, implying a large suppression for $Br\,(\tau \to e\gamma)$. Eq. (3.13) also implies that an increase of $Br\,(\tau \to e\gamma)$ by three orders of magnitude is possible if $\theta_{13} \approx 0$ or $\theta_{13} \approx 0.2$.

The Dirac phase δ can have a large impact on $Br\,(\tau \to e\gamma)$ and $Br\,(\mu \to e\gamma)$, as can be seen in Figs. 4.42 to 4.45. For the choice of parameters in these Figures, the effect of δ on the decay rates can be approximated using eq. (3.13) and inserting the best-fit values according to Tab. 4.1 numerically, leading to

$$
\begin{aligned}
\left(Y_\nu^\dagger L Y_\nu\right)_{21} &\approx 1 \cdot 10^{-17} \frac{M_R}{\text{GeV}} \ln \frac{M_{GUT}}{M_R} \left(9 + 9e^{i\delta}\right) \\
\left(Y_\nu^\dagger L Y_\nu\right)_{31} &\approx 1 \cdot 10^{-17} \frac{M_R}{\text{GeV}} \ln \frac{M_{GUT}}{M_R} \left(-9 + 9e^{i\delta}\right) \\
\left(Y_\nu^\dagger L Y_\nu\right)_{32} &\approx 1 \cdot 10^{-16} \frac{M_R}{\text{GeV}} \ln \frac{M_{GUT}}{M_R} \left(8 + 0.05e^{-i\delta} - 0.05e^{i\delta}\right),
\end{aligned}
\tag{4.22}
$$

where a value of $\tan\beta = 10$ is assumed. Eq. (4.22) shows that $Br\,(\mu \to e\gamma)$ is expected to be maximal for $\delta = 0$ and minimal for $\delta = \pi$ where the dominant terms cancel in $\left(Y_\nu^\dagger L Y_\nu\right)_{21}$. For $Br\,(\tau \to e\gamma)$ on the other hand, the situation is reversed: Maximal (minimal) values are expected for $\delta = \pi(0)$ due to the different sign in front of the real term in $\left(Y_\nu^\dagger L Y_\nu\right)_{31}$. Moreover, it is clear from eq. (4.22) that $Br\,(\tau \to \mu\gamma)$ is virtually unaffected by a variation of the Dirac phase in the case considered here, which can also be seen in Figs. 4.42 to 4.45.

On the other hand, there is no effect of the two Majorana phases in the case of degenerate M_i and real R-matrix, as can be seen from eqs. (2.55) or (3.12). Then the Majorana phases ϕ and ϕ' drop out in the combination $U_{jk}U_{ik}^*$ which is also true for non-degenerate M_i and $R = \mathbf{1}$, see eq. (3.15).

SPS 1a						
	θ_{23}	θ_{13}	θ_{12}	Δm^2_{21}	Δm^2_{31}	δ
$Br\left(\tau \to \mu\gamma\right)/10^{-11}$	6.2; 7.6	6.9; 7.7	7.4; 7.8	7.2; 7.8	3.7; 11	7.2; 7.6
$\dfrac{\left\|\left(\delta m^2_{\tilde{L}}\right)_{32}\right\|^2_{min}}{\left\|\left(\delta m^2_{\tilde{L}}\right)_{32}\right\|^2_{max}}$	0.82	0.90	0.94	0.93	0.33	0.95
$Br\left(\mu \to e\gamma\right)/10^{-11}$	2.1; 2.2	0.6; 8	2.1; 2.4	2.0; 2.6	1.7; 2.7	$4 \cdot 10^{-4}$; 2
$\dfrac{\left\|\left(\delta m^2_{\tilde{L}}\right)_{21}\right\|^2_{min}}{\left\|\left(\delta m^2_{\tilde{L}}\right)_{21}\right\|^2_{max}}$	0.95	0.07	0.89	0.77	0.60	$2 \cdot 10^{-4}$
SPS 9						
	θ_{23}	θ_{13}	θ_{12}	Δm^2_{21}	Δm^2_{31}	δ
$Br\left(\tau \to \mu\gamma\right)/10^{-10}$	1.0; 1.3	1.2; 1.3	1.2; 1.3	1.2; 1.3	0.7; 1.8	1.2; 1.3
$\dfrac{\left\|\left(\delta m^2_{\tilde{L}}\right)_{32}\right\|^2_{min}}{\left\|\left(\delta m^2_{\tilde{L}}\right)_{32}\right\|^2_{max}}$	0.82	0.90	0.94	0.93	0.34	0.95
$Br\left(\mu \to e\gamma\right)/10^{-11}$	3.9; 4.2	1.1; 15	3.9; 4.4	3.8; 4.9	3.2; 5.0	$1 \cdot 10^{-3}$; 4
$\dfrac{\left\|\left(\delta m^2_{\tilde{L}}\right)_{21}\right\|^2_{min}}{\left\|\left(\delta m^2_{\tilde{L}}\right)_{21}\right\|^2_{max}}$	0.94	0.07	0.89	0.77	0.61	$6 \cdot 10^{-5}$
$\tilde{G}$MSB						
	θ_{23}	θ_{13}	θ_{12}	Δm^2_{21}	Δm^2_{31}	δ
$Br\left(\tau \to \mu\gamma\right)/10^{-12}$	1.0; 1.3	1.2; 1.3	1.2; 1.3	1.2; 1.3	0.6; 1.8	1.2; 1.3
$\dfrac{\left\|\left(\delta m^2_{\tilde{L}}\right)_{32}\right\|^2_{min}}{\left\|\left(\delta m^2_{\tilde{L}}\right)_{32}\right\|^2_{max}}$	0.82	0.90	0.94	0.93	0.33	0.95
$Br\left(\mu \to e\gamma\right)/10^{-13}$	3.6; 3.8	0.9; 13	3.5; 3.9	3.4; 4.4	2.8; 4.6	$7 \cdot 10^{-4}$; 4
$\dfrac{\left\|\left(\delta m^2_{\tilde{L}}\right)_{21}\right\|^2_{min}}{\left\|\left(\delta m^2_{\tilde{L}}\right)_{21}\right\|^2_{max}}$	0.95	0.07	0.89	0.77	0.60	$2 \cdot 10^{-4}$
GMSB						
	θ_{23}	θ_{13}	θ_{12}	Δm^2_{21}	Δm^2_{31}	δ
$Br\left(\tau \to \mu\gamma\right)/10^{-12}$	3.2; 3.9	3.6; 4.0	3.8; 4.1	3.8; 4.1	1.9; 5.8	3.7;3.9
$\dfrac{\left\|\left(\delta m^2_{\tilde{L}}\right)_{32}\right\|^2_{min}}{\left\|\left(\delta m^2_{\tilde{L}}\right)_{32}\right\|^2_{max}}$	0.82	0.91	0.94	0.93	0.33	0.95
$Br\left(\mu \to e\gamma\right)/10^{-12}$	1.1; 1.2	0.3; 3.9	1.1; 1.3	1.1; 1.4	0.9; 1.5	$2 \cdot 10^{-4}$;1
$\dfrac{\left\|\left(\delta m^2_{\tilde{L}}\right)_{21}\right\|^2_{min}}{\left\|\left(\delta m^2_{\tilde{L}}\right)_{21}\right\|^2_{max}}$	0.95	0.08	0.89	0.77	0.60	$2 \cdot 10^{-4}$

Table 4.10: Ranges of $Br\left(l_i \to l_j\gamma\right)$ that correspond to the variation of the corresponding parameter in the 3σ CL intervals according to Tab. 4.1 in the case of SPS 1a, SPS 9, $\tilde{G}$MSB and GMSB. Additional rows show the estimate of the effects of these variations based on the LL approximations eqs. (2.50), (2.63), (2.88), (2.115).

Chapter 5

Conclusions

In this work the SUSY seesaw model and its effects on low-energy leptonic observables and thermal leptogenesis have been systematically investigated. Precision measurements will increase the sensitivity on lepton-flavor violating decays, particularly on $Br\,(l_j \to l_i\gamma)$ and also on electric and magnetic diplole moments in the near future. In order to improve also the accuracy of theoretical predictions for these processes, we have performed a full one-loop calculation of the underlying supersymmetric processes taking into account the lepton masses.

By the introduction of very heavy Majorana neutrinos, the supersymmetric seesaw model naturally leads to small neutrino masses. On the other hand it provides definite predictions for SSB mass terms, where in flavor space, non-diagonal elements of the slepton mass matrices induce LFV. The scale dependence of these SUSY mass parameters is determined by the RGEs. In order to obtain reliable and precise results for the mass terms, the complete set of one-loop RGEs between the electroweak scale and the unification scale has been solved numerically.

Since the mechanism of SSB is completely unknown, a novel analysis beyond the often studied mSUGRA models has been performed. This includes the formulation of the SUSY seesaw model in the "minimal" framework of gauge mediation, anomaly mediation and gaugino mediation. For the numerical results in mSUGRA and AMSB, we have referred to the benchmark scenarios SPS 1a and SPS 9 proposed in [39]. In the case of GMSB and $\tilde{G}$MSB, the fundamental parameters have been chosen such that the sparticle masses are in the range from 200 GeV to roughly 1 TeV, being also the mass range in the aforementioned benchmark scenarios. This way it has been demonstrated that in all of these models of SUSY breaking, the ongoing search for $Br(\mu \to e\gamma)$ can constrain fundamental SSB parameters and/or the seesaw parameters. In this context it should be mentioned that in GMSB lepton-flavor violating effects can be strongly suppressed, if the messenger scale is below the mass scales of right-handed neutrinos.

We have studied many useful relations for rare leptonic processes that are valid in all of these SSB scenarios, e. g. $Br\left(l_j \to l_i\bar{l}_i l_i\right) \propto Br\left(l_j \to l_i\gamma\right)$ and $Br\left(l_j \to l_i\gamma\right) \propto |\delta a_\mu|^2$. These correlations between different LFV decays will allow for many predictions for leptonic observables at low energies once charged LFV is observed. In each of the SSB

mechanisms considered, we have also demonstrated numerically that the decay rates for $l_j \rightarrow l_i \gamma$ generically scale with the "leading logarithmic" approximations for the RGE effects in the slepton sector. This might be useful for model building. Finally, because many SUSY flavor effects can also be studied in supersymmetric models that violate trilinear R-parity, we have pointed out correlations in lepton-flavor violating processes that are essentially different in R-parity conserving or violating approaches.

This analysis shows that for slepton and gaugino masses below roughly 700 GeV and a right-handed Majorana mass scale of at least $1 \cdot 10^{13}$ GeV, one can expect an observable signal for $\mu \rightarrow e\gamma$ in the PSI experiment in a large portion of the seesaw parameter space. If the light neutrinos are quasi-degenerate, the rates for $Br\,(\mu \rightarrow e\gamma)$ are reduced by more than two orders of magnitude. The CP-violating neutrino Dirac phase also has a great impact on $Br\,(\mu \rightarrow e\gamma)$ and $Br\,(\tau \rightarrow e\gamma)$: For the specific case of a real R-matrix, degenerate right-handed Majorana masses and hierarchical light neutrino masses, large cancellations occur in $Br\,(\mu \rightarrow e\gamma)$ for $\delta = \pi$ and in $Br\,(\tau \rightarrow e\gamma)$ for $\delta = 0$, respectively. If the masses of the right-handed neutrinos are non-degenerate, the ratios of $Br\,(l_j \rightarrow l_i\gamma)$ for different decays can probe the mass spectrum of the heavy Majorana masses M_i. For non-degenerate M_i, the real mixing angles x_i in the unknown complex orthogonal R-matrix are important for $Br\,(l_j \rightarrow l_i\gamma)$. It has been shown that $Br\,(\mu \rightarrow e\gamma)$ may be suppressed in some regions of x_1 by more than four orders of magnitude, while the suppression for $x_2 = \frac{\pi}{2}$ can be more than three orders of magnitude.

Finally the predictions for the baryon asymmetry of the universe generated through thermal leptogenesis have been analyzed in the context of the seesaw model. Thermal leptogenesis is only possible for non-degenerate heavy neutrinos. Assuming both hierarchical light and heavy neutrinos, the low-energy rare processes are dependent mainly on the mass of the heaviest right-handed neutrino M_3, whereas in thermal leptogenesis a lower bound on M_1 can be obtained. The baryon asymmetry generated in thermal leptogenesis is essentially independent of the mechanism of SUSY breaking and also on the neutrino MNS mixing matrix. The basic parameters of leptogenesis, such as the CP asymmetry ϵ_1 in the decays of N_1, provide probes of the unknown complex orthogonal R-matrix. We have shown that for a minimal model, i. e. parameterizing R in terms of one common imaginary angle, $y_i \equiv y$ and vanishing real mixing angles, successful thermal leptogenesis is possible provided $M_1 \gtrsim 10^{11}$ GeV.

The results of this work show that further information on $Br\,(\mu \rightarrow e\gamma)$ in the near future in connection with constraints from thermal leptogenesis will be an excellent probe of the parameters of the SUSY seesaw model and will allow for more precise predictions for other lepton-flavor violating processes.

Appendix A

SM input values

The input parameters of the SM have been taken from the Particle Data Group Collaboration [5] and the program package SOFTSUSY [33]. For the numerical analysis of the RG evolution we refer to the input values at m_Z listed in Tab. A.1 specifying the running masses at m_Z, see also [33], where accurate RG studies have been carried out. An additional fundamental parameter is the GUT scale, $M_{GUT} = 1.5 \cdot 10^{16}$ GeV corresponding to an unification of gauge couplings in the scenarios considered.

It should also be mentioned that we do not include quark mixing in this analysis which is appropriate for the purpose of this study, where we concentrate on lepton mixing rather than on the small quark mixing. Due to the dominance of top and bottom quark masses, the corresponding Yukawa couplings are strongly dominating among the quarks.

Variable	value	description
α, $\alpha\left(m_Z\right)$	$1/137.036$, $7.82 \cdot 10^{-3}$	fine-structure constant
$\alpha_s\left(m_Z\right)$	$1.17 \cdot 10^{-1}$	strong coupling constant
$\sin^2\theta_W\left(m_Z\right)$	0.2311	weak-mixing angle
v	174.19	VEV of Higgs field
m_Z	91.188	Z-boson mass
m_W	80.423	W-boson mass
$m_e\left(m_e\right)$, $m_e\left(m_Z\right)$	$5.11 \cdot 10^{-4}$, $5.01 \cdot 10^{-4}$	electron mass
$m_\mu\left(m_\mu\right)$, $m_\mu\left(m_Z\right)$	$1.057 \cdot 10^{-1}$, $1.039 \cdot 10^{-1}$	μ mass
$m_\tau\left(m_\tau\right)$, $m_\tau\left(m_Z\right)$	1.777, 1.752	τ mass
Γ_μ	$2.996 \cdot 10^{-19}$	full width of μ
Γ_τ	$2.2649 \cdot 10^{-12}$	full width of τ
$m_u\left(m_Z\right)$	$1.72 \cdot 10^{-3}$	u-quark mass
$m_d\left(m_Z\right)$	$3.89 \cdot 10^{-3}$	d-quark mass
$m_s\left(m_Z\right)$	$6.76 \cdot 10^{-2}$	s-quark mass
$m_c\left(m_Z\right)$	0.576	c-quark mass
$m_b\left(m_Z\right)$	2.91	b-quark mass
$m_t\left(m_Z\right)$	174.3	t-quark mass

Table A.1: SM input parameters, all masses and widths are in units of GeV.

Appendix B

Feynman rules

In this appendix we show the relevant vertices for sparticles arising from the interaction Lagrangians specified below.

Interaction Lagrangians   Charged lepton-sneutrino-chargino [31]:

$$\mathcal{L}_c^{\tilde{\nu}} = \overline{l}_i \left(C_{iax}^{R(l)} P_R + C_{iax}^{L(l)} P_L \right) \tilde{\chi}_a^- \tilde{\nu}_x + \tilde{\nu}_x^* \overline{\tilde{\chi}_a^-} \left(C_{iax}^{R(l)*} P_L + C_{iax}^{L(l)*} P_R \right) l_i \qquad \text{(B.1)}$$

Quark-squark-chargino [31]:

$$\begin{aligned}
\mathcal{L}_c^{\tilde{q}} &= \overline{d}_i \left(C_{iax}^{R(d)} P_R + C_{iax}^{L(d)} P_L \right) \tilde{\chi}_a^- \tilde{u}_x + \tilde{u}_x^* \overline{\tilde{\chi}_a^-} \left(C_{iax}^{R(d)*} P_L + C_{iax}^{L(d)*} P_R \right) d_i \\
&\quad + \overline{u}_i \left(C_{iax}^{R(u)} P_R + C_{iax}^{L(u)} P_L \right) \tilde{\chi}_a^+ \tilde{d}_x + \tilde{d}_x^* \overline{\tilde{\chi}_a^+} \left(C_{iax}^{R(u)*} P_L + C_{iax}^{L(u)*} P_R \right) u_i
\end{aligned}$$

$$\text{(B.2)}$$

Charged lepton-charged slepton-neutralino [31]:

$$\mathcal{L}_n^{\tilde{l}} = \overline{l}_i \left(N_{iax}^{R(l)} P_R + N_{iax}^{L(l)} P_L \right) \tilde{\chi}_a^0 \tilde{l}_x + \tilde{l}_x^* \overline{\tilde{\chi}_a^0} \left(N_{iax}^{R(l)*} P_L + N_{iax}^{L(l)*} P_R \right) l_i \qquad \text{(B.3)}$$

Quark-squark-neutralino [31]:

$$\begin{aligned}
\mathcal{L}_n^{\tilde{q}} &= \overline{d}_i \left(N_{iax}^{R(d)} P_R + N_{iax}^{L(d)} P_L \right) \tilde{\chi}_a^0 \tilde{d}_x + \tilde{d}_x^* \overline{\tilde{\chi}_a^0} \left(N_{iax}^{R(d)*} P_L + N_{iax}^{L(d)*} P_R \right) d_i \\
&\quad + \overline{u}_i \left(N_{iax}^{R(u)} P_R + N_{iax}^{L(u)} P_L \right) \tilde{\chi}_a^0 \tilde{u}_x + \tilde{u}_x^* \overline{\tilde{\chi}_a^0} \left(N_{iax}^{R(u)*} P_L + N_{iax}^{L(u)*} P_R \right) u_i
\end{aligned}$$

$$\text{(B.4)}$$

Photon-chargino-chargino [87]:

$$\mathcal{L}^{\tilde{\chi}^\pm} = -eA_\mu \overline{\tilde{\chi}_i^+} \gamma^\mu \tilde{\chi}_i^+ \qquad \text{(B.5)}$$

Photon-charged slepton-charged slepton [87]:

$$\mathcal{L}^{\tilde{l}^\pm} = ieA_\mu \tilde{l}_x^* \overset{\leftrightarrow}{\partial^\mu} \tilde{l}_x \qquad \text{(B.6)}$$

The coefficients of the vertex factors involving charginos are given by

$$
C_{iax}^{R(l)} = -g \left(O_R \right)_{a1} \left(U_{\tilde{\nu}} \right)_{xi} \tag{B.7}
$$

$$
C_{iax}^{L(l)} = g \frac{m_{l_i}}{\sqrt{2} m_W \cos \beta} \left(O_L \right)_{a2} \left(U_{\tilde{\nu}} \right)_{xi} \tag{B.8}
$$

$$
C_{iax}^{R(d)} = g \left(- \left(O_R \right)_{a1} \left(U_{\tilde{u}} \right)_{xi} + \frac{m_{u_i}}{\sqrt{2} m_W \sin \beta} \left(O_R \right)_{a2} \left(U_{\tilde{u}} \right)_{x(i+3)} \right) \tag{B.9}
$$

$$
C_{iax}^{L(d)} = g \frac{m_{d_i}}{\sqrt{2} m_W \cos \beta} \left(O_L \right)_{a2} \left(U_{\tilde{u}} \right)_{xi} \tag{B.10}
$$

$$
C_{iax}^{R(u)} = g \left(- \left(O_L \right)_{a1} \left(U_{\tilde{d}} \right)_{xi} + \frac{m_{d_i}}{\sqrt{2} m_W \cos \beta} \left(O_L \right)_{a2} \left(U_{\tilde{d}} \right)_{x(i+3)} \right) \tag{B.11}
$$

$$
C_{iax}^{L(u)} = g \frac{m_{u_i}}{\sqrt{2} m_W \sin \beta} \left(O_R \right)_{a2} \left(U_{\tilde{d}} \right)_{xi} . \tag{B.12}
$$

The vertex factors involving neutralinos have the following coefficients

$$
\begin{aligned}
N_{iax}^{R(l)} = {} & -\frac{g}{\sqrt{2}} \left(\left(- \left(O_N \right)_{a2} - \left(O_N \right)_{a1} \tan \theta_W \right) \left(U_{\tilde{l}} \right)_{xi} \right. \\
& \left. + \frac{m_{l_i}}{m_W \cos \beta} \left(O_N \right)_{a3} \left(U_{\tilde{l}} \right)_{x(i+3)} \right)
\end{aligned} \tag{B.13}
$$

$$
\begin{aligned}
N_{iax}^{L(l)} = {} & -\frac{g}{\sqrt{2}} \left(\frac{m_{l_i}}{m_W \cos \beta} \left(O_N \right)_{a3} \left(U_{\tilde{l}} \right)_{xi} \right. \\
& \left. + 2 \left(O_N \right)_{a1} \tan \theta_W \left(U_{\tilde{l}} \right)_{x(i+3)} \right)
\end{aligned} \tag{B.14}
$$
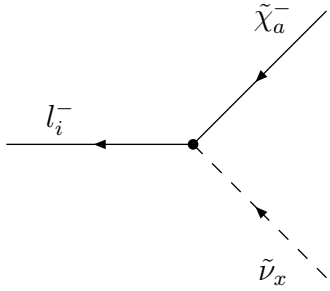
$$
\begin{aligned}
N_{iax}^{R(d)} = {} & -\frac{g}{\sqrt{2}} \left(\left(- \left(O_N \right)_{a2} + \frac{1}{3} \left(O_N \right)_{a1} \tan \theta_W \right) \left(U_{\tilde{d}} \right)_{xi} \right. \\
& \left. + \frac{m_{d_i}}{m_W \cos \beta} \left(O_N \right)_{a3} \left(U_{\tilde{d}} \right)_{x(i+3)} \right)
\end{aligned} \tag{B.15}
$$

$$
\begin{aligned}
N_{iax}^{L(d)} = {} & -\frac{g}{\sqrt{2}} \left(\frac{m_{d_i}}{m_W \cos \beta} \left(O_N \right)_{a3} \left(U_{\tilde{d}} \right)_{xi} \right. \\
& \left. + \frac{2}{3} \left(O_N \right)_{a1} \tan \theta_W \left(U_{\tilde{d}} \right)_{x(i+3)} \right)
\end{aligned} \tag{B.16}
$$

$$
\begin{aligned}
N_{iax}^{R(u)} = {} & -\frac{g}{\sqrt{2}} \left(\left(- \left(O_N \right)_{a2} + \frac{1}{3} \left(O_N \right)_{a1} \tan \theta_W \right) \left(U_{\tilde{u}} \right)_{xi} \right. \\
& \left. + \frac{m_{u_i}}{m_W \sin \beta} \left(O_N \right)_{a4} \left(U_{\tilde{u}} \right)_{x(i+3)} \right)
\end{aligned} \tag{B.17}
$$
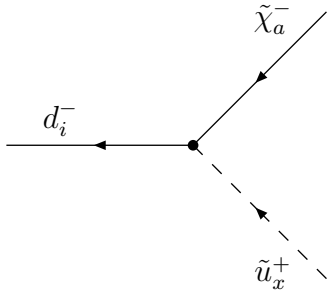
$$
\begin{aligned}
N_{iax}^{L(u)} = {} & -\frac{g}{\sqrt{2}} \left(\frac{m_{u_i}}{m_W \sin \beta} \left(O_N \right)_{a4} \left(U_{\tilde{u}} \right)_{xi} \right. \\
& \left. - \frac{4}{3} \left(O_N \right)_{a1} \tan \theta_W \left(U_{\tilde{u}} \right)_{x(i+3)} \right) .
\end{aligned} \tag{B.18}
$$

Vertices From the above interaction Lagrangians the vertex factor for diagrams involving one scalar and two fermions when all arrows are reversed, is obtained from the "original" one as follows: If the vertex factor is of the form $c^L P_L + c^R P_R$, then reversing all arrows yields the vertex factor $c^{R*} P_L + c^{L*} P_R$, see also [87]. The arrows on scalar lines denote the flow of the corresponding lepton number or baryon number.
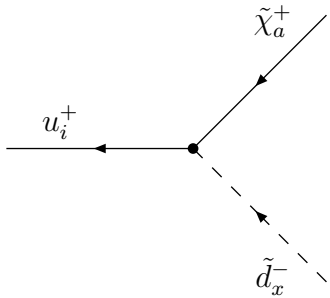
$$C_{iax}^{R(l)} P_R + C_{iax}^{L(l)} P_L$$

$$C_{iax}^{R(d)} P_R + C_{iax}^{L(d)} P_L$$

$$C_{iax}^{R(u)} P_R + C_{iax}^{L(u)} P_L$$

$$N_{iax}^{R(l)} P_R + N_{iax}^{L(l)} P_L$$

$$N_{iax}^{R(d)} P_R + N_{iax}^{L(d)} P_L$$

$$N_{iax}^{R(u)} P_R + N_{iax}^{L(u)} P_L$$

$$ie\gamma^\mu$$

$$ie(p_1 + p_2)^\mu$$

Appendix C

Masses and mixings

Neutralinos The symmetric neutralino mass matrix $M_{\tilde{\chi}^0}$ is introduced by [31]

$$-\mathcal{L}_{\tilde{\chi}^0} = \frac{1}{2}\psi_{\tilde{\chi}^0} M_{\tilde{\chi}^0} \psi_{\tilde{\chi}^0}^T + h.c., \tag{C.1}$$

in the neutralino basis

$$\psi_{\tilde{\chi}^0} = \left(\tilde{B}_L^0, \tilde{W}_L^0, \tilde{h}_{1_L}^0, \tilde{h}_{2_L}^0 \right), \tag{C.2}$$

as

$$M_{\tilde{\chi}^0} = \begin{pmatrix} \tilde{M}_1 & 0 & -m_Z s_{\theta_W} c_\beta & m_Z s_{\theta_W} s_\beta \\ 0 & \tilde{M}_2 & m_Z c_{\theta_W} c_\beta & -m_Z c_{\theta_W} s_\beta \\ -m_Z s_{\theta_W} c_\beta & m_Z c_{\theta_W} c_\beta & 0 & -\mu \\ m_Z s_{\theta_W} s_\beta & -m_Z c_{\theta_W} s_\beta & -\mu & 0 \end{pmatrix}, \tag{C.3}$$

where $s_\alpha \equiv \sin\alpha$ and $c_\alpha \equiv \cos\alpha$.

The gauge eigenstates are the bino, the neutral wino and two higgsino states where each component is a two-component Majorana fermion field. The real matrix $M_{\tilde{\chi}^0}$ is diagonalized by the orthogonal matrix O_N,

$$O_N M_{\tilde{\chi}^0} O_N^T = \text{Diag}\left(m_{\tilde{\chi}_1^0}, m_{\tilde{\chi}_2^0}, m_{\tilde{\chi}_3^0}, m_{\tilde{\chi}_4^0} \right), \tag{C.4}$$

leading to four left-handed neutralino mass eigenstates which are defined by

$$\tilde{\chi}_{i_L}^0 = (O_N)_{ij} \left(\psi_{\tilde{\chi}^0} \right)_j, \qquad i, j : 1, \ldots, 4. \tag{C.5}$$

Four-component Majorana spinors $\tilde{\chi}_i^0$ of mass $m_{\tilde{\chi}_i^0}$ are obtained as $\tilde{\chi}_i^0 = \tilde{\chi}_{i_L}^0 + \tilde{\chi}_{i_R}^0$ [31].

Charginos The mass matrix of charginos $\mathcal{L}_{\tilde{\chi}^-}$ is given by [31]

$$-\mathcal{L}_{\tilde{\chi}^-} = \left(\overline{\tilde{W}_R^-}, \overline{\tilde{h}_{2_R}^-} \right) M_{\tilde{\chi}^-} \begin{pmatrix} \tilde{W}_L^- \\ \tilde{h}_{1_L}^- \end{pmatrix} + h.c., \tag{C.6}$$

as

$$M_{\tilde{\chi}^-} = \begin{pmatrix} \tilde{M}_2 & \sqrt{2}m_W \cos\beta \\ \sqrt{2}m_W \sin\beta & \mu \end{pmatrix}. \tag{C.7}$$

A real $M_{\tilde{\chi}^-}$ matrix is diagonalized by two orthogonal matrices O_R and O_L such that

$$O_R M_{\tilde{\chi}^-} O_L^T = \text{Diag}\left(M_{\tilde{\chi}_1^-}, M_{\tilde{\chi}_2^-}\right). \tag{C.8}$$

Defining

$$\begin{pmatrix} \tilde{\chi}_{1_L}^- \\ \tilde{\chi}_{2_L}^- \end{pmatrix} = O_L \begin{pmatrix} \tilde{W}_L^- \\ \tilde{h}_{1_L}^- \end{pmatrix}, \quad \begin{pmatrix} \tilde{\chi}_{1_R}^- \\ \tilde{\chi}_{2_R}^- \end{pmatrix} = O_R \begin{pmatrix} \tilde{W}_R^- \\ \tilde{h}_{2_R}^- \end{pmatrix}, \tag{C.9}$$

leads to two chargino Dirac states

$$\tilde{\chi}_a^- = \tilde{\chi}_{a_L}^- + \tilde{\chi}_{a_R}^-, \qquad a = 1, 2 \tag{C.10}$$

with masses $m_{\tilde{\chi}_1^-}$ and $m_{\tilde{\chi}_2^-}$ [31].

Sfermions   The charged slepton (mass)^2 matrix has the form

$$m_{\tilde{l}}^2 = \begin{pmatrix} m_{\tilde{l}_L}^2 & (m_{\tilde{l}_{LR}}^2)^\dagger \\ m_{\tilde{l}_{LR}}^2 & m_{\tilde{l}_R}^2 \end{pmatrix}, \tag{C.11}$$

where $m_{\tilde{l}_L}^2$, $m_{\tilde{l}_R}^2$ and $m_{\tilde{l}_{LR}}^2$ are 3×3 matrices, $m_{\tilde{l}_L}^2$ and $m_{\tilde{l}_R}^2$ being hermitian, see [31] and [51]. The matrix elements are given by

$$(m_{\tilde{l}_L}^2)_{ij} = (m_{\tilde{L}}^2)_{ij} + \delta_{ij}\left(m_{l_i}^2 + m_Z^2 \cos(2\beta)\left(-\frac{1}{2} + \sin^2\theta_W\right)\right) \tag{C.12}$$

$$(m_{\tilde{l}_R}^2)_{ij} = (m_{\tilde{e}}^2)_{ij} + \delta_{ij}(m_{l_i}^2 - m_Z^2 \cos(2\beta)\sin^2\theta_W) \tag{C.13}$$

$$(m_{\tilde{l}_{LR}}^2)_{ij} = (A_e)_{ij}\, v \cos\beta - \delta_{ij} m_{l_i} \mu \tan\beta. \tag{C.14}$$

From eq. (C.11) the mass eigenvalues of $m_{\tilde{l}}^2$ are found through diagonalization by a 6×6 unitary matrix $U_{\tilde{l}}$,

$$U_{\tilde{l}} m_{\tilde{l}}^2 U_{\tilde{l}}^\dagger = \text{Diag}(m_{\tilde{l}_1}^2, ..., m_{\tilde{l}_j}^2, ..., m_{\tilde{l}_6}^2), \tag{C.15}$$

where the masses increase from $m_{\tilde{l}_1}^2$ to $m_{\tilde{l}_6}^2$. The slepton mass eigenstates are expressed in terms of the gauge eigenstates by

$$\tilde{l}_j = (U_{\tilde{l}})_{j\alpha}\tilde{l}_{L_\alpha} + (U_{\tilde{l}})_{j(\alpha+3)}\tilde{l}_{R_\alpha}, \qquad j = 1, ..., 6;\ \alpha = e, \mu, \tau. \tag{C.16}$$

The (mass)^2 matrix of the SUSY partners of the left-handed neutrinos is given by

$$(m_{\tilde{\nu}}^2)_{ij} = (m_{\tilde{L}}^2)_{ij} + \frac{1}{2}\delta_{ij} m_Z^2 \cos 2\beta, \qquad i, j = 1, 2, 3. \tag{C.17}$$

In the SUSY seesaw model, the partners of the right-handed neutrinos are very heavy and their admixture to the left-handed sneutrino mass matrix can therefore be disregarded in $m_{\tilde{\nu}}^2$ at energy scales much below the heavy Majorana neutrino masses. After diagonalization with the unitary 3×3 matrix $U_{\tilde{\nu}}$,

$$U_{\tilde{\nu}} m_{\tilde{\nu}}^2 U_{\tilde{\nu}}^\dagger = \text{Diag}(m_{\tilde{\nu}_1}^2, m_{\tilde{\nu}_2}^2, m_{\tilde{\nu}_3}^2), \tag{C.18}$$

the mass eigenstates $\tilde{\nu}_i$ are related to the gauge eigenstates by

$$\tilde{\nu}_j = (U_{\tilde{\nu}})_{j\alpha}\tilde{\nu}_{L\alpha}, \qquad j = 1, 2, 3; \ \alpha = e, \mu, \tau. \tag{C.19}$$

The $(\text{mass})^2$ matrices for up- and down-squarks have a form analogous to that of the charged sleptons. For down-squarks it is given by

$$m_{\tilde{D}}^2 = \begin{pmatrix} m_{\tilde{D}_L}^2 & (m_{\tilde{D}_{LR}}^2)^\dagger \\ m_{\tilde{D}_{LR}}^2 & m_{\tilde{D}_R}^2 \end{pmatrix}, \tag{C.20}$$

where $m_{\tilde{D}_L}^2$, $m_{\tilde{D}_R}^2$ and $m_{\tilde{D}_{LR}}^2$ are 3×3 matrices, $m_{\tilde{D}_L}^2$ and $m_{\tilde{D}_R}^2$ being hermitian. The matrix elements are given by

$$(m_{\tilde{D}_L}^2)_{ij} = (m_{\tilde{Q}}^2)_{ij} + \delta_{ij}\left(m_{d_i}^2 + m_Z^2\cos(2\beta)\left(-\frac{1}{2} + \frac{\sin^2\theta_W}{3}\right)\right) \tag{C.21}$$

$$(m_{\tilde{D}_R}^2)_{ij} = (m_{\tilde{d}}^2)_{ij} + \delta_{ij}(m_{d_i}^2 - \frac{1}{3}m_Z^2\cos(2\beta)\sin^2\theta_W) \tag{C.22}$$

$$(m_{\tilde{D}_{LR}}^2)_{ij} = (A_d)_{ij}\, v\cos\beta - \delta_{ij}m_{d_i}\mu\tan\beta. \tag{C.23}$$

From eq. (C.20) the mass eigenvalues of $m_{\tilde{D}}^2$ are obtained by diagonalization with a 6×6 unitary matrix $U_{\tilde{d}}$,

$$U_{\tilde{d}}m_{\tilde{D}}^2 U_{\tilde{d}}^\dagger = \text{Diag}(m_{\tilde{d}_1}^2, ..., m_{\tilde{d}_j}^2, ..., m_{\tilde{d}_6}^2). \tag{C.24}$$

The down-squark mass eigenstates are expressed in terms of the gauge eigenstates by

$$\tilde{d}_j = (U_{\tilde{d}})_{j\alpha}\tilde{d}_{L\alpha} + (U_{\tilde{d}})_{j(\alpha+3)}\tilde{d}_{R\alpha}, \qquad j = 1, ..., 6; \ \alpha = d, s, b. \tag{C.25}$$

For up-squarks the $(\text{mass})^2$ matrix reads

$$m_{\tilde{U}}^2 = \begin{pmatrix} m_{\tilde{U}_L}^2 & (m_{\tilde{U}_{LR}}^2)^\dagger \\ m_{\tilde{U}_{LR}}^2 & m_{\tilde{U}_R}^2 \end{pmatrix}, \tag{C.26}$$

where $m_{\tilde{U}_L}^2$, $m_{\tilde{U}_R}^2$ and $m_{\tilde{U}_{LR}}^2$ are 3×3 matrices, $m_{\tilde{U}_L}^2$ and $m_{\tilde{U}_R}^2$ being hermitian. The matrix elements are given by

$$(m_{\tilde{U}_L}^2)_{ij} = (m_{\tilde{Q}}^2)_{ij} + \delta_{ij}\left(m_{u_i}^2 + m_Z^2\cos(2\beta)\left(\frac{1}{2} - \frac{2\sin^2\theta_W}{3}\right)\right) \tag{C.27}$$

$$(m_{\tilde{U}_R}^2)_{ij} = (m_{\tilde{u}}^2)_{ij} + \delta_{ij}(m_{u_i}^2 + \frac{2}{3}m_Z^2\cos(2\beta)\sin^2\theta_W) \tag{C.28}$$

$$(m_{\tilde{U}_{LR}}^2)_{ij} = (A_u)_{ij}\, v\sin\beta - \delta_{ij}m_{u_i}\mu\cot\beta. \tag{C.29}$$

From eq. (C.20) the mass eigenvalues of $m_{\tilde{U}}^2$ are found through diagonalization by a 6×6 unitary matrix $U_{\tilde{u}}$,

$$U_{\tilde{u}}m_{\tilde{U}}^2 U_{\tilde{u}}^\dagger = \text{Diag}(m_{\tilde{u}_1}^2, ..., m_{\tilde{u}_j}^2, ..., m_{\tilde{u}_6}^2). \tag{C.30}$$

The up-squark mass eigenstates are expressed in terms of the gauge eigenstates by

$$\tilde{u}_j = (U_{\tilde{u}})_{j\alpha}\tilde{u}_{L\alpha} + (U_{\tilde{u}})_{j(\alpha+3)}\tilde{u}_{R\alpha}, \qquad j = 1, ..., 6; \ \alpha = u, c, t. \tag{C.31}$$

Appendix D

Dirac algebra and Gordon identity

The Dirac equation for spinors u_j and $\bar{u}_i \equiv u_i^\dagger \gamma^0$ is given by

$$\bar{u}_i\,(p')\,(\,\not{p}' - m_i) = (\,\not{p} - m_j)\,u_j(p) = 0, \tag{D.1}$$

where

$$\not{p} \equiv p_\mu \gamma^\mu \equiv p \cdot \gamma. \tag{D.2}$$

Dirac matrices fulfill anticommutation relations,

$$\{\gamma^\mu, \gamma^\nu\} = 2g^{\mu\nu}, \qquad \{\gamma^\mu, \gamma^5\} = 0. \tag{D.3}$$

Useful relations of Dirac matrices are [52]

$$\gamma^\nu \;=\; \gamma^0 \gamma^{\nu\dagger} \gamma^0 \tag{D.4}$$
$$\gamma^{0\dagger} \;=\; \gamma^0, \qquad \gamma^0\gamma^0 = \mathbf{1} \tag{D.5}$$
$$\gamma_\mu \gamma^\nu \gamma^\mu \;=\; -2\gamma^\nu \tag{D.6}$$
$$\gamma^{5\dagger} \;=\; \gamma^5 \tag{D.7}$$

Using

$$[\gamma^\mu, \gamma^\nu] = -2i\sigma^{\mu\nu}, \tag{D.8}$$

one can show that

$$\not{a}\,\not{b} = a \cdot b - ia_\mu b_\nu \sigma^{\mu\nu}. \tag{D.9}$$

Then one can derive the following Gordon identity, see e. g. [88] and [54],

$$\bar{u}_i\,(p')\,\gamma^\alpha u_j(p) \;=\; \frac{1}{m_i + m_j}\bar{u}_i\,(p')\left[(p'^\alpha + p^\alpha) + i\sigma^{\alpha\beta}\left(p'_\beta - p_\beta\right)\right]u_j(p)$$

$$\bar{u}_i\,(p')\,\gamma \cdot \epsilon^* u_j(p) \;=\; \frac{1}{m_i + m_j}\bar{u}_i\,(p')\left[2p \cdot \epsilon^* - i\epsilon_\alpha^* \sigma^{\alpha\beta} q_\beta\right]u_j(p), \tag{D.10}$$

where the four-momentum q is defined as $q_\mu = p_\mu - p'_\mu$ and for an on-shell photon $\epsilon \cdot q = \epsilon^* \cdot q = 0$. Making use of eq. (D.3) and

$$\left[\gamma^5, \sigma^{\mu\nu}\right] = 0, \tag{D.11}$$

one can show that

$$
\overline{u}_i\left(p'\right)\gamma^\alpha\gamma^5 u_j(p) = \frac{1}{m_i - m_j}\overline{u}_i\left(p'\right)\left[\left(p'^\alpha + p^\alpha\right) + i\sigma^{\alpha\beta}\left(p'_\beta - p_\beta\right)\right]\gamma_5 u_j(p)
$$

$$
\overline{u}_i\left(p'\right)\gamma\cdot\epsilon^*\gamma_5 u_j(p) = \frac{1}{m_i - m_j}\overline{u}_i\left(p'\right)\left[2p\cdot\epsilon^* - i\epsilon_\alpha^*\sigma^{\alpha\beta}q_\beta\right]\gamma_5 u_j(p). \tag{D.12}
$$

Only helicity-changing terms contribute to leptonic dipole operators at the one-loop level, so that helicity conserving terms, i. e. $\gamma\cdot\epsilon^* = 0$ can be neglected [54]. Therefore, for an on-shell photon $q^2 = 0$, the helicity-changing part of the penguin-type diagrams can be written as

$$
\overline{u}_i\left(p'\right)2p\cdot\epsilon^*\,P_{L(R)}u_j(p) = \overline{u}_i\left(p'\right)i\epsilon_\alpha^*\sigma^{\alpha\beta}q_\beta P_{L(R)}u_j(p). \tag{D.13}
$$

Appendix E

Formulae for calculation of loop integrals

The following identity is used to combine denominator factors [54],

$$\frac{1}{a_1 a_2 \cdots a_n} = (n-1)! \int_0^1 \frac{dz_1 dz_2 \cdots dz_n}{(a_1 z_1 + a_2 z_2 + \cdots + a_n z_n)^n} \delta\left(1 - \sum_{i=1}^n z_i\right), \qquad \text{(E.1)}$$

where the z_i's are called Feynman parameters. In the case of three denominator factors, which arises in the calculation of penguin-type diagrams, the above formula yields

$$\frac{1}{a_1 a_2 a_3} = 2 \int_0^1 dz_1 \int_0^{1-z_1} dz_2 \frac{1}{(z_1 a_1 + z_2 a_2 + (1 - z_1 - z_2) a_3)^3}. \qquad \text{(E.2)}$$

The subsequent relations can be derived by the technique of dimensional regularization in d-dimensions [54],

$$I_0(\alpha, n) = \int \frac{d^n k}{(2\pi)^n} \frac{1}{(k^2 + 2p \cdot k + M^2 + i\epsilon)^\alpha} \qquad \text{(E.3)}$$

$$= i \frac{(-\pi)^{n/2}}{(2\pi)^n} \frac{\Gamma(\alpha - n/2)}{\Gamma(\alpha)} \frac{1}{(M^2 - p^2 + i\epsilon)^{\alpha - (n/2)}} \qquad \text{(E.4)}$$

$$I_\mu(\alpha, n) = \int \frac{d^n k}{(2\pi)^n} \frac{k_\mu}{(k^2 + 2p \cdot k + M^2 + i\epsilon)^\alpha} = -p_\mu I_0(\alpha, n) \qquad \text{(E.5)}$$

$$I_{\mu\nu}(\alpha, n) = \int \frac{d^n k}{(2\pi)^n} \frac{k_\mu k_\nu}{(k^2 + 2p \cdot k + M^2 + i\epsilon)^\alpha} \qquad \text{(E.6)}$$

$$= I_0(\alpha, n) \left(p_\mu p_\nu + \frac{1}{2} g_{\mu\nu} \frac{M^2 - p^2}{\alpha - \frac{n}{2} - 1}\right). \qquad \text{(E.7)}$$

Here k denotes the loop four-momentum. These formulae lead to

$$\int \frac{d^4k}{(2\pi)^4} \frac{1}{(k^2 + 2p \cdot k - M^2 + i\epsilon)^3} = -\frac{i}{32\pi^2} \frac{1}{p^2 + M^2 + i\epsilon} \qquad (E.8)$$

$$\int \frac{d^4k}{(2\pi)^4} \frac{k_\mu}{(k^2 + 2p \cdot k - M^2 + i\epsilon)^3} = \frac{i}{32\pi^2} \frac{p_\mu}{p^2 + M^2 + i\epsilon} \qquad (E.9)$$

$$\left(\int \frac{d^4k}{(2\pi)^4} \frac{k_\mu k_\nu}{(k^2 + 2p \cdot k - M^2 + i\epsilon)^3} \right)_{fin} = -\frac{i}{32\pi^2} \frac{p_\mu p_\nu}{p^2 + M^2 + i\epsilon}. \qquad (E.10)$$

In expression eq. (E.10) we show only the finite part of the integral. The infinite part proportional to $g_{\mu\nu}$ does not contribute to leptonic dipole moments in the leading order of the perturbative calculation, because it cannot be absorbed by counter-terms at this order. As we only consider one-loop integrals, i. e. the amplitudes at leading order, we can safely ignore the infinite part [54]. Due to the same reason the anomalous magnetic moment $(g-2)_e$ of the electron must be finite at the one-loop level in QED [54].

Appendix F

Calculation of $l_j \to l_i\gamma$ at one-loop level

F.1 Neutralino part

For the analytical calculation of the amplitude $\mathcal{M}^n$ for the neutralino-charged slepton diagram in Fig. 3.1, we choose x and a as indices for slepton and neutralino mass eigenstates, respectively. Using the definition of momenta in Fig. F.1, the amplitude is

$$
\begin{aligned}
-i\mathcal{M}^n \;=\; & \overline{u}_i(p') \sum_{x,a} \int \frac{d^4k}{(2\pi)^4} \left[N_{iax}^{R(l)} P_R + N_{iax}^{L(l)} P_L \right] \frac{-i}{\slashed{k} + m_{\tilde{\chi}_a^0}} \left[N_{jax}^{R(l)*} P_L + N_{jax}^{L(l)*} P_R \right] \\
& \times \frac{i}{(p+k)^2 - m_{\tilde{l}_x}^2} ie(2p + 2k - q)_\mu \epsilon^{\mu*} \frac{i}{(p+k-q)^2 - m_{\tilde{l}_x}^2} u_j(p) \qquad \text{(F.1)} \\
\;=\; & -e\epsilon^{\mu*} \overline{u}_i(p') \sum_{x,a} \int \frac{d^4k}{(2\pi)^4} \frac{1}{den_n} \left[N_{iax}^{R(l)} P_R + N_{iax}^{L(l)} P_L \right] (\slashed{k} - m_{\tilde{\chi}_a^0}) \\
& \times \left[N_{jax}^{R(l)*} P_L + N_{jax}^{L(l)*} P_R \right] (2p + 2k - q)_\mu u_j(p), \qquad \text{(F.2)}
\end{aligned}
$$

where the denominator factors can be written as

$$
\begin{aligned}
\frac{1}{den_n} \;=\; & \frac{1}{\left(k^2 - m_{\tilde{\chi}_a^0}^2 \right) \left[(p+k)^2 - m_{\tilde{l}_x}^2 \right] \left[(p+k-q)^2 - m_{\tilde{l}_x}^2 \right]} \qquad \text{(F.3)} \\
\;=\; & 2 \int_0^1 dz_1 \int_0^{1-z_1} dz_2 \frac{1}{A_n^3}, \qquad \text{(F.4)} \\
A_n \;=\; & z_1 \left(k^2 - m_{\tilde{\chi}_a^0}^2 \right) + z_2 \left[(p+k)^2 - m_{\tilde{l}_x}^2 \right] \\
& + (1 - z_1 - z_2) \left[(p+k-q)^2 - m_{\tilde{l}_x}^2 \right] \qquad \text{(F.5)} \\
\;=\; & k^2 + 2k \left[(1-z_1) p + (-1 + z_1 + z_2) q \right] - m_{\tilde{l}_x}^2 (1-z_1) - m_{\tilde{\chi}_a^0}^2 z_1 \\
& + m_{l_j}^2 (1-z_1) + 2p \cdot q (-1 + z_1 + z_2). \qquad \text{(F.6)}
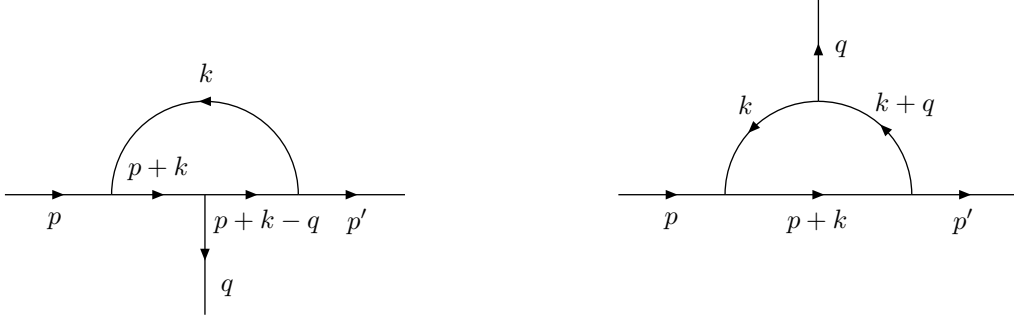\end{aligned}
$$

Figure F.1: Definition of the momenta for the neutralino-charged slepton diagram (left) and the chargino-sneutrino diagram (right) corresponding to Fig. 3.1.

In the last expression we have used the fact that the incoming lepton l_j and the outgoing photon are on-shell, i. e. $p^2 = m_{l_j}^2$ and $q^2 = 0$. From the kinematics of two-body decays [52], it follows that

$$p \cdot q = \frac{1}{2} \left(m_{l_j}^2 - m_{l_i}^2 \right), \tag{F.7}$$

so that the factor A_n in the denominator of eq. (F.2) can be written in the compact form

$$
\begin{aligned}
A_n &= k^2 + 2k \left[(1 - z_1) \, p + (-1 + z_1 + z_2) \, q \right] - b_n^2 - c_n^2, \tag{F.8} \\
b_n^2 &= m_{\tilde{l}_x}^2 \, (1 - z_1) + m_{\tilde{\chi}_a^0}^2 z_1, \tag{F.9} \\
c_n^2 &= -m_{l_j}^2 z_2 - m_{l_i}^2 \, (1 - z_1 - z_2) . \tag{F.10}
\end{aligned}
$$

We use $\epsilon^* \cdot q = 0$ and write the Dirac index structure explicitly,

$$
\begin{aligned}
-i\mathcal{M}^n &= -e\epsilon^{\mu*}\overline{u}_i(p') \sum_{x,a} 2 \int_0^1 dz_1 \int_0^{1-z_1} dz_2 \int \frac{d^4k}{(2\pi)^4} \frac{1}{A_n^3} \\
&\times \left(\left[N_{iax}^{R(l)} N_{jax}^{R(l)*} P_R + N_{iax}^{L(l)} N_{jax}^{L(l)*} P_L \right] (2p_\mu k_\nu \gamma^\nu + 2k_\mu k_\nu \gamma^\nu) \right. \\
&\left. - m_{\tilde{\chi}_a^0} \left[N_{iax}^{R(l)} N_{jax}^{L(l)*} P_R + N_{iax}^{L(l)} N_{jax}^{R(l)*} P_L \right] (2p_\mu + 2k_\mu) \right) u_j(p). \tag{F.11}
\end{aligned}
$$

Using eqs. (E.8) to (E.10) for the calculation of $\int \frac{d^4k}{(2\pi)^4}$ integrals in dimensional regularization, and taking the finite part from the integral over $k_\mu k_\nu$ yields

$$
\begin{aligned}
\mathcal{M}^n &= \frac{e}{16\pi^2}\overline{u}_i(p') \\
&\times \sum_{x,a} \frac{\int dz_1 \int dz_2}{b_n^2 + c_n^2 + (1 - z_1)^2 \, m_{l_j}^2 + (1 - z_1)(-1 + z_1 + z_2) \left(m_{l_j}^2 - m_{l_i}^2 \right)} \\
&\times \left(\left[N_{iax}^{R(l)} N_{jax}^{R(l)*} P_R + N_{iax}^{L(l)} N_{jax}^{L(l)*} P_L \right] 2p \cdot \epsilon^* z_1 \left[(1 - z_1) \not{p} + (-1 + z_1 + z_2) \not{q} \right] \right. \\
&\left. + m_{\tilde{\chi}_a^0} \left[N_{iax}^{R(l)} N_{jax}^{L(l)*} P_R + N_{iax}^{L(l)} N_{jax}^{R(l)*} P_L \right] 2p \cdot \epsilon^* z_1 \right) u_j(p). \tag{F.12}
\end{aligned}
$$

Writing $\not{q} = \not{p} - \not{p}'$ and using the Dirac equation (D.1) for incoming and outgoing lepton leads to

$$
\begin{aligned}
\mathcal{M}^n &= \frac{e}{16\pi^2} \bar{u}_i(p') 2p \cdot \epsilon^* \sum_{x,a} \Big(m_{l_i} \left[N_{iax}^{R(l)} N_{jax}^{R(l)*} P_L + N_{iax}^{L(l)} N_{jax}^{L(l)*} P_R \right] I_i^n \\
&\quad + m_{l_j} \left[N_{iax}^{R(l)} N_{jax}^{R(l)*} P_R + N_{iax}^{L(l)} N_{jax}^{L(l)*} P_L \right] I_j^n \\
&\quad + m_{\tilde{\chi}_a^0} \left[N_{iax}^{R(l)} N_{jax}^{L(l)*} P_R + N_{iax}^{L(l)} N_{jax}^{R(l)*} P_L \right] I_a^n \Big) u_j(p).
\end{aligned}
\tag{F.13}
$$

In the terms proportional to the lepton masses, the helicity flip takes place in the external lepton lines, whereas in the term proportional to the neutralino mass, the helicity is flipped in the neutralino propagator, see also [37], where the mass-insertion technique in the calculation of $Br\,(l_{j \to l_i \gamma})$ is discussed. The loop integrals are given as follows

$$
I_i^n = \int dz \frac{z_1 (1 - z_1 - z_2)}{d_n}
\tag{F.14}
$$

$$
I_j^n = \int dz \frac{z_1 z_2}{d_n}
\tag{F.15}
$$

$$
I_a^n = \int dz \frac{z_1}{d_n},
\tag{F.16}
$$

where integration over Feynman parameters is abbreviated,

$$
\int dz \equiv \int_0^1 dz_1 \int_0^{1-z_1} dz_2,
\tag{F.17}
$$

and the common denominator is

$$
d_n = m_{l_x}^2 (1 - z_1) + m_{\tilde{\chi}_a^0}^2 z_1 - m_{l_j}^2 z_1 z_2 - m_{l_i}^2 z_1 (1 - z_1 - z_2).
\tag{F.18}
$$

F.2 Chargino part

For the analytical calculation of the amplitude $\mathcal{M}^c$ for the chargino-sneutrino diagram in Fig. 3.1, we choose x and a as indices for sneutrino and chargino mass eigenstates, respectively. The momenta for this diagram are defined in Fig. F.1, so that the amplitude is given by

$$
\begin{aligned}
-i\mathcal{M}^c &= \bar{u}_i(p') \sum_{x,a} \int \frac{d^4 k}{(2\pi)^4} \left[C_{iax}^{R(l)} P_R + C_{iax}^{L(l)} P_L \right] \frac{-i}{\not{k} + \not{q} + m_{\tilde{\chi}_a^-}} ie\gamma^\mu \epsilon_\mu^* \\
&\quad \times \frac{-i}{\not{k} + m_{\tilde{\chi}_a^-}} \left[C_{jax}^{R(l)*} P_L + C_{jax}^{L(l)*} P_R \right] \frac{i}{(p+k)^2 - m_{\tilde{\nu}_x}^2} u_j(p).
\end{aligned}
\tag{F.19}
$$

The denominator factors can be written as

$$\frac{1}{den_c} = \frac{1}{\left[(k+q)^2 - m_{\tilde\chi_a^-}^2\right]\left[k^2 - m_{\tilde\chi_a^-}^2\right]\left[(p+k)^2 - m_{\tilde\nu_x}^2\right]} \tag{F.20}$$

$$= 2\int_0^1 dz_1 \int_0^{1-z_1} dz_2 \frac{1}{A_c^3}, \tag{F.21}$$

$$A_c = z_1\left[k^2 + 2k\cdot q - m_{\tilde\chi_a^-}^2\right] + z_2\left[k^2 - m_{\tilde\chi_a^-}^2\right]$$
$$+ (1 - z_1 - z_2)\left[(p+k)^2 - m_{\tilde\nu_x}^2\right] \tag{F.22}$$

$$= k^2 + 2k\cdot\left[(1 - z_1 - z_2)p + z_1 q\right] - b_c^2 - c_c^2, \tag{F.23}$$

where

$$b_c^2 = m_{\tilde\chi_a^-}^2 (z_1 + z_2) + m_{\tilde\nu_x}^2 (1 - z_1 - z_2)$$
$$c_c^2 = m_{l_j}^2 (-1 + z_1 + z_2). \tag{F.24}$$

Making use of

$$\epsilon^* \cdot q = 0, \qquad \overline{u}_i(p')\,p\!\!\!/' = \overline{u}_i(p')\,m_{l_i}, \tag{F.25}$$

and specifying the Dirac index structure of the terms, the amplitude of the chargino part becomes

$$-i\mathcal{M}^c = e\overline{u}_i(p')\sum_{x,a} 2\int dz \int \frac{d^4k}{(2\pi)^4}\frac{1}{den_c}\left(\left[-g^{\mu\nu}k_\mu k_\nu \epsilon\!\!\!/^* + m_{\tilde\chi_a^-}^2\epsilon\!\!\!/^* - 2p^\nu k_\nu \epsilon\!\!\!/^*\right.\right.$$
$$+2\epsilon^{*\mu}k_\mu k_\nu\gamma^\nu + \epsilon\!\!\!/^* k_\nu\gamma^\nu p\!\!\!/ - m_{l_i}\epsilon\!\!\!/^* k_\nu\gamma^\nu + 2p\cdot\epsilon^* k_\nu\gamma^\nu\right]$$
$$\times\left[C_{iax}^{R(l)}C_{jax}^{R(l)*}P_L + C_{iax}^{L(l)}C_{jax}^{L(l)*}P_R\right] - m_{\tilde\chi_a^-}\left[-m_{l_i}\epsilon\!\!\!/^* - \epsilon\!\!\!/^* p\!\!\!/ + 2\epsilon^{*\nu}k_\nu + 2p\cdot\epsilon^*\right]$$
$$\times\left.\left[C_{iax}^{R(l)}C_{jax}^{L(l)*}P_R + C_{iax}^{L(l)}C_{jax}^{R(l)*}P_L\right]\right)u_j(p). \tag{F.26}$$

Using eqs. (E.8) to (E.10) for the calculation of $\int\frac{d^4k}{(2\pi)^4}$ integrals in dimensional regularization, and taking the finite part from the integral over $k_\mu k_\nu$ leads to

$$-\mathcal{M}^c = \overline{u}_i(p')\frac{e}{16\pi^2}$$
$$\times\sum_{x,a}\frac{\int dz}{b_c^2 + c_c^2 + (1 - z_1 - z_2)^2 m_{l_j}^2 + (1 - z_1 - z_2)z_1\left(m_{l_j}^2 - m_{l_i}^2\right)}$$
$$\times\left(\left(-2(1 - z_1 - z_2)p\cdot\epsilon^*\left[(1 - z_1 - z_2)p\!\!\!/ + z_1 q\!\!\!/\right] + z_1\epsilon\!\!\!/^* q\!\!\!/ p\!\!\!/\right.\right.$$
$$-m_{l_i}(1 - z_1 - z_2)\epsilon\!\!\!/^* p\!\!\!/ - m_{l_i}z_1\epsilon\!\!\!/^* q\!\!\!/ + 2p\cdot\epsilon^*(1 - z_1 - z_2)p\!\!\!/$$
$$+2p\cdot\epsilon^* z_1 q\!\!\!/\right)\left[C_{iax}^{R(l)}C_{jax}^{R(l)*}P_L + C_{iax}^{L(l)}C_{jax}^{L(l)*}P_R\right]$$
$$+m_{\tilde\chi_a^-}\left[2p\cdot\epsilon^*(z_1 + z_2)\right]\left.\left[C_{iax}^{R(l)}C_{jax}^{L(l)*}P_R + C_{iax}^{L(l)}C_{jax}^{R(l)*}P_L\right]\right)u_j(p). \tag{F.27}$$

To derive the last expression, we use $p \cdot q = \frac{1}{2}\left(m_{l_j}^2 - m_{l_i}^2\right)$ and also that a term of the form $const \not{\epsilon}^*$ does not lead to dipole-type amplitudes and thus can be disregarded. After some Dirac algebra, in particular using eq. (D.1), the amplitude of the chargino part is given by

$$
\begin{aligned}
\mathcal{M}^c \;=\;& -\frac{e}{16\pi^2}\overline{u}_i(p')2p \cdot \epsilon^* \sum_{x,a}\left(m_{l_i}\left[C_{iax}^{R(l)}C_{jax}^{R(l)*}P_L + C_{iax}^{L(l)}C_{jax}^{L(l)*}P_R\right] I_i^c \right.\\
&+ m_{l_j}\left[C_{iax}^{R(l)}C_{jax}^{R(l)*}P_R + C_{iax}^{L(l)}C_{jax}^{L(l)*}P_L\right] I_j^c \\
&\left.+ m_{\tilde{\chi}_a^-}\left[C_{iax}^{R(l)}C_{jax}^{L(l)*}P_R + C_{iax}^{L(l)}C_{jax}^{R(l)*}P_L\right] I_a^c \right) u_j(p).
\end{aligned}
\tag{F.28}
$$

In analogy to the neutralino part, the helicity flip takes place in the external lepton lines in those terms of eq. (F.28) proportional to lepton masses, whereas in the term proportional to the chargino mass, the helicity is flipped in the chargino propagator. The loop integrals are given as follows

$$
I_i^c \;=\; \int dz \frac{z_1\left(1 - z_1 - z_2\right)}{d_c} \tag{F.29}
$$

$$
I_j^c \;=\; \int dz \frac{z_2\left(1 - z_1 - z_2\right)}{d_c} \tag{F.30}
$$

$$
I_a^c \;=\; \int dz \frac{z_1 + z_2}{d_c}, \tag{F.31}
$$

where

$$
\begin{aligned}
d_c \;=\;& m_{\tilde{\nu}_x}^2\left(1 - z_1 - z_2\right) + m_{\tilde{\chi}_a^-}^2\left(z_1 + z_2\right) + m_{l_j}^2 z_2\left(-1 + z_1 + z_2\right)\\
&+ m_{l_i}^2 z_1\left(-1 + z_1 + z_2\right).
\end{aligned}
\tag{F.32}
$$

Exchanging the indices $i \leftrightarrow j$ and the integration variables $z_1 \leftrightarrow z_2$ simultaneously transforms I_i^c into I_j^c and vice versa.

In summary, the coefficients for the one-loop leptonic dipole factors are given by

$$
\begin{aligned}
16\pi^2 A_L^{ij} m_{l_j} \;=\;& m_{l_i}I_i^n N_{iax}^{R(l)}N_{jax}^{R(l)*} + m_{l_j}I_j^n N_{iax}^{L(l)}N_{jax}^{L(l)*} + m_{\tilde{\chi}_a^0}I_a^n N_{iax}^{L(l)}N_{jax}^{R(l)*}\\
&- m_{l_i}I_i^c C_{iax}^{R(l)}C_{jax}^{R(l)*} - m_{l_j}I_j^c C_{iax}^{L(l)}C_{jax}^{L(l)*} - m_{\tilde{\chi}_a^-}I_a^c C_{iax}^{L(l)}C_{jax}^{R(l)*}
\end{aligned}
\tag{F.33}
$$

$$
\begin{aligned}
16\pi^2 A_R^{ij} m_{l_j} \;=\;& m_{l_i}I_i^n N_{iax}^{L(l)}N_{jax}^{L(l)*} + m_{l_j}I_j^n N_{iax}^{R(l)}N_{jax}^{R(l)*} + m_{\tilde{\chi}_a^0}I_a^n N_{iax}^{R(l)}N_{jax}^{L(l)*}\\
&- m_{l_i}I_i^c C_{iax}^{L(l)}C_{jax}^{L(l)*} - m_{l_j}I_j^c C_{iax}^{R(l)}C_{jax}^{R(l)*} - m_{\tilde{\chi}_a^-}I_a^c C_{iax}^{R(l)}C_{jax}^{L(l)*}.
\end{aligned}
\tag{F.34}
$$

F.3   Limiting behavior of loop functions

Neglecting the leptonic masses in the loop integration, the loop functions including the sparticle masses are given by [89]:

$$F_i^c = \frac{1}{2m_{\tilde{\nu}_x}^2} \frac{2 + 3r - 6r^2 + r^3 + 6r\ln r}{6(1-r)^4} \equiv I_{j,i}^c\left(m_{l_i}^2, m_{l_j}^2 \to 0\right) \tag{F.35}$$

$$F_a^c = \frac{m_{\tilde{\chi}_a^-}}{2m_{\tilde{\nu}_x}^2} \frac{-3 + 4r - r^2 - 2\ln r}{(1-r)^3} \equiv m_{\tilde{\chi}_a^-} I_a^c\left(m_{l_i}^2, m_{l_j}^2 \to 0\right) \tag{F.36}$$

$$F_i^n = \frac{1}{2m_{\tilde{l}_x}^2} \frac{1 - 6r + 3r^2 + 2r^3 - 6r^2\ln r}{6(1-r)^4} \equiv I_{j,i}^n\left(m_{l_i}^2, m_{l_j}^2 \to 0\right) \tag{F.37}$$

$$F_a^n = \frac{m_{\tilde{\chi}_a^0}}{2m_{\tilde{l}_x}^2} \frac{1 - r^2 + 2r\ln r}{(1-r)^3} \equiv m_{\tilde{\chi}_a^0} I_a^c\left(m_{l_i}^2, m_{l_j}^2 \to 0\right), \tag{F.38}$$

where in the loop functions of the chargino diagram (superscript c) r denotes $\frac{m_{\tilde{\chi}_a^-}^2}{m_{\tilde{\nu}_x}^2}$ and in those corresponding to the neutralino diagram (superscript n) $\frac{m_{\tilde{\chi}_a^0}^2}{m_{\tilde{l}_x}^2}$, respectively.

In the limit of $r = 1$, i. e. $m_{\tilde{\nu}_x} = m_{\tilde{\chi}_a^-}$ or $m_{\tilde{l}_x} = m_{\tilde{\chi}_a^0}$, these fuctions obtain the following values,

$$F_i^c(r = 1) = \frac{1}{24m_{\tilde{\nu}_x}^2} \tag{F.39}$$

$$F_a^c(r = 1) = \frac{m_{\tilde{\chi}_a^-}}{3m_{\tilde{\nu}_x}^2} = \frac{1}{3m_{\tilde{\nu}_x}} \tag{F.40}$$

$$F_i^n(r = 1) = \frac{1}{24m_{\tilde{l}_x}^2} \tag{F.41}$$

$$F_a^n(r = 1) = \frac{m_{\tilde{\chi}_a^0}}{6m_{\tilde{l}_x}^2} = \frac{1}{6m_{\tilde{l}_x}}. \tag{F.42}$$

For $r \gg 1$, these functions behave as

$$F_i^c(r \gg 1) = \frac{1}{12m_{\tilde{\chi}_a^-}^2} \tag{F.43}$$

$$F_a^c(r \gg 1) = \frac{1}{2m_{\tilde{\chi}_a^-}} \tag{F.44}$$

$$F_i^n(r \gg 1) = \frac{1}{6m_{\tilde{\chi}_a^0}^2} \tag{F.45}$$

$$F_a^n(r \gg 1) = \frac{1}{2m_{\tilde{\chi}_a^0}}. \tag{F.46}$$

For $r \ll 1$, these functions are approximated by

$$F_i^c(r \ll 1) \quad = \quad \frac{1}{6m_{\tilde{\nu}_x}^2} \tag{F.47}$$

$$F_a^c(r \ll 1) \quad = \quad -\frac{m_{\tilde{\chi}_a^-}}{m_{\tilde{\nu}_x}^2} \ln \frac{m_{\tilde{\chi}_a^-}^2}{m_{\tilde{\nu}_x}^2} \tag{F.48}$$

$$F_i^n(r \ll 1) \quad = \quad \frac{1}{12m_{\tilde{l}_x}^2} \tag{F.49}$$

$$F_a^n(r \ll 1) \quad = \quad \frac{m_{\tilde{\chi}_a^0}}{2m_{\tilde{l}_x}^2}. \tag{F.50}$$

Appendix G

Evaluation of loop functions for other leptonic low-energy processes

The calculation of the decay rates for lepton-flavor violating decays $l_j^- \to l_i^- l_i^+ l_i^-$ and μ-e conversion on nuclei can be found in [31]. As we follow the conventions and the calculation for these processes, we do not repeat their full results here.

In the calculation of box diagrams to the process $l_j^- \to l_i^- l_i^+ l_j^-$, the following types of loop integrals occur:

$$I_3^0 = \int \frac{d^4k}{\left(k^2 - m_1^2\right)\left(k^2 - m_2^2\right)\left(k^2 - m_3^2\right)} \tag{G.1}$$

$$I_4^0 = \frac{-i}{(2\pi)^4} \int \frac{d^4k}{\left(k^2 - m_1^2\right)\left(k^2 - m_2^2\right)\left(k^2 - m_3^2\right)\left(k^2 - m_4^2\right)} \tag{G.2}$$

$$J_4^0 = \frac{-i}{(2\pi)^4} \int \frac{d^4k\, k^2}{\left(k^2 - m_1^2\right)\left(k^2 - m_2^2\right)\left(k^2 - m_3^2\right)\left(k^2 - m_4^2\right)}. \tag{G.3}$$

Obviously, the functions I_3^0, I_4^0 and J_4^0 are functions of the squared masses m_1^2, m_2^2, m_3^2 and for the latter two also of m_4^2. Making use of Feynman parameters, see eq. (E.2), and performing the loop-momentum integration in Euclidean space, one obtains

$$I_3^0 = -i\pi^2 \int_0^1 \frac{dz_1 dz_2 dz_3 \delta\left(1 - z_1 - z_2 - z_3\right)}{z_1 m_1^2 + z_2 m_2^2 + z_3 m_3^2}, \tag{G.4}$$

which can be evaluated to be

$$I_3^0 = -i\pi^2 \left[\frac{m_1^2 \ln m_1^2}{\left(m_1^2 - m_2^2\right)\left(m_1^2 - m_3^2\right)} + \frac{m_2^2 \ln m_2^2}{\left(m_2^2 - m_1^2\right)\left(m_2^2 - m_3^2\right)} + \frac{m_3^2 \ln m_3^2}{\left(m_3^2 - m_1^2\right)\left(m_3^2 - m_2^2\right)}\right]. \tag{G.5}$$

The loop function I_4^0 can be written in terms of I_3^0,

$$I_4^0\left(m_1^2, m_2^2, m_3^2, m_4^2\right) = \frac{-i}{(2\pi)^4} \frac{1}{m_1^2 - m_2^2} \left(I_3^0\left(m_1^2, m_3^2, m_4^2\right) - I_3^0\left(m_2^2, m_3^2, m_4^2\right)\right), \tag{G.6}$$

leading to

$$I_4^0 = -\frac{1}{16\pi^2}\left[\frac{m_1^2 \ln m_1^2}{(m_1^2 - m_2^2)(m_1^2 - m_3^2)(m_1^2 - m_4^2)} + \frac{m_2^2 \ln m_2^2}{(m_2^2 - m_1^2)(m_2^2 - m_3^2)(m_2^2 - m_4^2)}\right.$$
$$\left. + \frac{m_3^2 \ln m_3^2}{(m_3^2 - m_1^2)(m_3^2 - m_2^2)(m_3^2 - m_4^2)} + \frac{m_4^2 \ln m_4^2}{(m_4^2 - m_1^2)(m_4^2 - m_2^2)(m_4^2 - m_3^2)}\right].$$
(G.7)

Then the loop function J_4^0 can be expressed through I_3^0 and I_4^0,

$$J_4^0\left(m_1^2, m_2^2, m_3^2, m_4^2\right) = m_4^2 I_4^0\left(m_1^2, m_2^2, m_3^2, m_4^2\right) - \frac{i}{(2\pi)^4}I_3^0\left(m_1^2, m_2^2, m_3^2\right). \tag{G.8}$$

If some of the masses appearing in the loops are equal, the following limits of I_3^0 occur

$$I_3^0\left(m_1^2, m_2^2, m_2^2\right) = -\frac{i\pi^2}{m_2^2 - m_1^2}\left[1 + \frac{m_1^2}{m_2^2 - m_1^2}\ln\frac{m_1^2}{m_2^2}\right] \tag{G.9}$$

$$I_3^0\left(m_1^2, m_1^2, m_2^2\right) = -\frac{i\pi^2}{m_1^2 - m_2^2}\left[1 + \frac{m_2^2}{m_1^2 - m_2^2}\ln\frac{m_2^2}{m_1^2}\right]. \tag{G.10}$$

In order to derive these results for equal masses, some interesting calculations have to be performed, as shall be demonstrated in the case of $I_3^0\left(m_1^2, m_1^2, m_2^2\right)$:
We express the difference between m_1^2 and m_2^2 through the infinitesimal quantity ϵ,

$$m_2^2 = (1 + \epsilon)m_1^2, \qquad m_1^2 - m_2^2 = -\epsilon m_1^2. \tag{G.11}$$

In the limit $\epsilon \to 0$ we obtain for the terms involving $\ln m_1^2$ and $\ln m_2^2$ in $I_3^0\left(m_1^2, m_2^2, m_3^2\right)$, see eq. (G.5),

$$-i\pi^2 \lim_{\epsilon \to 0}\left[\frac{\ln m_1^2}{(m_1^2 - m_3^2)(-\epsilon)} + \frac{(1 + \epsilon)(\ln m_1^2 + \ln(1 + \epsilon))}{\epsilon((1 + \epsilon)m_1^2 - m_3^2)}\right]$$

$$= -i\pi^2 \lim_{\epsilon \to 0}\left[\frac{\ln m_1^2}{m_1^2 - m_3^2}\left(-\frac{1}{\epsilon} + \frac{1 + \epsilon}{\epsilon\left(1 + \frac{\epsilon m_1^2}{m_1^2 - m_3^2}\right)}\right) + \frac{(1 + \epsilon)\ln(1 + \epsilon)}{(m_1^2 - m_3^2)\epsilon\left(1 + \frac{m_1^2\epsilon}{m_1^2 - m_3^2}\right)}\right]$$

$$= -i\pi^2\left[-\frac{m_3^2 \ln m_1^2}{(m_1^2 - m_3^2)^2} + \frac{1}{m_1^2 - m_3^2}\right]. \tag{G.12}$$

In deriving this limit we have used

$$\ln(1 + \epsilon) \simeq \epsilon - \frac{\epsilon^2}{2} \tag{G.13}$$

for small $|\epsilon| \ll 1$, so that

$$(1 + \epsilon)\ln(1 + \epsilon) \simeq \epsilon(1 + \epsilon) \simeq \epsilon. \tag{G.14}$$

The third term in $I_3^0\left(m_1^2, m_2^2, m_3^2\right)$, see eq. (G.5), proportional to $\ln m_3^2$ is simply given by $\frac{m_3^2 \ln m_3^2}{\left(m_3^2 - m_1^2\right)^2}$, so that the above limit eq. (G.10) is verified.

It should be mentioned that the other limits of I_3^0 and I_4^0 for equal masses can be derived in an analogous way,

$$
\begin{aligned}
I_4^0\left(m_1^2, m_1^2, m_2^2, m_3^2\right) &= -\frac{1}{16\pi^2}\left[\frac{m_2^2 \ln m_2^2}{\left(m_2^2 - m_1^2\right)^2\left(m_2^2 - m_3^2\right)} + \frac{m_3^2 \ln m_3^2}{\left(m_3^2 - m_1^2\right)^2\left(m_3^2 - m_2^2\right)}\right. \\
&\left. + \frac{\left(m_1^2 - m_2^2\right)\left(m_1^2 - m_3^2\right) - \left(m_1^4 - m_2^2 m_3^2\right)\ln m_1^2}{\left(m_1^2 - m_2^2\right)^2\left(m_1^2 - m_3^2\right)^2}\right] \quad\text{(G.15)}
\end{aligned}
$$

$$
\begin{aligned}
I_4^0\left(m_1^2, m_2^2, m_3^2, m_3^2\right) &= -\frac{1}{16\pi^2}\left[\frac{m_1^2 \ln m_1^2}{\left(m_1^2 - m_2^2\right)\left(m_1^2 - m_3^2\right)^2} + \frac{m_2^2 \ln m_2^2}{\left(m_2^2 - m_1^2\right)\left(m_2^2 - m_3^2\right)^2}\right. \\
&\left. + \frac{\left(m_3^2 - m_1^2\right)\left(m_3^2 - m_2^2\right) - \left(m_3^4 - m_1^2 m_2^2\right)\ln m_3^2}{\left(m_3^2 - m_1^2\right)^2\left(m_3^2 - m_2^2\right)^2}\right] \quad\text{(G.16)}
\end{aligned}
$$

$$
I_4^0\left(m_1^2, m_1^2, m_2^2, m_2^2\right) = -\frac{1}{16\pi^2}\frac{1}{\left(m_1^2 - m_2^2\right)^2}\left[2 + \frac{m_1^2 + m_2^2}{m_1^2 - m_2^2}\ln\frac{m_2^2}{m_1^2}\right]. \quad\text{(G.17)}
$$

For definiteness, we also show the functions arising from Z-boson penguin-type diagrams [31] and present relevant limits with equal masses,

$$
F\left(m_x^2, m_a^2, m_b^2\right) = \ln\frac{m_a^2}{m_x^2} + \frac{1}{m_a^2 - m_b^2}\left(\frac{m_a^4 \ln\frac{m_a^2}{m_x^2}}{m_x^2 - m_a^2} - \frac{m_b^4 \ln\frac{m_b^2}{m_x^2}}{m_x^2 - m_b^2}\right) \quad\text{(G.18)}
$$

$$
F\left(m_x^2, m_a^2, m_a^2\right) = \ln\frac{m_a^2}{m_x^2} - \frac{m_a^2}{m_x^2 - m_a^2}\left(-1 + \frac{2m_x^2 - m_a^2}{m_x^2 - m_a^2}\ln\frac{m_x^2}{m_a^2}\right) \quad\text{(G.19)}
$$

$$
G\left(m_x^2, m_a^2, m_b^2\right) = \frac{m_a m_b}{m_a^2 - m_b^2}\left(\frac{m_a^2 \ln\frac{m_a^2}{m_x^2}}{m_x^2 - m_a^2} - \frac{m_b^2 \ln\frac{m_b^2}{m_x^2}}{m_x^2 - m_b^2}\right) \quad\text{(G.20)}
$$

$$
G\left(m_x^2, m_a^2, m_a^2\right) = \frac{m_a^2}{m_x^2 - m_a^2}\left(1 + \frac{m_x^2}{m_x^2 - m_a^2}\ln\frac{m_a^2}{m_x^2}\right). \quad\text{(G.21)}
$$

It should also be mentioned that we have corrected equation (25) in [31] according to [90], in such a way that the term in brackets now reads $F_{X,A,B} + G_{X,A,B}$ instead of $F_{X,A,B} + 2G_{X,A,B}$. Moreover, the logarithmically enhanced contribution of photon penguin diagrams in $\Gamma\left(l_j^- \to l_i^- l_i^+ l_i^-\right)$ is taken to be $\left(\frac{8}{3}\ln\frac{m_{l_j}^2}{m_{l_i}^2} - \frac{22}{3}\right)$ instead of $\left(\frac{16}{3}\ln\frac{m_{l_j}}{2m_{l_i}} - \frac{14}{9}\right)$ in equation (52) of [31].

Appendix H

Renormalization group equations

In the following RGEs, the renormalization scale is denoted by μ. At first, we list the one-loop RGEs for the Yukawa couplings, gauge couplings and the effective neutrino mass matrix, valid in the SM extended by right-handed neutrino singlets, see [91] and [92],

$$
16\pi^2 \mu \frac{dY_u}{d\mu} = Y_u \left(\left(-\frac{17}{20}g_1^2 - \frac{9}{4}g_2^2 - 8g_3^2 + Tr\left(3Y_u^\dagger Y_u + 3Y_d^\dagger Y_d + Y_e^\dagger Y_e\right) \right) \mathbf{1} \right.
$$
$$
\left. + \frac{3}{2}\left(Y_u^\dagger Y_u - Y_d^\dagger Y_d\right) \right) \tag{H.1}
$$

$$
16\pi^2 \mu \frac{dY_d}{d\mu} = Y_d \left(\left(-\frac{1}{4}g_1^2 - \frac{9}{4}g_2^2 - 8g_3^2 + Tr\left(3Y_u^\dagger Y_u + 3Y_d^\dagger Y_d + Y_e^\dagger Y_e\right) \right) \mathbf{1} \right.
$$
$$
\left. + \frac{3}{2}\left(Y_d^\dagger Y_d - Y_u^\dagger Y_u\right) \right) \tag{H.2}
$$

$$
16\pi^2 \mu \frac{dY_e}{d\mu} = Y_e \left(\left(-\frac{9}{4}g_1^2 - \frac{9}{4}g_2^2 + Tr\left(3Y_u^\dagger Y_u + 3Y_d^\dagger Y_d + Y_e^\dagger Y_e\right) \right) \mathbf{1} \right.
$$
$$
\left. + \frac{3}{2}Y_e^\dagger Y_e \right) \tag{H.3}
$$

$$
16\pi^2 \mu \frac{dg_a}{d\mu} = b_a^{SM} g_a^3 \tag{H.4}
$$

$$
16\pi^2 \mu \frac{d\kappa}{d\mu} = -\frac{3}{2}\left(Y_e^\dagger Y_e\right)^T \kappa - \frac{3}{2}\kappa\left(Y_e^\dagger Y_e\right) + 2Tr\left(Y_e^\dagger Y_e\right)\mathbf{1}\kappa
$$
$$
+ \left(6Tr\left(Y_u^\dagger Y_u + Y_d^\dagger Y_d\right)\mathbf{1} - 3g_2^2\mathbf{1} + \lambda_h\mathbf{1}\right)\kappa, \tag{H.5}
$$

where in GUT normalization for $U(1)_Y$, $b_a^{SM} = \left(\frac{41}{10}, -\frac{19}{6}, -7\right)$ and we have used that Y_ν vanishes below the mass scales of the right-handed neutrino singlets which are assumed to be many orders of magnitudes above the SUSY-scale in the SUSY seesaw model. Due to the underlying supersymmetric theory, the Higgs self-coupling λ_h is given by $\lambda_h = \frac{1}{4}\left(g_1^2 + g_2^2\right)$, see also [34]. Note that the top Yukawa couplings are integrated in above their running mass threshold $m_t\left(m_Z\right)$.

The one-loop RGEs for Yukawa coupling matrices in the SUSY seesaw model are given by

$$
16\pi^2\mu\frac{dY_u}{d\mu} = Y_u\left(\left(-\frac{13}{15}g_1^2 - 3g_2^2 - \frac{16}{3}g_3^2 + Tr\left(3Y_u^\dagger Y_u + Y_\nu^\dagger Y_\nu\right)\right)\mathbf{1}\right.
$$
$$
\left. +3Y_u^\dagger Y_u + Y_d^\dagger Y_d\right) \tag{H.6}
$$

$$
16\pi^2\mu\frac{dY_d}{d\mu} = Y_d\left(\left(-\frac{7}{15}g_1^2 - 3g_2^2 - \frac{16}{3}g_3^2 + Tr\left(3Y_d^\dagger Y_d + Y_e^\dagger Y_e\right)\right)\mathbf{1}\right.
$$
$$
\left. +3Y_d^\dagger Y_d + Y_u^\dagger Y_u\right) \tag{H.7}
$$

$$
16\pi^2\mu\frac{dY_e}{d\mu} = Y_e\left(\left(-\frac{9}{5}g_1^2 - 3g_2^2 + Tr\left(3Y_d^\dagger Y_d + Y_e^\dagger Y_e\right)\right)\mathbf{1}\right.
$$
$$
\left. +3Y_e^\dagger Y_e + Y_\nu^\dagger Y_\nu\right) \tag{H.8}
$$

$$
16\pi^2\mu\frac{dY_\nu}{d\mu} = Y_\nu\left(\left(-\frac{3}{5}g_1^2 - 3g_2^2 + Tr\left(3Y_u^\dagger Y_u + Y_\nu^\dagger Y_\nu\right)\right)\mathbf{1}\right.
$$
$$
\left. +3Y_\nu^\dagger Y_\nu + Y_e^\dagger Y_e\right), \tag{H.9}
$$

see also [31], [35] and [45]. For the RGEs of supersymmetric gauge couplings and gaugino masses we also take into account important two-loop effects, see also [34],

$$
16\pi^2\mu\frac{dg_a}{d\mu} = g_a^3 B_a^{(1)} + \frac{g_a^3}{16\pi^2}\left(\sum_{b=1}^3 B_{ab}^{(2)} g_b^2\right) \tag{H.10}
$$

$$
16\pi^2\mu\frac{d\tilde{M}_a}{d\mu} = 2g_a^2 B_a^{(1)}\tilde{M}_a + \frac{2g_a^2}{16\pi^2}\sum_{b=1}^3 B_{ab}^{(2)} g_b^2\left(\tilde{M}_a + \tilde{M}_b\right). \tag{H.11}
$$

Here the coefficients are $B^{(1)} = \left(\frac{33}{5}, 1, -3\right)$ for $U(1)_Y$ in GUT normalization, $SU(2)_L$ and $SU(3)_C$, respectively, and

$$
B^{(2)} = \begin{pmatrix} \frac{199}{25} & \frac{27}{5} & \frac{88}{5} \\ \frac{9}{5} & 25 & 24 \\ \frac{11}{5} & 9 & 14 \end{pmatrix}. \tag{H.12}
$$

In GUT normalization for $U(1)_Y$, the one-loop RGEs for the effective neutrino mass matrix and the right-handed Majorana mass matrix in the SUSY seesaw model are as follows [36],

$$
16\pi^2\mu\frac{d\kappa}{d\mu} = \left(Y_e^\dagger Y_e\right)^T\kappa + \kappa\left(Y_e^\dagger Y_e\right) + \left(Y_\nu^\dagger Y_\nu\right)^T\kappa + \kappa\left(Y_\nu^\dagger Y_\nu\right)
$$
$$
+ \left(2Tr\left(3Y_u^\dagger Y_u + Y_\nu^\dagger Y_\nu\right) - \frac{6}{5}g_1^2 - 6g_2^2\right)\kappa \tag{H.13}
$$

$$
16\pi^2\mu\frac{dM}{d\mu} = 2\left(Y_\nu Y_\nu^\dagger\right)M + 2M\left(Y_\nu Y_\nu^\dagger\right)^T. \tag{H.14}
$$

The one-loop RGEs for soft-breaking terms in the MSSM [50], extended to the SUSY seesaw model read [34]

$$16\pi^2\mu\frac{dm_{\tilde{Q}}^2}{d\mu} = m_{\tilde{Q}}^2 Y_u^\dagger Y_u + Y_u^\dagger Y_u m_{\tilde{Q}}^2 + m_{\tilde{Q}}^2 Y_d^\dagger Y_d + Y_d^\dagger Y_d m_{\tilde{Q}}^2$$
$$+2\left(Y_d^\dagger m_{\tilde{d}}^2 Y_d + m_{h_1}^2 Y_d^\dagger Y_d + A_d^\dagger A_d + Y_u^\dagger m_{\tilde{u}}^2 Y_u + m_{h_2}^2 Y_u^\dagger Y_u + A_u^\dagger A_u\right)$$
$$-\left(\frac{2}{15}g_1^2|\tilde{M}_1|^2 + 6g_2^2|\tilde{M}_2|^2 + \frac{32}{3}g_3^2|\tilde{M}_3|^2 - \frac{1}{5}g_1^2 S\right)\mathbf{1} \tag{H.15}$$

$$16\pi^2\mu\frac{dm_{\tilde{L}}^2}{d\mu} = m_{\tilde{L}}^2 Y_e^\dagger Y_e + Y_e^\dagger Y_e m_{\tilde{L}}^2 + m_{\tilde{L}}^2 Y_\nu^\dagger Y_\nu + Y_\nu^\dagger Y_\nu m_{\tilde{L}}^2$$
$$+2\left(Y_e^\dagger m_{\tilde{e}}^2 Y_e + m_{h_1}^2 Y_e^\dagger Y_e + A_e^\dagger A_e + Y_\nu^\dagger m_{\tilde{\nu}}^2 Y_\nu + m_{h_2}^2 Y_\nu^\dagger Y_\nu + A_\nu^\dagger A_\nu\right)$$
$$-\left(\frac{6}{5}g_1^2|\tilde{M}_1|^2 + 6g_2^2|\tilde{M}_2|^2 + \frac{3}{5}g_1^2 S\right)\mathbf{1} \tag{H.16}$$

$$16\pi^2\mu\frac{dm_{\tilde{u}}^2}{d\mu} = 2\left(m_{\tilde{u}}^2 Y_u Y_u^\dagger + Y_u Y_u^\dagger m_{\tilde{u}}^2\right) + 4\left(Y_u m_{\tilde{Q}}^2 Y_u^\dagger + m_{h_2}^2 Y_u Y_u^\dagger + A_u A_u^\dagger\right)$$
$$-\left(\frac{32}{15}g_1^2|\tilde{M}_1|^2 + \frac{32}{3}g_3^2|\tilde{M}_3|^2 + \frac{4}{5}g_1^2 S\right)\mathbf{1} \tag{H.17}$$

$$16\pi^2\mu\frac{dm_{\tilde{d}}^2}{d\mu} = 2\left(m_{\tilde{d}}^2 Y_d Y_d^\dagger + Y_d Y_d^\dagger m_{\tilde{d}}^2\right) + 4\left(Y_d m_{\tilde{Q}}^2 Y_d^\dagger + m_{h_1}^2 Y_d Y_d^\dagger + A_d A_d^\dagger\right)$$
$$-\left(\frac{8}{15}g_1^2|\tilde{M}_1|^2 + \frac{32}{3}g_3^2|\tilde{M}_3|^2 - \frac{2}{5}g_1^2 S\right)\mathbf{1} \tag{H.18}$$

$$16\pi^2\mu\frac{dm_{\tilde{e}}^2}{d\mu} = 2\left(m_{\tilde{e}}^2 Y_e Y_e^\dagger + Y_e Y_e^\dagger m_{\tilde{e}}^2\right) + 4\left(Y_e m_{\tilde{L}}^2 Y_e^\dagger + m_{h_1}^2 Y_e Y_e^\dagger + A_e A_e^\dagger\right)$$
$$-\left(\frac{24}{5}g_1^2|\tilde{M}_1|^2 - \frac{6}{5}g_1^2 S\right)\mathbf{1} \tag{H.19}$$

$$16\pi^2\mu\frac{dm_{\tilde{\nu}}^2}{d\mu} = 2\left(m_{\tilde{\nu}}^2 Y_\nu Y_\nu^\dagger + Y_\nu Y_\nu^\dagger m_{\tilde{\nu}}^2\right) + 4\left(Y_\nu m_{\tilde{\nu}}^2 Y_\nu^\dagger + m_{h_2}^2 Y_\nu Y_\nu^\dagger + A_\nu A_\nu^\dagger\right) \tag{H.20}$$

$$16\pi^2\mu\frac{dm_{h_1}^2}{d\mu} = 6Tr\left(m_{\tilde{Q}}^2 Y_d^\dagger Y_d + Y_d^\dagger\left(m_{\tilde{d}}^2 + m_{h_1}^2\mathbf{1}\right)Y_d + A_d^\dagger A_d\right)$$
$$+2Tr\left(m_{\tilde{L}}^2 Y_e^\dagger Y_e + Y_e^\dagger\left(m_{\tilde{e}}^2 + m_{h_1}^2\mathbf{1}\right)Y_e + A_e^\dagger A_e\right)$$
$$-\frac{6}{5}g_1^2|\tilde{M}_1|^2 - 6g_2^2|\tilde{M}_2|^2 - \frac{3}{5}g_1^2 S \tag{H.21}$$

$$16\pi^2\mu\frac{dm_{h_2}^2}{d\mu} = 6Tr\left(m_{\tilde{Q}}^2 Y_u^\dagger Y_u + Y_u^\dagger\left(m_{\tilde{u}}^2 + m_{h_2}^2\mathbf{1}\right)Y_u + A_u^\dagger A_u\right)$$
$$+2Tr\left(m_{\tilde{L}}^2 Y_\nu^\dagger Y_\nu + Y_\nu^\dagger\left(m_{\tilde{\nu}}^2 + m_{h_2}^2\mathbf{1}\right)Y_\nu + A_\nu^\dagger A_\nu\right)$$
$$-\frac{6}{5}g_1^2|\tilde{M}_1|^2 - 6g_2^2|\tilde{M}_2|^2 + \frac{3}{5}g_1^2 S \tag{H.22}$$

$$16\pi^2\mu\frac{dA_u}{d\mu} = \left(-\frac{13}{15}g_1^2 - 3g_2^2 - \frac{16}{3}g_3^2 + Tr\left(3Y_u^\dagger Y_u + Y_\nu^\dagger Y_\nu\right)\right)A_u$$

$$+2\left(\frac{13}{15}g_1^2\tilde{M}_1 + 3g_2^2\tilde{M}_2 + \frac{16}{3}g_3^2\tilde{M}_3 + Tr\left(3Y_u^\dagger A_u + Y_\nu^\dagger A_\nu\right)\right)Y_u$$

$$+4Y_uY_u^\dagger A_u + 5A_uY_u^\dagger Y_u + 2Y_uY_d^\dagger A_d + A_uY_d^\dagger Y_d \qquad \text{(H.23)}$$

$$16\pi^2\mu\frac{dA_d}{d\mu} = \left(-\frac{7}{15}g_1^2 - 3g_2^2 - \frac{16}{3}g_3^2 + Tr\left(3Y_d^\dagger Y_d + Y_e^\dagger Y_e\right)\right)A_d$$

$$+2\left(\frac{7}{15}g_1^2\tilde{M}_1 + 3g_2^2\tilde{M}_2 + \frac{16}{3}g_3^2\tilde{M}_3 + Tr\left(3Y_d^\dagger A_d + Y_e^\dagger A_e\right)\right)Y_d$$

$$+4Y_dY_d^\dagger A_d + 5A_dY_d^\dagger Y_d + 2Y_dY_u^\dagger A_u + A_dY_u^\dagger Y_u \qquad \text{(H.24)}$$

$$16\pi^2\mu\frac{dA_e}{d\mu} = \left(-\frac{9}{5}g_1^2 - 3g_2^2 + Tr\left(3Y_d^\dagger Y_d + Y_e^\dagger Y_e\right)\right)A_e$$

$$+2\left(\frac{9}{5}g_1^2\tilde{M}_1 + 3g_2^2\tilde{M}_2 + Tr\left(3Y_d^\dagger A_d + Y_e^\dagger A_e\right)\right)Y_e$$

$$+4Y_eY_e^\dagger A_e + 5A_eY_e^\dagger Y_e + 2Y_eY_\nu^\dagger A_\nu + A_eY_\nu^\dagger Y_\nu \qquad \text{(H.25)}$$

$$16\pi^2\mu\frac{dA_\nu}{d\mu} = \left(-\frac{3}{5}g_1^2 - 3g_2^2 + Tr\left(3Y_u^\dagger Y_u + Y_\nu^\dagger Y_\nu\right)\right)A_\nu$$

$$+2\left(\frac{3}{5}g_1^2\tilde{M}_1 + 3g_2^2\tilde{M}_2 + Tr\left(3Y_u^\dagger A_u + Y_\nu^\dagger A_\nu\right)\right)Y_\nu$$

$$+4Y_\nu Y_\nu^\dagger A_\nu + 5A_\nu Y_\nu^\dagger Y_\nu + 2Y_\nu Y_e^\dagger A_e + A_\nu Y_e^\dagger Y_e, \qquad \text{(H.26)}$$

where

$$S = Tr\left(m_{\tilde{Q}}^2 + m_{\tilde{d}}^2 - 2m_{\tilde{u}}^2 - m_{\tilde{L}}^2 + m_{\tilde{e}}^2\right) - m_{h_1}^2 + m_{h_2}^2. \qquad \text{(H.27)}$$

We have adopted the convention of S. P. Martin and M. T. Vaughn [50] for the sign of terms proportional to the gaugino masses in the RGEs of trilinear A parameters. As the right-handed neutrinos are no active degrees of freedom below the M_i-thresholds, the corresponding trilinear terms A_ν are also integrated out below the respective M_i-thresholds, see also [34].

Bibliography

[1] Q. R. Ahmad *et al.* [SNO Collaboration], Phys. Rev. Lett. **87**, 071301 (2001) [arXiv:nucl-ex/0106015].

[2] Y. Fukuda *et al.* [Super-Kamiokande Collaboration], Phys. Rev. Lett. **81**, 1562 (1998) [arXiv:hep-ex/9807003].

[3] M. Maltoni, T. Schwetz, M. A. Tortola and J. W. F. Valle, Phys. Rev. D **68**, 113010 (2003) [arXiv:hep-ph/0309130].

[4] For a summary of current limits and future prospects of $\mu - e$ conversion and $\mu \to e\gamma$ experiments, see M. Hebert, "Status and prospects of MECO, the Muon to Electron Conversion Experiment", presented at *Beyond the Desert 2003*, Schloss Ringberg, June 9th to 14th, 2003, http://meco.ps.uci.edu/mecopages/presentations.html.

[5] K. Hagiwara *et al.* [Particle Data Group Collaboration], Phys. Rev. D **66**, 010001 (2002).

[6] MEG home page, http://meg.psi.ch.

[7] K. Inami, for the Belle Collaboration, Talk presented at the 19th International Workshop on Weak Interactions and Neutrinos (WIN-03) October 6th to 11th, 2003, Lake Geneva, Wisconsin, USA.

[8] K. Abe *et al.* [Belle Collaboration], arXiv:hep-ex/0310029.

[9] T. Oshima, "$\tau \to \mu\gamma$: Status and prospects", *3rd Workshop on Neutrino Oscillations and Their Origin (NOON 2001)*, Kashiwa, Japan, Dec 5th to 8th, 2001; K. Inami, "lepton flavor violation in tau decay: experiment", *Mini-workshop for Super KEKB LoI physics part Discovery and Identification of New Physics at 3 ab^{-1} and $30ab^{-1}$*, KEK, June 19th, 2003.

[10] J. Aysto *et al.*, arXiv:hep-ph/0109217.

[11] See MECO experiment home page, http://meco.ps.uci.edu.

[12] B. C. Regan, E. D. Commins, C. J. Schmidt and D. DeMille, Phys. Rev. Lett. **88**, 071805 (2002).

[13] S. K. Lamoreaux, arXiv:nucl-ex/0109014.

[14] J. Bailey *et al.* [CERN-Mainz-Daresbury Collaboration], Test Of Relativistic Time Dilation," Nucl. Phys. B **150**, 1 (1979).

[15] M. Gell-Mann, P. Ramond and R. Slansky, *Proceedings of the Supergravity Stony Brook Workshop*, New York 1979, eds. P. Van Nieuwenhuizen and D. Freedman; T. Yanagida, *Proceedings of the Workshop on Unified Theories and Baryon Number in the Universe*, Tsukuba, Japan 1979, eds. A. Sawada and A. Sugamoto; R. N. Mohapatra and G. Senjanovic, Phys. Rev. Lett. **44**, 912 (1980), *erratum ibid* Phys. Rev. **D 23**, 165 (1993).

[16] M. Fukugita and T. Yanagida, Phys. Lett B **174** 45 (1986).

[17] S. T. Petcov, Sov. J. Nucl. Phys. **25**, 340 (1977) [Yad. Fiz. **25**, 641 (1977); Erratum, **25**, 698 (1977); erratum **25**, 1336 (1977)]; S. M. Bilenkii, S. T. Petcov and B. Pontecorvo, Phys. Lett. B **67** 309 (1977).

[18] M. Davier, S. Eidelman, A. Hocker and Z. Zhang, arXiv:hep-ph/0308213; see also more conservative approach to interpret the muon $g-2$ results, S. P. Martin and J. D. Wells, Phys. Rev. D **67**, 015002 (2003) [arXiv:hep-ph/0209309].

[19] G. W. Bennett *et al.* [Muon g-2 Collaboration], Phys. Rev. Lett. **89**, 101804 (2002) [Erratum-ibid. **89**, 129903 (2002)] [arXiv:hep-ex/0208001].

[20] J. R. Ellis, J. S. Hagelin, D. V. Nanopoulos, K. A. Olive and M. Srednicki, Nucl. Phys. B **238**, 453 (1984); see also H. Goldberg Phys. Rev. Lett. **50**, 1419 (1983).

[21] D. Z. Freedman, P. van Nieuwenhuizen and S. Ferrara, Phys. Rev. D **13**, 3214 (1976); S. Deser and B. Zumino, Phys. Lett. B **62**, 335 (1976); D. Z. Freedman and P. van Nieuwenhuizen, Phys. Rev. D **14**, 912 (1976); E. Cremmer, B. Julia, J. Scherk, S. Ferrara, L. Girardello and P. van Nieuwenhuizen, Nucl. Phys. B **147**, 105 (1979); J. A. Bagger, Nucl. Phys. B **211**, 302 (1983); E. Cremmer, S. Ferrara, L. Girardello and A. Van Proeyen, Nucl. Phys. B **212**, 413 (1983).

[22] R. Barbieri, L. Hall and A. Strumia, Nucl. Phys. B **445** 219 (1995). G. K. Leontaris and N. D. Tracas, Phys. Lett. B **431** 90 (1998); W. Buchmüller, D. Delepine and F. Vissani, Phys. Lett. B **459** 171 (1999); M. E. Gomez, G. K. Leontaris, S. Lola and J. D. Vergados, Phys. Rev. D **59** 116009 (1999); S. F. King and M. Oliveira, Phys. Rev. D **60** 035003 (1999); W. Buchmüller, D. Delepine and L. T. Handoko, X. J. Bi and Y. B. Dai, [arXiv:hep-ph/0112077]; Nucl. Phys. B **576** 445 (2000); J. Ellis, M. E. Gomez, G. K. Leontaris, S. Lola and D. V. Nanopoulos, Eur. Phys. J. C **14** 319 (2000); D. F. Carvalho, M. E. Gomez and S. Khalil, [arXiv:hep-ph/0101250]; S. Davidson and A. Ibarra, JHEP **0109**, 013 (2001) [arXiv:hep-ph/0104076]; P. Ciafaloni, A. Romanino and A. Strumia, Nucl. Phys. B **458** 3 (1996); J. Hisano, T. Moroi, K. Tobe and M. Yamaguchi, Phys. Lett. B **391** 341

(1997); J. Hisano, D. Nomura, Y. Okada, Y. Shimizu and M. Tanaka, Phys. Rev. D **58** 116010 (1998); J. Hisano, D. Nomura and T. Yanagida, Phys. Lett. B **437** 351 (1998); G. Barenboim, K. Huitu and M. Raidal, Phys. Rev. D **63** 055006 (2001); S. Lavignac, I. Masina and C. A. Savoy, Phys. Lett. B **520**, 269 (2001) [arXiv:hep-ph/0106245]; A. Kageyama, S. Kaneko, N. Shimoyama and M. Tanimoto, Phys. Rev. D **65**, 096010 (2002) [arXiv:hep-ph/0112359]; F. Deppisch, H. Päs, A. Redelbach, R. Rückl and Y. Shimizu, Eur. Phys. J. C **28**, 365 (2003) [arXiv:hep-ph/0206122]; S. T. Petcov, S. Profumo, Y. Takanishi and C. E. Yaguna, Nucl. Phys. B **676**, 453 (2004) [arXiv:hep-ph/0306195].

[23] L. Randall and R. Sundrum, Nucl. Phys. B **557**, 79 (1999) [arXiv:hep-th/9810155]; G. F. Giudice, M. A. Luty, H. Murayama and R. Rattazzi, JHEP **9812**, 027 (1998) [arXiv:hep-ph/9810442].

[24] D. E. Kaplan, G. D. Kribs and M. Schmaltz, Phys. Rev. D **62**, 035010 (2000) [arXiv:hep-ph/9911293]; Z. Chacko, M. A. Luty, A. E. Nelson and E. Ponton, JHEP **0001**, 003 (2000) [arXiv:hep-ph/9911323].

[25] G. F. Giudice and R. Rattazzi, Phys. Rept. **322**, 419 (1999) [arXiv:hep-ph/9801271].

[26] K. Tobe, J. D. Wells and T. Yanagida, arXiv:hep-ph/0310148.

[27] S. P. Martin, arXiv:hep-ph/9709356; published in *Perspectives on Supersymmetry*, World Scientific Pub. Co. (1999), ed. G. L. Kane.

[28] H. P. Nilles, Phys. Rept. **110**, 1 (1984).

[29] L. Girardello and M. T. Grisaru, Nucl. Phys. B **194**, 65 (1982).

[30] S. Weinberg, *The Quantum Theory of Fields, Volume II, Modern Applications*, Cambridge University Press (1996).

[31] J. Hisano, T. Moroi, K. Tobe and M. Yamaguchi, Phys. Rev. D **53**, 2442 (1996) [arXiv:hep-ph/9510309].

[32] D. M. Pierce, J. A. Bagger, K. T. Matchev and R. J. Zhang, Nucl. Phys. B **491**, 3 (1997) [arXiv:hep-ph/9606211].

[33] B. C. Allanach, Comput. Phys. Commun. **143**, 305 (2002) [arXiv:hep-ph/0104145].

[34] S. T. Petcov, S. Profumo, Y. Takanishi and C. E. Yaguna, Nucl. Phys. B **676**, 453 (2004) [arXiv:hep-ph/0306195].

[35] J. A. Casas and A. Ibarra, Nucl. Phys. B **618** 171 (2001) [arXiv:hep-ph/0103065].

[36] S. Antusch, J. Kersten, M. Lindner and M. Ratz, Phys. Lett. B **538**, 87 (2002) [arXiv:hep-ph/0203233].

[37] J. Hisano and D. Nomura, Phys. Rev. D **59**, 116005 (1999) [arXiv:hep-ph/9810479].

[38] J. R. Ellis, J. Hisano, S. Lola and M. Raidal, Nucl. Phys. B **621**, 208 (2002) [arXiv:hep-ph/0109125]; J. R. Ellis, J. Hisano, M. Raidal and Y. Shimizu, Phys. Lett. B **528**, 86 (2002) [arXiv:hep-ph/0111324].

[39] B. C. Allanach *et al.*, in *Proc. of the APS/DPF/DPB Summer Study on the Future of Particle Physics (Snowmass 2001)* ed. N. Graf, Eur. Phys. J. C **25**, 113 (2002) [eConf **C010630**, P125 (2001)] [arXiv:hep-ph/0202233].

[40] M. Fujii and T. Yanagida, Phys. Lett. B **549**, 273 (2002) [arXiv:hep-ph/0208191]; M. Fujii, M. Ibe and T. Yanagida, arXiv:hep-ph/0309064.

[41] K. Hamaguchi, arXiv:hep-ph/0212305, and references therein.

[42] T. Moroi, H. Murayama and M. Yamaguchi, Phys. Lett. B **303**, 289 (1993); A. de Gouvea, T. Moroi and H. Murayama, Phys. Rev. D **56**, 1281 (1997) [arXiv:hep-ph/9701244].

[43] J. L. Feng and T. Moroi, Phys. Rev. D **61**, 095004 (2000) [arXiv:hep-ph/9907319].

[44] T. Gherghetta, G. F. Giudice and J. D. Wells, Nucl. Phys. B **559**, 27 (1999) [arXiv:hep-ph/9904378].

[45] S. Antusch and M. Ratz, JHEP **0207**, 059 (2002) [arXiv:hep-ph/0203027].

[46] M. Schmaltz and W. Skiba, Phys. Rev. D **62**, 095005 (2000) [arXiv:hep-ph/0001172]; M. Schmaltz and W. Skiba, Phys. Rev. D **62**, 095004 (2000) [arXiv:hep-ph/0004210].

[47] H. Baer, M. A. Diaz, P. Quintana and X. Tata, JHEP **0004**, 016 (2000) [arXiv:hep-ph/0002245].

[48] S. Baek, T. Goto, Y. Okada and K. I. Okumura, Phys. Rev. D **64**, 095001 (2001) [arXiv:hep-ph/0104146].

[49] J. I. Illana and M. Masip, arXiv:hep-ph/0307393.

[50] S. P. Martin and M. T. Vaughn, Phys. Rev. D **50**, 2282 (1994) [arXiv:hep-ph/9311340].

[51] Y. Okada, K. i. Okumura and Y. Shimizu, Phys. Rev. D **61** 094001 (2000) [arXiv:hep-ph/9906446].

[52] D. Griffiths, *Introduction to elementary particles*, John Wiley & Sons (1987).

[53] Y. Kuno and Y. Okada, Phys. Rev. Lett. **77**, 434 (1996) [arXiv:hep-ph/9604296]; Y. Kuno, A. Maki and Y. Okada, Phys. Rev. D **55**, 2517 (1997) [arXiv:hep-ph/9609307].

[54] T. P. Cheng and L. F. Li, *Gauge theory of elementary particle physics*, Oxford University Press (1984); T. P. Cheng and L. F. Li, *Gauge theory of elementary particle physics- problems and solutions*, Oxford University Press (2000).

[55] F. Deppisch, H. Päs, A. Redelbach, R. Rückl and Y. Shimizu, Eur. Phys. J. C **28**, 365 (2003) [arXiv:hep-ph/0206122].

[56] A. Bartl, W. Majerotto, W. Porod and D. Wyler, Phys. Rev. D **68**, 053005 (2003) [arXiv:hep-ph/0306050].

[57] D. F. Carvalho, J. R. Ellis, M. E. Gomez and S. Lola, Phys. Lett. B **515** 323 (2001) [arXiv:hep-ph/0103256].

[58] J. L. Feng, K. T. Matchev and Y. Shadmi, Nucl. Phys. B **613**, 366 (2001) [arXiv:hep-ph/0107182].

[59] H. C. Chiang, E. Oset, T. S. Kosmas, A. Faessler and J. D. Vergados, Nucl. Phys. A **559** (1993) 526; T. S. Kosmas, A. Faessler, F. Simkovic and J. D. Vergados, Phys. Rev. C **56**, 526 (1997) [arXiv:nucl-th/9704021].

[60] T. Suzuki, D. F. Measday and J. P. Roalsvig, Phys. Rev. C **35** (1987) 2212.

[61] S. Weinberg and G. Feinberg, Phys. Rev. Lett. **3** 111 (1959).

[62] R. Kitano, M. Koike and Y. Okada, Phys. Rev. D **66**, 096002 (2002) [arXiv:hep-ph/0203110].

[63] A. Ilakovac and A. Pilaftsis, Nucl. Phys. B **437**, 491 (1995) [arXiv:hep-ph/9403398].

[64] A. Dedes, J. R. Ellis and M. Raidal, Phys. Lett. B **549**, 159 (2002) [arXiv:hep-ph/0209207].

[65] A. de Gouvea, S. Lola and K. Tobe, Phys. Rev. D **63**, 035004 (2001) [arXiv:hep-ph/0008085].

[66] C. L. Bennett *et al.*, arXiv:astro-ph/0302207; D. N. Spergel *et al.*, arXiv:astro-ph/0302209.

[67] A. D. Sakharov, Pis'ma Zh Eksp. Teor. Fiz. **5** 32 (1967).

[68] E. W. Kolb and M. S. Turner, *The Early Universe*, Addison-Wesley, Reading, MA (1989).

[69] V. A. Kuzmin, V. A. Rubakov and M. E. Shaposhnikov, Phys. Lett. B **155**, 36 (1985).

[70] M. Plümacher, arXiv:hep-ph/9807557 and references therein.

[71] W. Buchmüller, P. Di Bari and M. Plümacher, Nucl. Phys. B **643**, 367 (2002) [arXiv:hep-ph/0205349]; W. Buchmuller, P. Di Bari and M. Plumacher, Nucl. Phys. B **665**, 445 (2003) [arXiv:hep-ph/0302092].

[72] W. Buchmüller and M. Plümacher, Int. J. Mod. Phys. A **15**, 5047 (2000) [arXiv:hep-ph/0007176].

[73] A. Pilaftsis, Int. J. Mod. Phys. A **14**, 1811 (1999) [arXiv:hep-ph/9812256].

[74] S. Davidson and A. Ibarra, Phys. Lett. B **535**, 25 (2002) [arXiv:hep-ph/0202239].

[75] M. Hirsch and S. F. King, Phys. Rev. D **64**, 113005 (2001) [arXiv:hep-ph/0107014].

[76] P. Di Bari, AIP Conf. Proc. **655**, 208 (2003) [arXiv:hep-ph/0211175].

[77] M. Plümacher, private communication.

[78] M. Y. Khlopov and A. D. Linde, Phys. Lett. B **138**, 265 (1984); J. R. Ellis, J. E. Kim and D. V. Nanopoulos, Phys. Lett. B **145**, 181 (1984).

[79] M. Kawasaki, K. Kohri and T. Moroi, Phys. Rev. D **63**, 103502 (2001) [arXiv:hep-ph/0012279].

[80] W. Buchmüller, K. Hamaguchi and M. Ratz, Phys. Lett. B **574**, 156 (2003) [arXiv:hep-ph/0307181].

[81] H. Päs and T. J. Weiler, Phys. Rev. D **63**, 113015 (2001) [arXiv:hep-ph/0101091].

[82] A. Osipowicz *et al.* [KATRIN Collaboration], arXiv:hep-ex/0109033; C. Weinheimer, private communication.

[83] M. Battaglia *et al.*, Eur. Phys. J. C **22**, 535 (2001) [arXiv:hep-ph/0106204].

[84] F. Deppisch, H. Päs, A. Redelbach, R. Rückl and Y. Shimizu, arXiv:hep-ph/0310053.

[85] S. Antusch, J. Kersten, M. Lindner and M. Ratz, Nucl. Phys. B **674**, 401 (2003) [arXiv:hep-ph/0305273].

[86] G. C. Cho, N. Haba and J. Hisano, Phys. Lett. B **529**, 117 (2002) [arXiv:hep-ph/0112163].

[87] H. E. Haber and G. L. Kane, Phys. Rept. **117**, 75 (1985).

[88] W. Greiner and B. Müller *Relativistische Quantenmechanik, Wellengleichungen*, Verlag Harri Deutsch (1987).

[89] S. Wolfram, *Mathematica*, version 4.

[90] J. Hisano, private communication.

[91] S. Antusch, M. Drees, J. Kersten, M. Lindner and M. Ratz, Phys. Lett. B **519**, 238 (2001) [arXiv:hep-ph/0108005].

[92] P. H. Chankowski and S. Pokorski, Int. J. Mod. Phys. A **17**, 575 (2002) [arXiv:hep-ph/0110249].

Acknowledgements